

Time Frequency Analysis of Railway Wagon Body Accelerations for a Low-Power Autonomous Device

Steven Shea Bleakley

Thesis submitted for the Degree of Master of Engineering

Faculty of Engineering and Physical Systems

Central Queensland University

October 2006

Executive Summary

This thesis examines the application of the techniques of Fourier spectrogram and wavelet analysis to a low power embedded microprocessor application in a novel railway and rollingstock monitoring system.

The safe and cost effective operation of freight railways is limited by the dynamic performance of wagons running on track. A monitoring system has been proposed comprising of low cost wireless sensing devices, dubbed “Health Cards”, to be installed on every wagon in the fleet. When marshalled into a train, the devices would sense accelerations and communicate via radio network to a master system in the locomotive. The integrated system would provide online information for decision support systems.

Data throughput was heavily restricted by the network architecture, so significant signal analysis was required at the device level. An electronics engineering team at Central Queensland University developed a prototype Health Card, incorporating a 27MHz microcontroller and four dual axis accelerometers. A sensing arrangement and online analysis algorithms were required to detect and categorise dynamic events while operating within the constraints of the system.

Time-frequency analysis reveals the time varying frequency content of signals, making it suitable to detect and characterise transient events. With efficient algorithms such as the Fast Fourier Transform, and Fast Wavelet Transform, time-frequency analysis methods can be implemented on a low power, embedded microcontroller.

This thesis examines the application of time-frequency analysis techniques to wagon body acceleration signals, for the purpose of detecting poor dynamic performance of the

wagon-track system. The Fourier spectrogram is implemented on the Health Card prototype and demonstrated in the laboratory. The research and algorithms provide a foundation for ongoing development as resources become available for system testing and validation.

Publications

1. Bleakley, S., Senini, S., “Autonomous Time Frequency Analysis of Wagon Body Accelerations”, Proceedings of the 5th Asia-Pacific Industrial Engineering and Management Systems Conference, Gold Coast, Australia, 12-15 Dec 2004
2. Xia, F., Bleakley, S., “The Estimation of Wheel-Rail Interaction Forces from Wagon Acceleration”, *Advances in Applied Mechanics*, Proceedings of the 4th Australasian Congress on Applied Mechanics (ACAM2005), Melbourne, Australia, 16-18 Feb 2005, pp333-338

Declaration of Authorship

I certify that the main text of this thesis is entirely my own work and that such work has not previously been submitted for award of a degree

Steven Bleakley

Acknowledgements

As the author of this thesis I would like to thank the following people for their support and contributions to this work:

- Dr Steven Senini* For his supervision throughout this work. For copious amounts of encouraging words. For clarity when the trees obscured the forest, and for humour when the heat was on.
- Prof. Peter Wolfs* “Our fearless leader”. For his resourceful leadership, capable electronics hardware design, and for keeping an open door.
- Dr Peter Thomas* For Health Card microcontroller programming and PC programming of the “master system” display. The only man I’ve ever seen who can program all night in a railway carriage on little more than coffee and not complain.
- Bryan Powell* For Health Card hardware development. For his inspiring organisation and attention to detail.
- Greg Capern* For battling with radio protocols and coming through victorious.
- Andrew Kearney* For prototype hardware - built on time and under budget. “We deliver”.
- Ian Tomlinson* For data acquisition system development. “The LABVIEW guru”.
- Queensland Rail* For access to test trains, use of the test car, and study assistance. Special thanks to Eryl Lynch for project support within QR.

And on a more personal note...

- My wife Helena* For marrying me in the middle of writing this thesis and for putting up with the “t” word throughout our engagement and the first year and a half of our life together. For her understanding, patience, support, prayers and encouragement.
- My parents,
family, and
friends* For their thoughts, prayers and encouragement throughout this work.
- Lighthouse
Baptist Church* For all their prayers and regular encouragement. Special thanks to Andrew & Barbara Wojtas for their focused prayer at a time of great need.
- The LORD God
Almighty* For answering prayer. For all the times during this work that He has heard my cry and delivered me out of my distresses. Most of all: for giving me life, forgiveness, and salvation for all eternity, by the finished work of God the Son - Jesus Christ - the great Author and Finisher - my Lord and my Saviour.

Table of Contents

EXECUTIVE SUMMARY	II
PUBLICATIONS.....	IV
ACKNOWLEDGEMENTS	V
TABLE OF CONTENTS.....	V
LIST OF FIGURES.....	X
1 INTRODUCTION.....	1
2 APPLICATION BACKGROUND	4
2.1 RAILWAY WAGON-TRACK SYSTEM	4
2.1.1 <i>Conventional Track Structure.....</i>	5
2.1.2 <i>Conventional Freight Wagon Structure.....</i>	8
2.2 DYNAMIC PERFORMANCE OF THE WAGON-TRACK SYSTEM	12
2.2.1 <i>Lateral Instability of the Railway Wagon.....</i>	12
2.2.1.1 Steering Mechanism.....	12
2.2.1.2 Lateral Instability	13
2.2.1.3 Detection of Bogie Hunting from the Wagon Body	15
2.2.2 <i>Vehicle Interaction with Track Irregularities.....</i>	16
2.2.2.1 Track Irregularities.....	17
2.2.2.2 Resonant Modes of Wagon Response	20
2.3 MANAGING THE PERFORMANCE OF THE WAGON TRACK SYSTEM	25
2.3.1 <i>Performance Testing of Rollingstock.....</i>	25
2.3.2 <i>Benefits of Monitoring Ride on Every Wagon</i>	27
2.3.3 <i>Existing Ride Monitoring Systems and Standards.....</i>	28
2.4 CONCLUSIONS	30
3 HEALTH CARD SYSTEM.....	32
3.1 THE PROPOSED SYSTEM	32
3.2 PROTOTYPE HEALTH CARD.....	34

3.2.1	<i>Network Throughput Constraints</i>	35
3.2.2	<i>Processing Capability</i>	36
3.2.3	<i>Sensor Location and Type</i>	36
3.2.4	<i>Sensing Arrangement</i>	37
3.2.5	<i>Signal Pre-Processing</i>	38
3.2.6	<i>Signal Filtering</i>	39
3.2.7	<i>Algorithm Requirements</i>	43
3.3	CONCLUSION.....	44
4	TIME FREQUENCY ANALYSIS OF ACCELERATION SIGNALS	46
4.1	ONLINE ANALYSIS OF ACCELERATION SIGNALS	46
4.1.1	<i>Online Analysis in Existing Systems and Standards</i>	46
4.1.2	<i>Frequency Content of Acceleration Signals</i>	48
4.2	TIME FREQUENCY ANALYSIS	53
4.3	FOURIER ANALYSIS.....	53
4.3.1	<i>Continuous Fourier Transform</i>	53
4.3.2	<i>Discrete Fourier Transform</i>	54
4.3.3	<i>Fast Fourier Transform</i>	58
4.4	ANALYSIS OF NON-STATIONARY SIGNALS.....	59
4.4.1	<i>Short Term Fourier Transform and Spectrogram</i>	60
4.4.2	<i>Windowing</i>	61
4.4.3	<i>Limitation of Time Frequency Resolution</i>	64
4.5	WAVELET ANALYSIS.....	65
4.5.1	<i>Wavelet Transform</i>	66
4.5.2	<i>Fast Wavelet Algorithm</i>	69
4.5.3	<i>Wavelet Type Selection</i>	72
4.5.4	<i>Relating Scales to Frequencies</i>	73
4.5.5	<i>Example of Wavelet Analysis vs Fourier Spectrogram</i>	74
4.6	CONCLUSION.....	76

5	TIME FREQUENCY ANALYSIS OF FIELD DATA.....	77
5.1	FIELD DATA ACQUISITION	77
5.1.1	<i>Purpose</i>	78
5.1.2	<i>Test Wagon</i>	78
5.1.3	<i>Test Track</i>	79
5.1.4	<i>Test Journey</i>	80
5.1.5	<i>Data Acquisition Equipment</i>	81
5.1.6	<i>Sensing Arrangement</i>	81
5.1.7	<i>Signal Conditioning, Sampling and Storage</i>	83
5.2	OFFLINE ANALYSIS OF DATA	85
5.3	DATA ANALYSIS IN MATLAB™.....	87
5.4	RESULTS	89
5.5	DISCUSSION OF RESULTS.....	90
5.5.1	<i>Detection of Bogie Hunting</i>	90
5.5.2	<i>Detection of Severe Vehicle-Track Interaction</i>	94
5.5.3	<i>Deficiencies in Australian and North American Standard Measures</i>	96
5.5.4	<i>Detection of Loading State from Spectral Average</i>	97
5.5.5	<i>Comparison of Wavelet and Fourier Time-Frequency Analysis</i>	100
5.6	CONCLUSION.....	101
6	IMPLEMENTING SHORT TERM FOURIER ANALYSIS ON HEALTH CARD	104
6.1	PURPOSE	104
6.2	REQUIREMENTS.....	104
6.3	IMPLEMENTATION OF STDFT ANALYSIS	104
6.4	OUTPUT VARIABLE	108
6.5	DISPLAY METHOD FOR THE MASTER DEVICE	113
6.6	DEMONSTRATION IN LABORATORY	114
6.7	RECOMMENDATION FOR AUTOMATED DETECTION OF TIME-FREQUENCY SIGNATURES	117
6.8	CONCLUSION.....	121

7	CONCLUSION	122
	REFERENCES	125
	BIBLIOGRAPHY	132

List of Figures

Figure 2-1 Conventional Track Structure.....	6
Figure 2-2 Diagram of Track Parameters.....	7
Figure 2-3 A Conventional Wagon Design.....	8
Figure 2-4 A Conventional Three Piece Bogie.....	9
Figure 2-5 Wheel-rail profile.....	10
Figure 2-6 Simulation Model of a Hopper Wagon.....	11
Figure 2-7 Wheelset Steering Mechanism.....	13
Figure 2-8 Track Irregularity Parameters.....	17
Figure 2-9 Examples of temporal track irregularities.....	18
Figure 2-10 Track Degradation and Maintenance Cycle.....	19
Figure 2-11 Excitation of oscillatory modes in the wagon body.....	21
Figure 2-12 Example Vertical Track Irregularity.....	23
Figure 2-13 RMS vertical body acceleration vs vertical excitation frequency in the vertical mode.....	24
Figure 2-14 Resonant conditions of speed and irregularity wavelength for bounce, pitch and roll modes.....	25
Figure 2-15 Hallade machine and recorded traces (source [2]).....	28
Figure 2-16 RideMon Example Desktop Display (Source [18]).....	29
Figure 3-1 Proposed System Arrangement.....	33
Figure 3-2 Health Card prototype installed on a ballast wagon.....	34
Figure 3-3 Health Card Prototype System Arrangement.....	35
Figure 3-4 Accelerometer Locations and Axis Naming Convention.....	38
Figure 3-5 Relating corner accelerations to 5 degrees of freedom.....	38

Figure 3-6 Prototype Health Card Signal Pre-Processing (one of eight axes)	39
Figure 3-7 Example of Signal Aliasing	40
Figure 3-8 Ideal Low Pass Filter for 200Hz sampling	41
Figure 3-9 Low Pass Filtering for Prototype Health Card.....	41
Figure 3-10 Low Pass Filtering for Prototype with Additional Mechanical Filter.	43
Figure 4-1 Root Mean Square (RMS) and Peak to Peak Values.....	48
Figure 4-2 Acceleration Frequency Sweep from 0 to 10Hz (1) with Velocity (2) and Displacement (3).....	50
Figure 4-3 Large Bounce Site: Acceleration, Velocity and Displacement.....	51
Figure 4-4 Discrete Fourier Transform Example	57
Figure 4-5 Comparison of DFT and FFT Processing Load.....	58
Figure 4-6 Time Signals and Corresponding Power Spectra: Sum of Sinusoids at 10, 20 and 30Hz (top); Sequence of Sinusoids at 10, 20 and 30Hz (middle); Frequency Sweep of 0-10Hz (bottom).	60
Figure 4-7 Time Signals and Corresponding Spectrogram: Sum of Sinusoids at 10, 20 and 30Hz (top); Sequence of Sinusoids at 10, 20 and 30Hz (middle); Frequency Sweep of 0-10Hz (bottom).	61
Figure 4-8 DFT Assumed Periodicity and Boundary Discontinuities.....	62
Figure 4-9 Windowing.....	63
Figure 4-10 Time-Frequency Plane and Time Frequency Resolution	65
Figure 4-11 Example Wavelet.....	66
Figure 4-12 Wavelet Scaling	67
Figure 4-13: Fourier Basis Function (left) vs Wavelet Basis Function (right).....	68
Figure 4-14: WT Time-Freq Relationship.....	69

Figure 4-15 Diadic (powers of 2) Scaling	70
Figure 4-16: Fast Wavelet Analysis Transform	71
Figure 4-17 Diadic Wavelet Analysis of a Transient Signal	72
Figure 4-18 Haar Wavelet	72
Figure 4-19 Approximating the Centre Frequency of a Wavelet with a Best Fit Sinusoid	74
Figure 4-20 Lateral Wagon Body Acceleration with Wavelet and FFT Spectrogram Compared.....	75
Figure 5-1 Field Data Acquisition	78
Figure 5-2 ballast hopper wagon used for signal acquisition	79
Figure 5-3 Journey Description from GPS Locations	80
Figure 5-4 Accelerometer units used for data acquisition	81
Figure 5-5 Accelerometer locations and xyz coordinate system.....	82
Figure 5-6 Relating corner accelerations to 5 degrees of freedom.....	83
Figure 5-7 - Signal Processing for Data Acquisition using PC and DAC Card	84
Figure 5-8 Wagon Body and Sideframe Accelerations in the Loaded and Empty Case	85
Figure 5-9 Example Data Analysis Page (source - CD01:\FBY(01-04 to 06-08).pdf page 5)	87
Figure 5-10 Journey Description with File Locations	90
Figure 5-11 Body Lateral (top) vs Bogie lateral (bottom) during lateral oscillation of an empty wagon.....	91
Figure 5-12 Body Lateral (top) vs Bogie lateral (bottom) during lateral oscillation of a loaded wagon.....	91
Figure 5-13 Discerning Hunting from Other Lateral Oscillations	93

Figure 5-14 Hunting Initiated By Irregularity	94
Figure 5-15 “Large Bounce” Site, Onward Journey, Loaded.....	95
Figure 5-16 “Large Bounce” Site, Return Journey, Unloaded	96
Figure 5-17 Average of Local Spectra for Loaded Wagon on Onward Journey.....	99
Figure 5-18 Average of Local Spectra for Empty Wagon on Return Journey	99
Figure 6-1 Raw Data Buffers – 8 Channels.....	105
Figure 6-2 Concept of Time Frequency Analysis with Pattern Recognition to Achieve Health Card Requirements.....	108
Figure 6-3 Overview of Algorithm for One Variable (roll)	110
Figure 6-4 Algorithm Output Variable (0-10Hz) Lateral	111
Figure 6-5 Algorithm Output Variable (0-5Hz) Lateral	112
Figure 6-6 Algorithm Output Variable (0-10Hz) Vertical	112
Figure 6-7 Algorithm Output Variable (0-4Hz) Vertical	113
Figure 6-8: Health Card Accelerometer and Transmitter Mounted on a Wagon in the Laboratory	115
Figure 6-9 Master System on Laptop Receiving Health Card Data via Radio Link ...	115
Figure 6-10 Master Display Showing (0.5-10Hz) Energy in Each DOF. (roll action excited, one wagon only).....	116
Figure 6-11 Expected Result for Four Wagons with Equal Characteristics (fabricated result).....	117
Figure 6-12 Spectrogram of Moving Signal (upper) and FFT of the Spectrogram Rows (lower)	120

1 Introduction

The safe and cost-effective operation of freight railways is limited by the dynamic performance of the wagons running on the track. The dynamic performance is determined by the characteristics of the wagon and the irregularities in the track. Wagon-track interaction can be monitored to a large degree by measuring the accelerations of the wagon body. Ride monitoring systems are currently available, suitable for installation on selected vehicles. However, the ride performance of every individual wagon on every track location cannot be measured viably with the existing technology.

A system has been proposed comprising of low cost wireless sensing devices, dubbed “Health Cards”, to be installed on every wagon in the fleet. When wagons are marshalled into a train, the devices would sense accelerations and communicate via radio network to a master system in the locomotive.

A set of four prototype Health Cards has been developed by an engineering team at Central Queensland University. Each prototype Health Card incorporates a 27MHz microcontroller with 256kB of onboard RAM, four dual axis accelerometers, a GPS receiver, two low power radios, lithium ion batteries with management circuits, and a solar panel. The purpose of the prototype was firstly to prove the capability of the equipment, and secondly to enable ongoing research into the capabilities of the proposed system.

Online signal processing and analysis algorithms were required for the prototype to operate and give meaningful information. The current ride monitoring systems detect events using peak or average vibration magnitude levels. Acceleration waveforms are

then stored or transmitted for further offline analysis. However, the proposed system has limited data throughput and therefore does not have the capability of storing or transmitting waveforms. Significant signal analysis must be performed onboard the device to extract features from the signal that can be used to classify events.

Time-frequency analysis is a signal processing technique which reveals the frequency content of transient signals. It has been applied in various signal analysis and detection applications. With efficient algorithms, such as the fast Fourier transform and fast wavelet transform, time-frequency analysis methods should be suitable for a low power, embedded microcontroller.

This research investigates whether time frequency analysis can be implemented within the constraints of the prototype device, and how effective the technique is for detection of poor vehicle dynamic performance and severe vehicle track interaction. In particular, two forms of time frequency analysis are investigated. These are the short term Fourier transform, and the wavelet transform.

Firstly, an understanding is developed in the areas of: the structure and dynamics of rail vehicles on track; the phenomena that are desirable to detect; existing rail industry practices in vehicle ride monitoring. Secondly, the prototype Health Card and associated constraints is presented. Thirdly, Fourier time-frequency analysis and wavelet analysis is introduced. Fourthly, wavelet analysis and Fourier time-frequency analysis is compared with standard root mean square (RMS) and peak to peak measures using field data. Finally, an algorithm for the prototype Health Card, based upon the Fourier time-frequency method is implemented on the prototype and demonstrated in the laboratory.

Through carrying out this research, significant contributions have been made towards the development of the Health Card system. These contributions include:

1. specification of sensor locations and signal pre-processing for a field data acquisition
2. strategic placement of four dual axis accelerometers in order for Health Card to capture the modes of dynamic motion in the vehicle body
3. determination of requirements for signal filtering and data sampling within the prototype device
4. specification of signal processing methods for the device including
 - a. online handling of data from the four dual axis accelerometers
 - b. online conversion of raw data into measurement of five modes of vehicle body motion including vertical, lateral, pitch, yaw and roll.
 - c. a time frequency analysis algorithm reporting energy levels in each mode while providing a means for frequency selective detection.

This thesis examines the application and implementation of time-frequency analysis techniques on the Health Card prototype, for the purpose of detecting poor dynamic performance of the wagon-track system. The research and algorithms provide a foundation for ongoing development towards a fully automated intelligent system.

2 Application Background

The purpose of the Health Card system is to monitor the dynamic performance of the railway system by placing an acceleration sensing device on every wagon. Algorithms for Health Card, like any signal analysis, cannot be developed without a good understanding of the application.

This chapter firstly introduces the basic structure and nomenclature of the wagon and track. Secondly, it identifies the dynamic principles that limit the performance of a wagon running on track. Finally, existing systems and standards are identified and compared with the proposed Health Card system.

2.1 RAILWAY WAGON-TRACK SYSTEM

This section introduces the physical structure of conventional freight wagons and track which will be referred to throughout the body of the thesis. Rollingstock and track design are substantial fields of engineering, and a coverage of these fields will not be attempted here. Although there are many variations, the majority of railways in Australia and worldwide use the basic elements of track and freight wagon structure which is shown in this section. For readers who are familiar with railway systems and terminology, this section is not needed. However, for those new to railway concepts, it is necessary to establish some basic terminology.

2.1.1 Conventional Track Structure

Railway track is designed to interface with railway vehicles to support the load while providing a permanent way of travel. A thorough coverage of railway track design and maintenance is given by [1][2]. Figure 2-1 pictures the basic elements of conventional track structure including the formation, capping layer, ballast, sleepers, fasteners and rails. The formation is the prepared support base for the structure. The capping layer is designed to cause water to shed to the sides of the track instead of seeping into the formation. Ballast is coarsely crushed rock which distributes the track load evenly from the sleepers to the formation, while providing ample drainage. The sleepers support the rails and providing lateral position and strength. The rails are rolled steel sections designed to interface with the wheel with minimal wear rolling resistance. The rails are fixed with fastenings to the sleepers. These elements combine to support the loads of a passing train, while maintaining the designed geometry of the track. Bridges, level crossings, tunnels etc, may be supported with structures differing from the track structure shown.

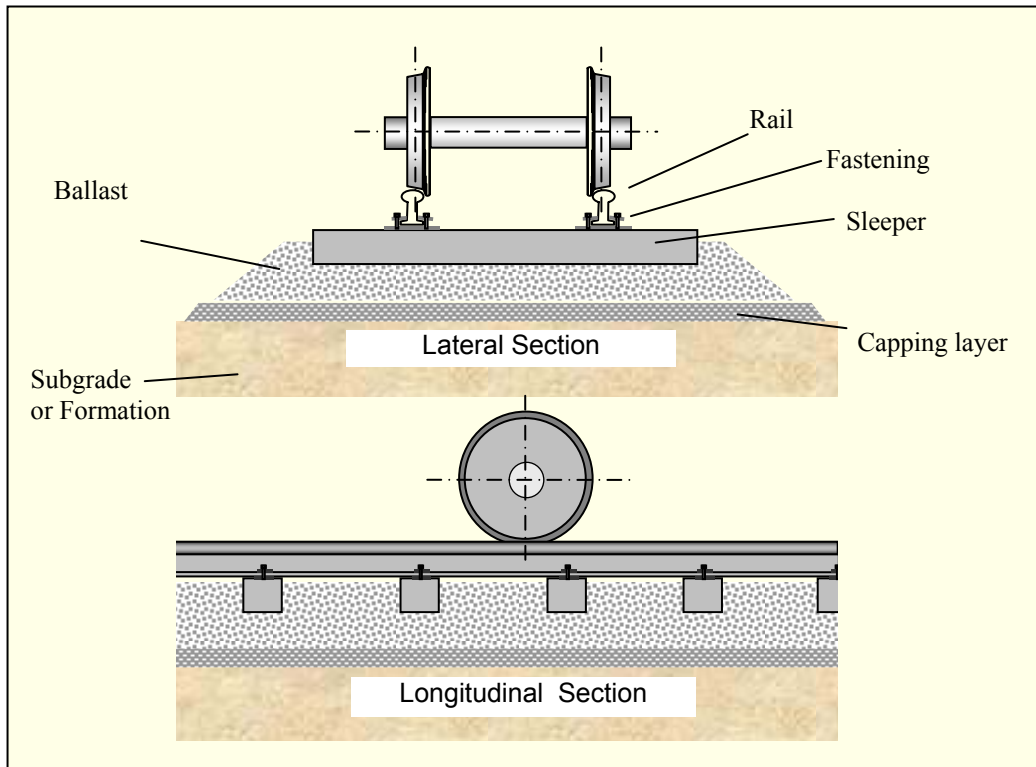


Figure 2-1 Conventional Track Structure

Geometric parameters that describe the track are shown in Figure 2-2 and the terms are defined in Table 2-1. Tangent, spiral and curved track are terms that describe the layout of the track. The geometry of the track is normally defined in terms of gauge, alignment, level, cant, and twist.

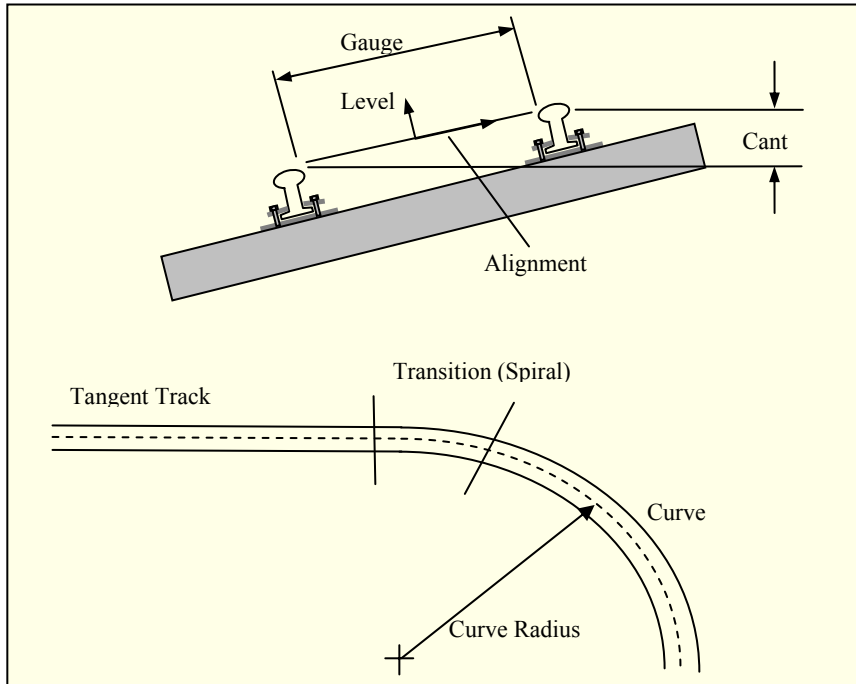


Figure 2-2 Diagram of Track Parameters

Table 2-1 Description of Track Parameters

<i>Term</i>	<i>Definition</i>
Gauge	Distance between the wheel rail contact points on the two rails.
Alignment, or Line	Deviation from the designed track centreline in the direction lateral to the designed plane of the track.
Level, Top, or Elevation	Deviation from the designed track centreline in the direction perpendicular to the designed plane of the track.
Cant, Cross-level, or Superelevation	Difference in vertical height between one rail and the other rail, describing the angle of the track plane to the horizontal plane.
Twist	The change in cant with respect to distance. Often defined over a nominated distance.
Spiral, or Transition	The section of curved track that has a changing radius from one curve radius to another.
Tangent (track)	Straight track, i.e. not curved.
Curve	A section of track that is not straight, normally defined by a curve radius.

2.1.2 Conventional Freight Wagon Structure

The railway wagon is designed to guide the load along the track safely with minimal damage to the track and the load. The most common wagon design has a bogie at each end as does the example shown in Figure 2-3. The bogie is a steerable unit which distributes the vehicle load between four wheels. The ride quality is improved by spring and damper elements within the bogie.

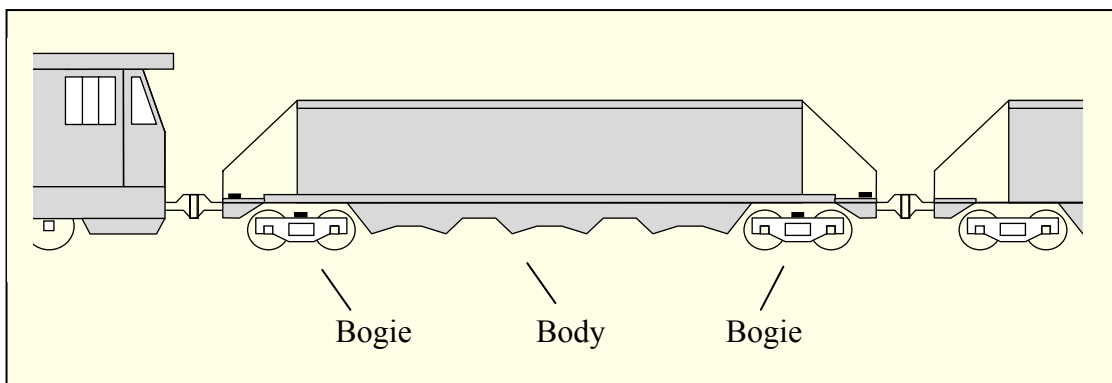


Figure 2-3 A Conventional Wagon Design

The “three-piece bogie” is the most common design used for Australian freight wagons. An example of a three piece bogie is shown in Figure 2-4. The three pieces refer to major structural components. These are the wheelsets, sideframes and bolster. There are two wheelsets, two sideframes and one bolster. The wheelsets consist of two steel wheels pressed onto a fixed axle with bearings at each end. The bearings are contained in bearing cases which fit into journals in the sideframes. The sideframes align the two wheelset axles and transfer the load between the bolster and the wheelsets. Suspension comprises of a nest of springs between each sideframe and its bolster end, with damping provided by a pair of friction pads between the sides of the bolster and the sideframes.

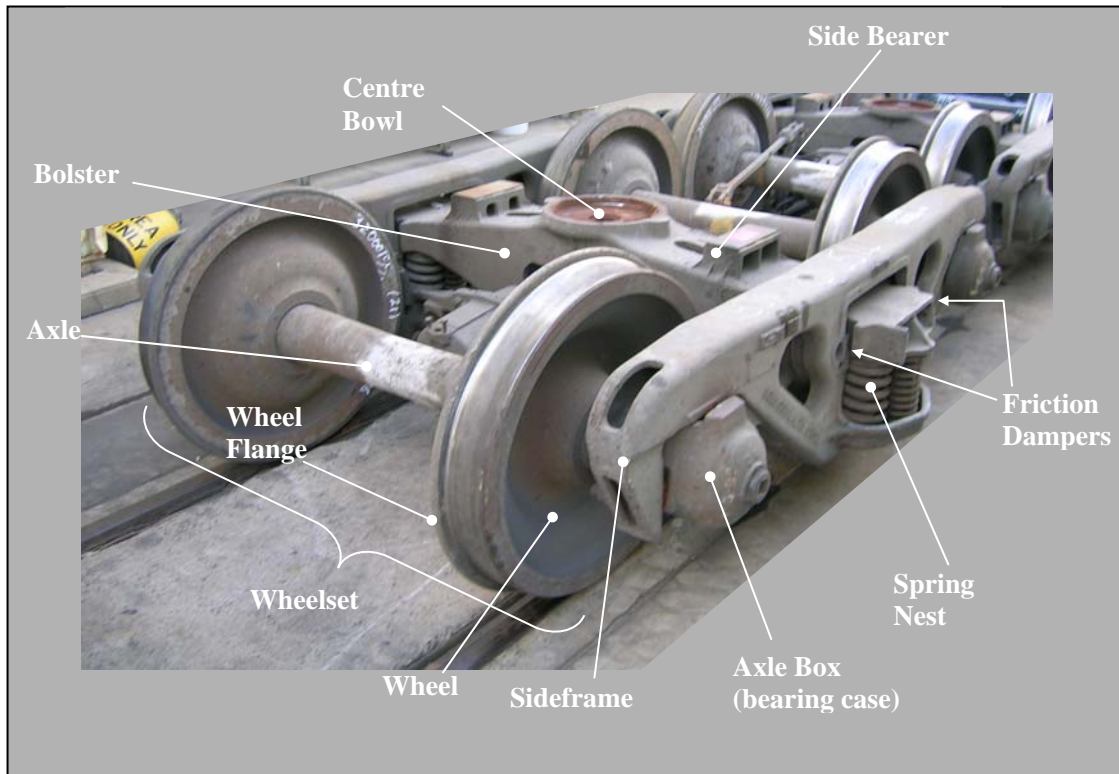


Figure 2-4 A Conventional Three Piece Bogie

Each wheel has a conical profile tapering from a larger radius on the inside edge to a smaller radius on the outside. The wheel rail interface profile is designed to minimise rolling resistance and provide the steering mechanism which will be described in Section 2.2.1. The inside edge of each wheel has a flange designed to provide additional guidance to the wheelset when the wheel conicity is inadequate. Excessive flange contact increases rail wear and risk of derailment.

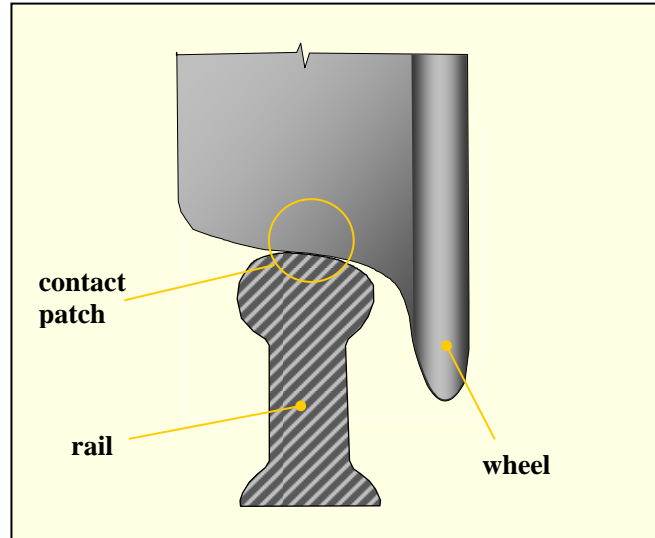


Figure 2-5 Wheel-rail profile

Figure 2-6 shows a graphical representation of a hopper wagon modelled in the simulation package Vampire™. A conventional railway wagon has 11 major masses including body(1), bolsters (2), sideframes (4) and wheelsets (4). Some example masses are listed in Table 2-2. (Note that Vampire™ uses units of mega-grams (Mg) to represent metric tonnes)

Table 2-2 Example Masses

<i>Component</i>	<i>Mass (Mg)</i>
Body (loaded)	66
Body (unloaded)	8
Bogie side frame	0.5
Bogie bolster	0.5
Wheelset	1.1
Total Each Bogie	3.7
Total Wagon (loaded)	73.4
(unloaded)	15.4

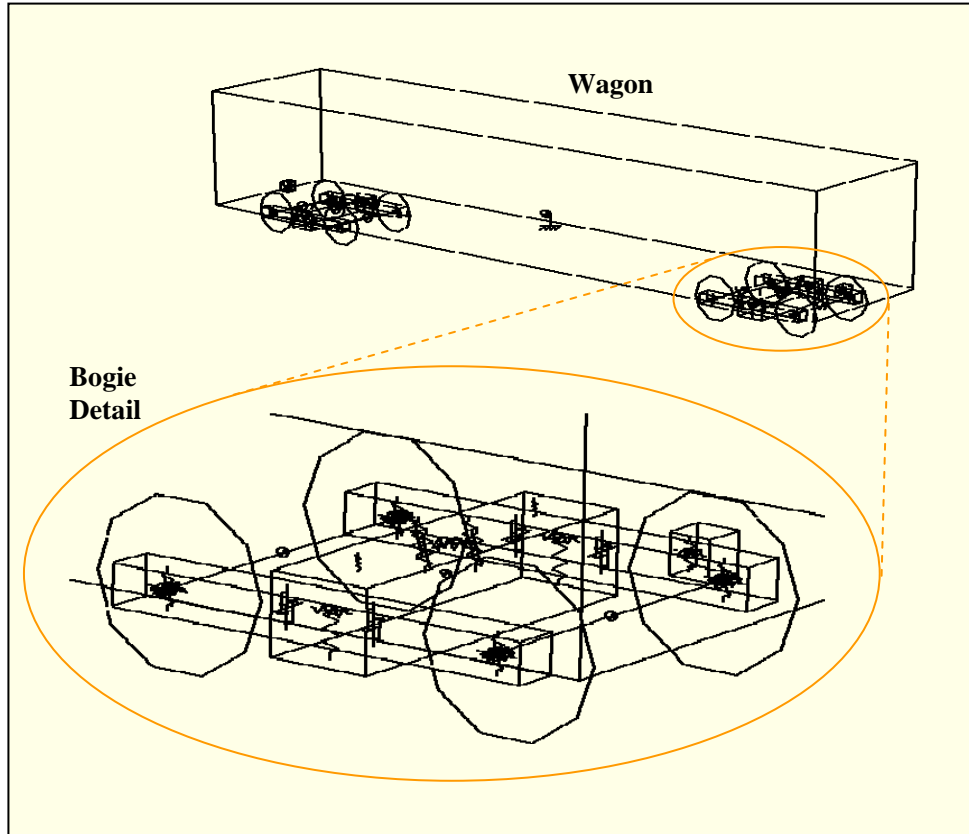


Figure 2-6 Simulation Model of a Hopper Wagon

2.2 DYNAMIC PERFORMANCE OF THE WAGON-TRACK SYSTEM

The safe and cost effective operation of freight railways is limited by the dynamic performance of wagons running on track. [3] identifies that the performance of rail vehicles running on tangent track is limited by two main problem areas. These are: the lateral instability inherent to the design of the steering of a railway wagon; and the response of the railway wagon to individual or combined track irregularities. These problem areas will be addressed, in that order, in the following sections. Particular attention will be given to how these can be detected from the accelerations of the wagon body.

2.2.1 Lateral Instability of the Railway Wagon

Railway wagons exhibit a self-excited lateral instability when running on tangent track. This instability is commonly known as *hunting*. Although it can be initiated by irregularities in the track, it is mainly attributable to the characteristics of the wagon. The mechanism that drives the instability is the same mechanism that steers the bogie smoothly through curves.

2.2.1.1 Steering Mechanism

The railway wagon is designed to negotiate gradual curves without contacting the wheel flanges. This negotiation is achieved by an intriguing steering mechanism produced by conical wheels on a fixed axle. Figure 2-7 illustrates the steering mechanism.

When a conical wheelset is given a lateral offset from the centreline of the track, the effective diameter at the wheel rail contact point is larger for the outermost wheel and smaller for the innermost wheel. However, the rotational speed of the two wheels is maintained equal by the fixed axle. Thus an unequal forward motion occurs which

rotates the wheelset towards the centre of the track, resulting in a lateral displacement opposing the initial offset.

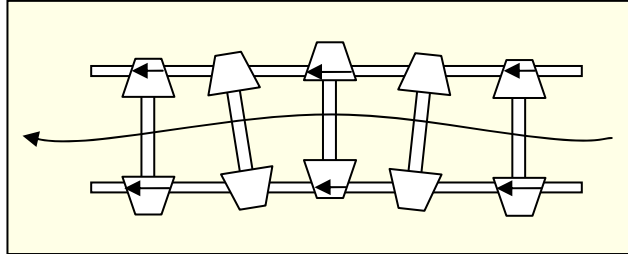


Figure 2-7 Wheelset Steering Mechanism

The steering mechanism acts to keep the wheelset in a central position on the track, guiding the wheelset effortlessly around curves with minimal wear. However, without some form of resistance, the wheelset will oscillate indefinitely. This oscillatory movement was first described mathematically by Klingel in 1883, and a derivation is given in [1].

2.2.1.2 Lateral Instability

The natural oscillation of the wheelset due to the steering mechanism is normally constrained by the rotational friction of the bogie and the inertia of the vehicle. However at critical running speeds the steering mechanism will resonate with the lateral properties of the vehicle to produce an underdamped oscillation commonly referred to as hunting.

Lateral instability, or hunting, is a key dynamic limitation of a rail vehicle, and the main speed-limiting factor on tangent track. Negative impacts of hunting include: increased wear of track, rail, wheel and bogie components; poor freight handling; and increased risk of derailment. Key factors that can influence lateral instability include: running

speed; loading state; bogie rotational resistance; wheel-rail contact profile; and friction of the wheel rail interface.

Gross mass has a large effect on hunting such that loaded vehicles are less likely to hunt than empty vehicles. This was verified in the analysis of field data, Section 5.5.1, which showed large increase in lateral oscillation when the wagon was empty compared to when it was full.

Hunting is the primary speed limiting factor for wagons running on tangent track. The speed at which hunting will occur for a particular wagon is difficult to determine. Simulation studies reported in [4] have shown that the existence of a single critical speed is questionable, even for a deterministic wagon model. Other studies, in [5], show that lateral oscillation is bifurcated, occurring at different speeds depending on the initial conditions. [3] reports that there are two major modes of lateral oscillation. One occurs at lower speeds and involves the resonant modes of the wagon body. The other occurs at higher speeds and appears as violent oscillation of the bogie components. Generally, the lowest speed at which severe hunting occurs must be taken as the speed limiting factor.

Increasing the rotational resistance of the bogie is an obvious control measure. However, this reduces the curving performance of the vehicle. Rotational stiffness and friction cause inadequate turning of the bogie when entering a curve, and a residual rotation of the bogie when exiting the curve. The bogie tends to warp to negotiate the curve, and the poor geometry through the curve dramatically increases wheel-rail wear and wheel squeal. Consequently, a significant trade-off exists between lateral stability of the wagon on tangent track, and the steering performance of the wagon when

negotiating curves. (This problem is not unique to railway vehicles. Riders of surf boards, skate boards, motorbikes, or the like will attest to the instability of a highly manoeuvrable vehicle on a straight at high speed.) In practice, rotational friction of the bogie will vary depending on the wear condition and lubrication of the centre bowl and side bearers.

Wheel-rail contact profile and friction are factors that can influence bogie hunting. As the wheels and rails wear, the contact profile changes so that the effective conicity becomes irregular across the profile. The friction of the contact point can also change with weather conditions and application of lubricants.

The occurrence of lateral bogie oscillation is difficult to predict, and depends of several variable factors. The complete elimination of hunting is highly improbable due to the need to maintain curving performance. However, hunting must be managed in order to maximise safety and minimise maintenance of rollingstock and track infrastructure.

Hunting is currently managed by ride testing new and modified rollingstock types before they enter service. Once a vehicle type has been accepted, there is no means of monitoring the hunting performance of individual wagons. An intended capability of Health Card is to detect hunting of freight wagons during normal operation.

2.2.1.3 Detection of Bogie Hunting from the Wagon Body

For Health Card to reliably detect lateral instability of the bogie, it must be able to detect the phenomena from the wagon body. North American standards [6] for high speed passenger and freight vehicles specify lateral accelerometers mounted on the bogie for detecting bogie hunting. This is not possible for the Health Card system on

freight wagons where sensing is restricted to the wagon body. However, measurement of the bogie is not required under the Australian [8][9][16] vehicle performance standards, which require measurement at the floor of the vehicle directly above the bogie centres.

[8] and [9] define unacceptable hunting as “*Sustained lateral sinusoidal acceleration of frequency greater than 0.5 Hz, producing average peak accelerations at the bogie centre in excess of +/- 0.35g over a period of at least 10 seconds.*” Both standards stipulate that accelerometers be placed on the body at floor level as close as possible to the bogie centre.

Simulation studies have shown that lateral oscillations of the front and back bogies reflect strongly in the wagon body motion. Field data collected from an in-service instrumented freight wagon [10] has shown that the wagon body responded with either a lateral motion when front and back bogies oscillate in phase, or a yaw motion when front and back bogies oscillate out of phase, as illustrated in Figure 2-11.

From the available standards and literature, it is reasonable to expect that unacceptable hunting can be reliably detected from the wagon body. For rollingstock maintenance planning, it is desirable to detect levels of lateral oscillation below the acceptable limits. This is further investigated in the analysis of field data in Section 5.5.1

2.2.2 Vehicle Interaction with Track Irregularities

The purpose of Health Card is to monitor the performance of the vehicle-track system. As stated in the introduction to Section 2.2, there are two problem areas that affect the dynamic performance of railway wagons running on track. The first is lateral instability

due to the wheelset steering mechanism. The second problem area is interaction with track irregularities.

2.2.2.1 Track Irregularities

Railway track is designed to interface with railway vehicles and provide a permanent way of travel. Deviation from the initial design geometry, otherwise known as irregularity, increases as the track condition degrades with use. Irregularity can be specified in terms of horizontal alignment, vertical alignment, cross-level and gauge (or equivalent terms) as shown in Figure 2-8. These quantities are recorded periodically by track measurement vehicles to ensure that the track is maintained to an agreed standard. Irregularity tolerances and recommended maintenance responses are specified in [7] and in Volume 4, Part 3, of [11].

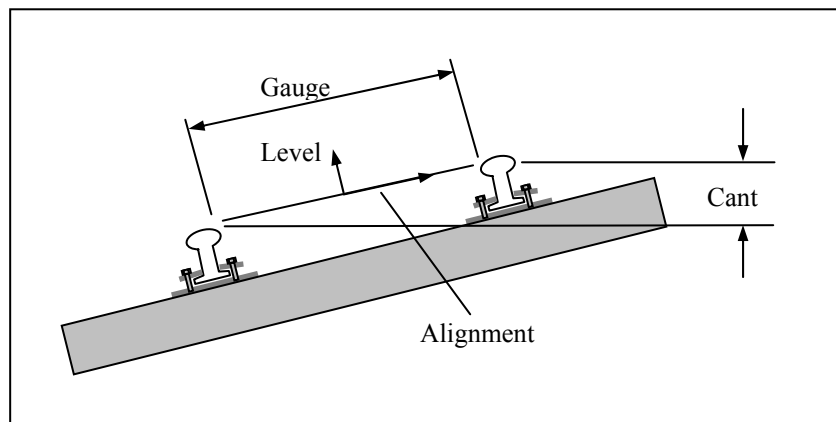


Figure 2-8 Track Irregularity Parameters

Examples of track irregularities and typical occurrences are described in Figure 2-9 and Table 2-3 adapted from [3].

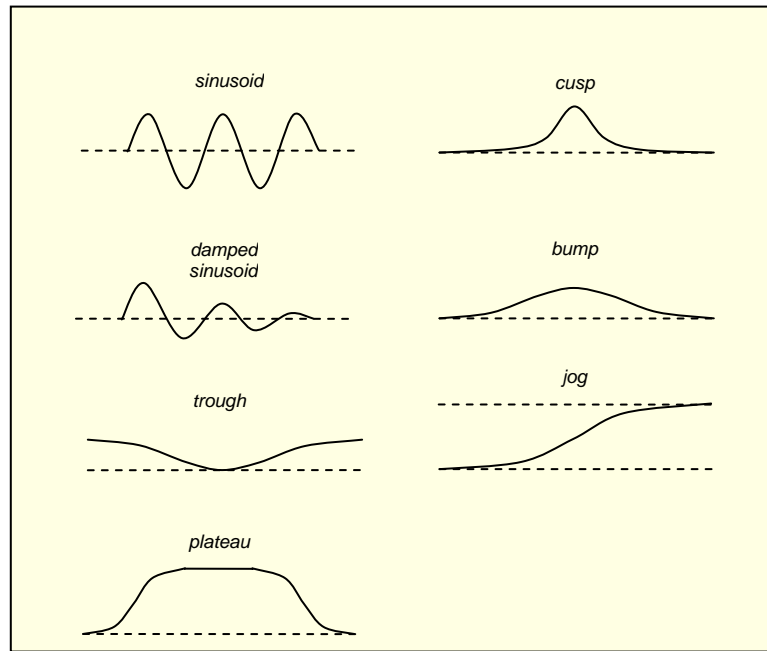


Figure 2-9 Examples of temporal track irregularities

Table 2-3 Typical Occurrences of Temporal Irregularities

<i>Irregularity</i>	<i>Typical Occurrence</i>
Cusp	Rail joints, turnouts, sun kinks, piers at bridges
Bump	Soft spots, washouts, mud spots, fouled ballast, joints, spirals, level crossings, bridges, overpasses, turnouts
Jog	Spirals, bridges, crossings, fill-cut transitions
Plateau	Bridges, grade crossings, areas of spot maintenance
Trough	Soft spots, soft and unstable subgrade, spirals
Damped sinusoid	Spirals, turnouts, localised soft spots
Sinusoid	Soft spots, bridges, periodic rail lengths

Track degradation and maintenance is an ongoing process that can be monitored against accumulated number of tonnes of traffic (gross tonnage). The cycle of track degradation and maintenance is illustrated in Figure 2-10 adapted from [1]. Newly laid track degrades very quickly during subgrade and ballast settlement. Once the initial

settlement occurs, the rate of degradation becomes linear. As the irregularity magnitudes increase further, the degradation once again starts to accelerate towards critical limits. Track maintenance is normally scheduled during the linear region as close as possible to the accelerated region. However, the degradation slope is increased compared to new track and ballast. [1] demonstrates this process with irregularity data trends measured at intervals before and after track maintenance and renewal.

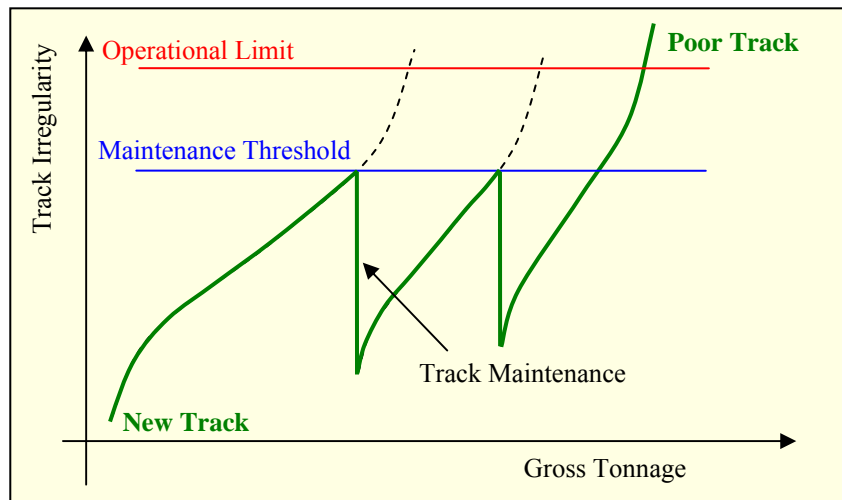


Figure 2-10 Track Degradation and Maintenance Cycle

Irregularities in the track accelerate due to their interaction with the rolling stock. The irregularities induce dynamic responses in the rolling stock. These dynamic responses will in turn produce track forces which further degrade the track. This can account for the accelerated degradation between the maintenance limit and the operational limit in Figure 2-10. In a study into vehicle track interaction [12], examples were shown where short defects can induce resonant modes involving body oscillation, leading to cyclic deformation in the track for some distance after the point irregularity.

2.2.2.2 Resonant Modes of Wagon Response

The response of an individual vehicle to track irregularities is not always proportional to the magnitude of the irregularities. A vehicle ride monitoring study [13] identified that the measured response of the vehicle to the track is often specific to the suspension characteristics of the vehicle carrying the ride monitoring equipment. Other wagon instrumentation studies [10][14][15] have shown that large dynamic events occur when the wavelength of a track variation combined with the train speed matches a resonant mode and frequency in the wagon.

Figure 2-11 shows the oscillatory modes of a wagon body and the track irregularity formations that excite those modes. In the figure: L is the distance between the centre of the front bogie and the centre of the rear bogie; n is a positive integer; and *phase* is the relative alignment of the sinusoidal irregularity on each rail.

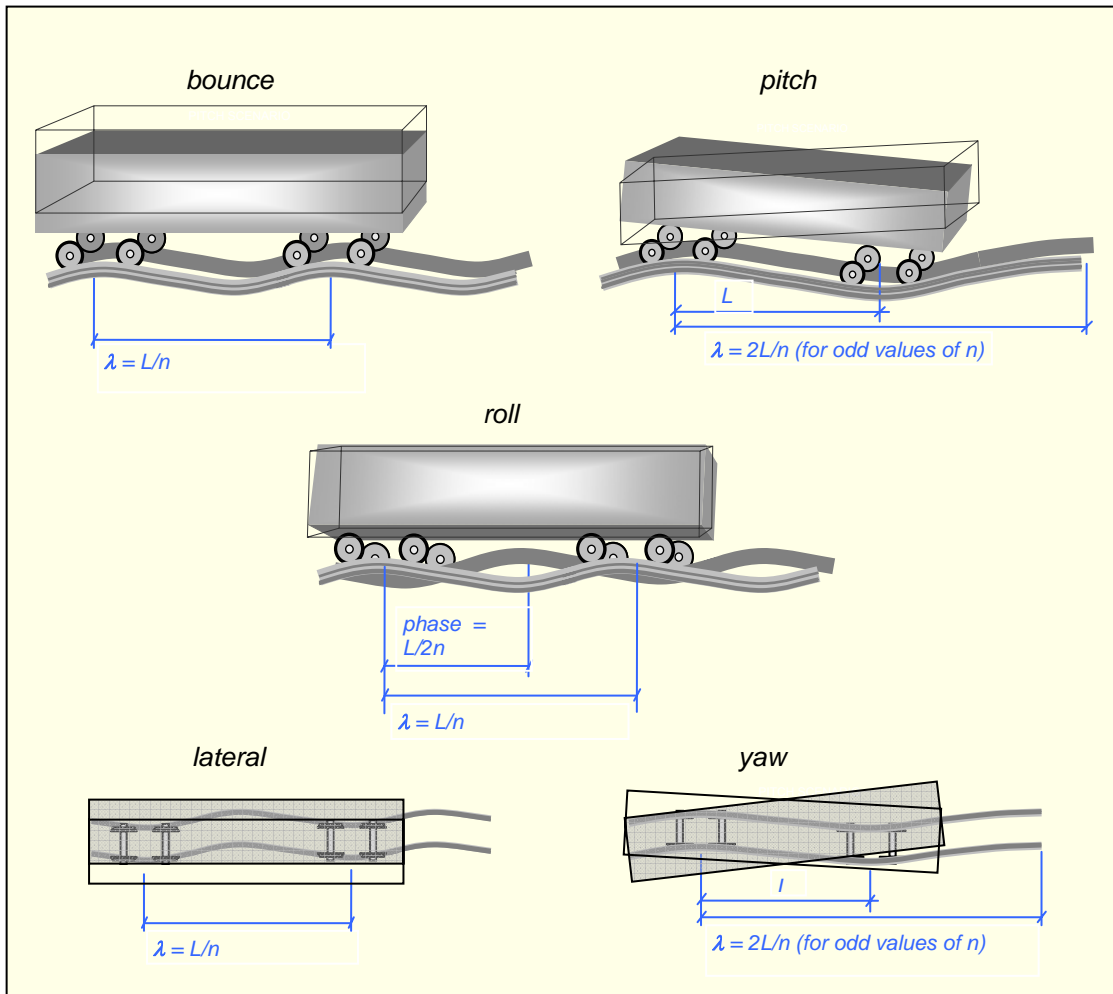


Figure 2-11 Excitation of oscillatory modes in the wagon body

Large dynamic responses are not limited to sustained sinusoidal irregularities. [3] identifies that large responses can also occur from spatial combinations of temporal irregularities, such as those described in Figure 2-9.

The resonant modes of oscillation in a wagon and the frequencies at which they occur can be identified with modal analysis of a linear dynamic model. The vehicle simulation package Vampire™ has a modal analysis function which was used on the hopper wagon model of Figure 2-6 with the parameters listed in Appendix A. (The model contains non-linear damping elements for dry friction. These elements are removed and replaced with linear damping for the modal analysis). The resulting

resonant frequencies for the body modes are shown in Table 2-4 for the loaded and empty case.

Table 2-4 Oscillation mode frequencies (Hz)

<i>Mode</i>	<i>loaded (Hz)</i>	<i>unloaded (Hz)</i>
Body Roll	1.237	5.426
Body Bounce	2.415	35.411
Body Pitch	4.104	30.344
Body Yaw (bogie lateral anti-phase)	1.237	0.986
Body Lateral (bogie lateral in-phase)	1.356	0.986

An example of the effect of resonance is shown in Figure 2-13. Vampire™ transient analysis was used to simulate the response of a wagon to track irregularities. A series of simulations were done with the same model as the modal analysis (with non-linear friction elements). Vertical track irregularities were designed such that the wavelength λ was equal to the distance between the bogies L . The irregularities were sinusoidal with smoothly increasing magnitude envelope to minimise transient effects. An example irregularity is shown in Figure 2-12.

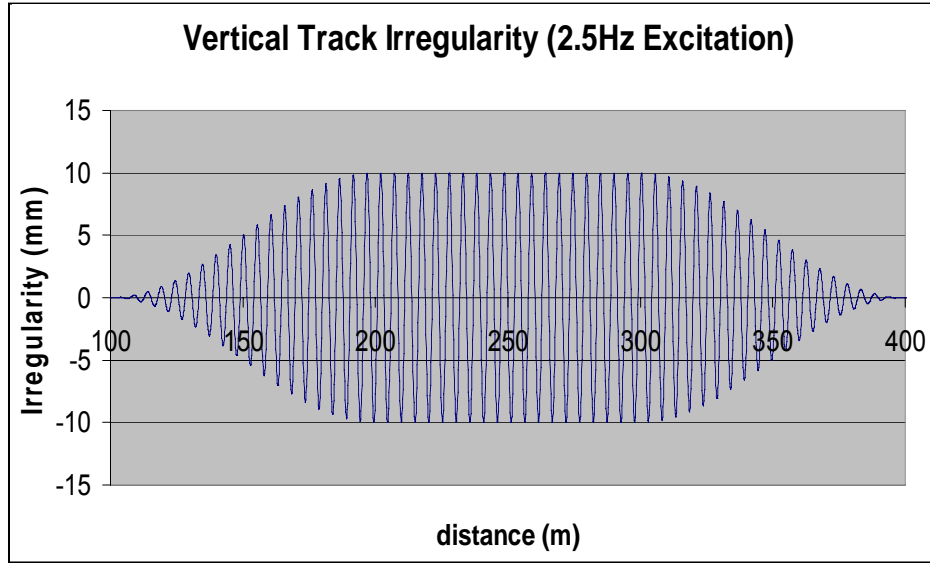


Figure 2-12 Example Vertical Track Irregularity

The running speed and wavelength was varied to produce frequency excitation in steps of 0.5Hz. The excitation frequency (f) generated is given by

$$v = f\lambda$$

eq. 2-1

For higher frequencies, the wavelength was divided by an integer n to keep running speeds below 80km/h. The RMS vertical accelerations of the body centre was plotted against each excitation frequency to produce Figure 2-13.

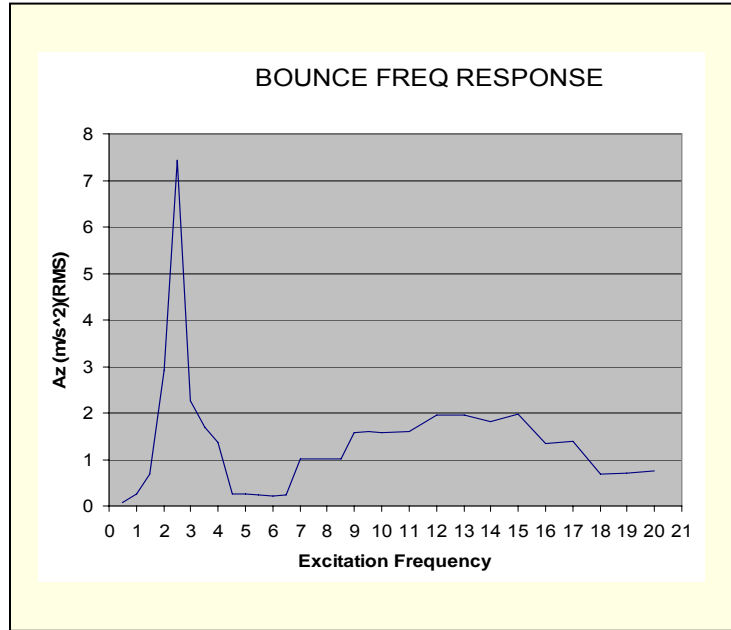


Figure 2-13 RMS vertical body acceleration vs vertical excitation frequency in the vertical mode

The plot shows a resonant peak at 2.5Hz, which corresponds to the modal analysis result of 2.415Hz in Table 2-4. The 2.5Hz peak was excited with $\lambda = 5.18\text{m}$ and speed = 46.62km/h.

Similar conditions exist that will excite resonance in other modes. Figure 2-14 is a plot of the resonant conditions for roll, pitch and vertical bounce with bogie spacing of 10.36m and an alternative length of 12m for comparison. This figure highlights the fact that wagons with different dimensions and suspension characteristics will resonate with different track irregularity formations and at different speeds.

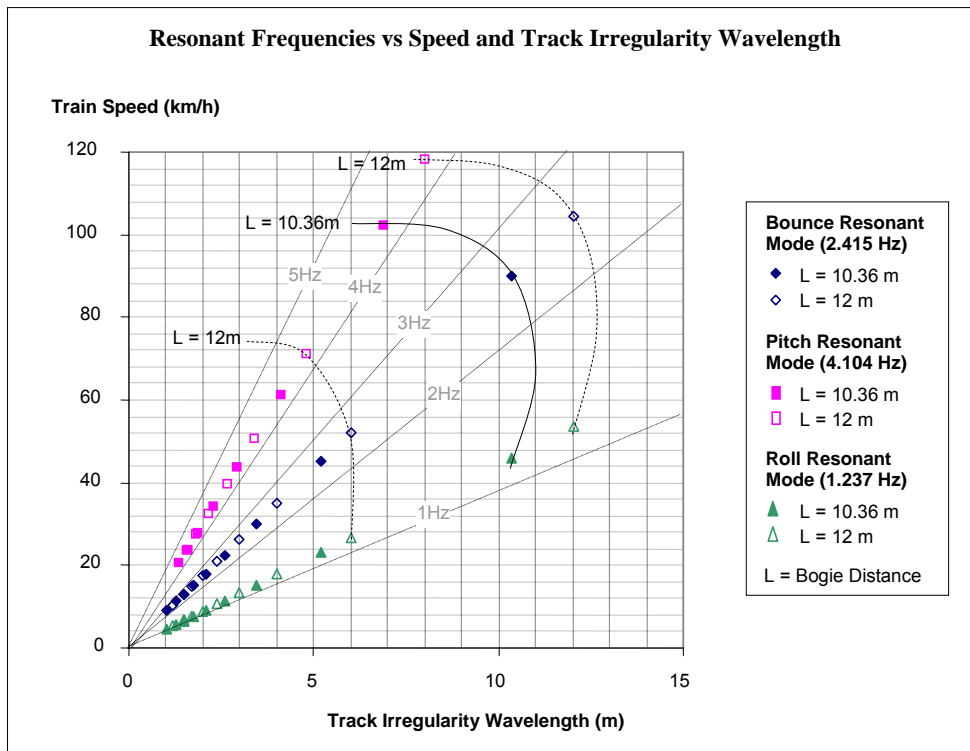


Figure 2-14 Resonant conditions of speed and irregularity wavelength for bounce, pitch and roll modes

It is clear that the response of wagons to track irregularities is highly dependent on the physical arrangement and suspension characteristics of the wagon and how they interact with track irregularities on a case by case basis.

2.3 MANAGING THE PERFORMANCE OF THE WAGON TRACK SYSTEM

The previous section establishes that the system of a wagon running on track is limited by the lateral stability of the individual wagon, and the combined interaction between the individual wagon and specific formations of track irregularity. These limitations must be managed to improve the performance of the rail system.

2.3.1 Performance Testing of Rollingstock

Australian vehicle acceptance standards [16][7][9] stipulate that all new or modified types of rollingstock are tested dynamically. Test regimes include passing the vehicle

over standard irregularities built into the test track, and monitoring the vehicle ride of track sections with a nominated irregularity level classification. Tests are performed with lateral and vertical accelerometers mounted on the vehicle body as close as possible to the bogie centre. Wheel profiles and loading states are designed to ensure that the test is performed under the most adverse conditions likely to be experienced in service.

Rail Infrastructure Corporation (NSW) [9] stipulates that previously accepted vehicles may require ride performance testing in the following instances:

1. Proposed modification to the suspension characteristics
2. Proposed change in bogie rotational resistance
3. Proposed change in wheel profile
4. Proposed change in bogie type
5. Proposed change in vehicle operating conditions
6. Any proposed vehicle modification which may affect the vehicle ride performance
7. Significant change in the vehicle tare mass
8. Where, in the Rail Infrastructure Corporation's opinion, there is suspected poor ride performance.

The first seven points emphasise the factors that have considerable impact on vehicle performance. Most of these factors can vary throughout the service life of the vehicle

and remain undetected for a period of time. Suspension characteristics can change due to degraded springs and worn or lubricated friction dampers. Bogie rotational resistance can change with the lubrication and wear condition of the centre bowl and side bearers. Wheel profiles change considerably as the wheel wears. Vehicle operating conditions can change with fleet demand. The eighth point aptly expresses the benefit of monitoring ride of every vehicle in service to verify dynamic performance.

2.3.2 Benefits of Monitoring Ride on Every Wagon

Monitoring the wagon fleet for instances of lateral instability has promising implications. The speed limiting nature of hunting, and the trade-off between lateral stability and curving performance creates an opportunity for optimisation which could have cost and safety benefits for both rollingstock and railway administrators. The fact that lateral instability is affected by the wear condition of the bogie suggests that its detection would be a useful indicator for maintenance planning. Operational safety would also increase with real time indication of hunting wagons, allowing the driver to adjust train speed accordingly.

Monitoring the fleet for instances of severe dynamic interaction would also benefit rollingstock and track maintainers. If a large proportion of the fleet responds poorly to a track location, that location could be given higher maintenance priority. [17] reports a similar concept where several cars in a passenger train were monitored simultaneously. Conversely, if a particular wagon responds poorly compared to the other wagons, it can be given a higher maintenance priority.

2.3.3 Existing Ride Monitoring Systems and Standards

Track maintainers have used vehicle ride measurement to monitor track condition since the 1920's. The first use of a ride measurement system found in literature was in 1926 when a Hallade machine was installed on a New South Wales track inspection car. The Hallade recorder was a mechanical system of pendulums linked to pens on a chart recorder. The pendulums were sensitive to roll, lateral, vertical and longitudinal accelerations, and the resulting traces were inspected to identify track sections that needed maintenance. An example of a Hallade machine and some sample charts used here by permission from [2] is shown in Figure 2-15. Although Hallade recorders have been replaced with electronic equivalents, the machines were still in use in British rail in 1979.

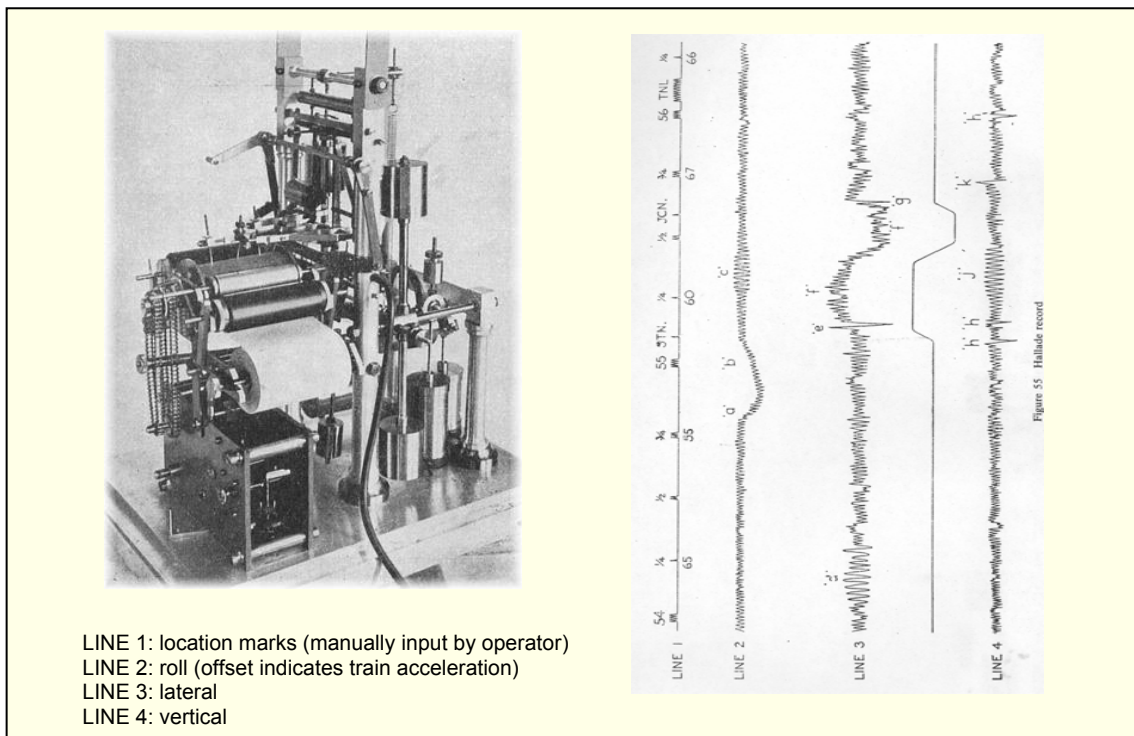


Figure 2-15 Hallade machine and recorded traces (source [2])

Modern systems measure accelerations with accelerometers and log the data digitally [18] [19]. The installation for [18] comprises of a sealed box containing a computer, satellite navigator, cellular telephone and modem. A single twin axis accelerometer is mounted on the wagon in a separate box. The computer records root mean square (RMS) lateral and vertical accelerations. The RMS values are calculated over 200m sections of track and reported to a land based desktop machine which displays a geographical view of the track network. Ride roughness is displayed in colour code. Figure 2-16 shows an example of the desktop display.

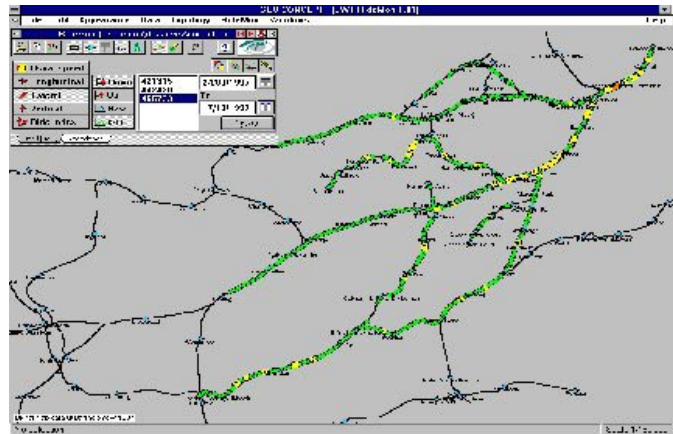


Figure 2-16 RideMon Example Desktop Display (Source [18])

[13] presents a similar ride monitoring system operating in North America. This system monitors acceleration levels stipulated in Federal Railroad Association (FRA) safety standards [6][21] for vehicle-track interaction. The system also applies more stringent maintenance thresholds for prioritising track maintenance.

The existing ride measurement systems are intended for installation on selected rollingstock to represent the different types of vehicles using the track. These are not intended to monitor the condition of the rollingstock fleet, but rather to monitor the condition of the track.

Typically these systems use embedded PC technology, and the power ratings for the units are in the order of tens of watts, prohibiting their use in permanent self powered installations. Furthermore, the existing systems limit online processing to level detection. If closer analysis of the signal is to be done at all, it is done by logging the waveforms that caused the trigger and downloading them to a land-based database for offline human analysis.

2.4 CONCLUSIONS

This chapter developed an understanding of the structure and dynamics of rail vehicles on track. Some key phenomena that are desirable to detect were identified, and existing rail industry practices and standards for vehicle ride testing and monitoring were reviewed. The following key considerations were identified:

- The dynamic performance of the system of a wagon running on track affects safe running speeds of rollingstock and wear rates of track infrastructure and rollingstock components.
- The dynamic performance on tangent track is limited by the lateral instability of the wagon due to the steering mechanism; hence a trade-off exists between tangent running performance and curving performance.
- The dynamic performance is also limited by and the interaction of the wagon with irregularities in the track, which depends upon the design parameters, wear condition, and loading state of the wagon.
- Ride monitoring systems are available for the purpose of prioritising track maintenance based upon the ride performance of sample rollingstock. However,

the existing systems are not viable for installation on every wagon to monitor the relative ride performance of the rollingstock.

The developmental Health Card system aims to monitor every vehicle in the fleet using low cost, intelligent devices. The benefits of this system would be to:

- Prioritise track maintenance based upon actual responses of the working rollingstock fleet.
- Prioritise rollingstock maintenance based upon relative behaviour of wagons on the same track sections.
- Provide safety benefits by alerting drivers in real time of excessive lateral and vertical dynamics of train elements.
- Provide a research and validation mechanism for studying the lateral and vertical dynamics of rollingstock, including the optimisation of the trade-off between curving performance and lateral instability on tangent track, and the validation of speed limits based upon actual dynamic performance.

The following chapter describes the developmental Health Card system and initial prototype in detail. Particular attention is given to the signal processing aspects and constraints that impact upon the signal analysis task.

3 Health Card System

Online monitoring of body accelerations on every wagon in the fleet is a concept that would not have been conceivable without recent developments in sensing and wireless communication technology. This chapter introduces the proposed Health Card system which aims to monitor every wagon in the fleet using low cost, intelligent devices. The first prototype Health Card was developed by a team of engineers at Central Queensland University during the course of this research. Online signal analysis algorithms were required for the device to operate. This chapter will focus upon the signal processing and analysis aspects of the prototype system.

3.1 THE PROPOSED SYSTEM

A system has been proposed to be installed on freight rollingstock to monitor the dynamic behaviour of a fleet of wagons throughout their service life. A small, low cost, self powered, wireless device, called a “Health Card”, was to be mounted on the body of each wagon. Each device would be capable of measuring accelerations, analysing them online, and producing report codes on either a periodic or event-driven basis.

When a number of wagons are marshalled together into a train, the devices would form a radio network and report information to a master system in the locomotive. Once the train is in motion, the cards would sense the ride motion of their host wagons and report behaviour to the master system. The master system in the locomotive would receive both stored information and real time indications from the Health Cards in the network. The holistic information gathered from the Health Cards would allow the system to monitor the running condition of the wagons and the track as they interact together.

The system would provide real time indications to the driver and/or supervisory system. The onboard system would communicate periodically with a centralised system. The centralised system would maintain a database to accumulate a history of dynamic behaviour. The database would be used to assess trends and possibly to determine safe speed limits on a trip by trip basis.

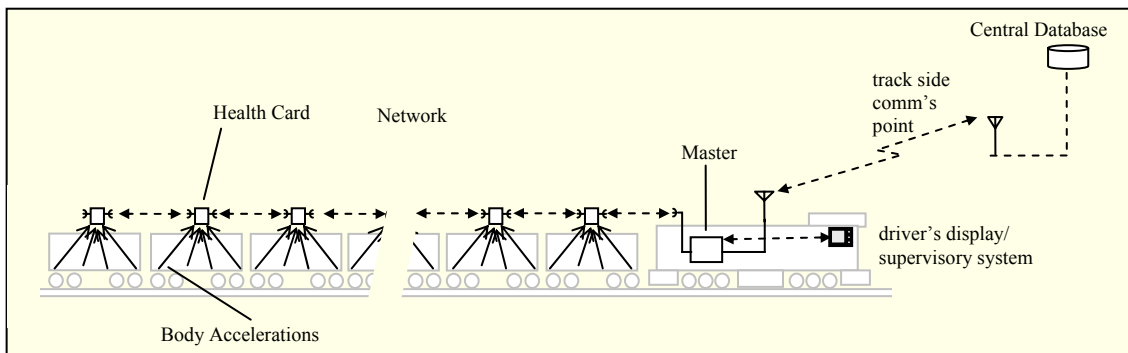


Figure 3-1 Proposed System Arrangement

The system was expected to produce benefits to both railway and rollingstock maintainers and operators. It would also provide a platform for ongoing research and optimisation of the rail system. Information from the system could be used to:

- prioritise wagon maintenance based upon relative dynamic performance of wagons
- prioritise track maintenance based upon the dynamic response of traffic
- determine speed limits based upon recent history of dynamic behaviour

The Health Card is the key device that would enable the system to operate. The proposed Health Card is a small, unobtrusive device that is self powered and communicates wirelessly. The device incorporates motion sensors and algorithms for

online signal analysis. Due to the limited throughput of the network, all signal analysis was to be done onboard the device.

3.2 PROTOTYPE HEALTH CARD

A set of four prototype Health Cards was developed by an engineering team at Central Queensland University during the first nine months of this research. Each prototype Health Card incorporated a 27MHz microcontroller with 256kB of onboard RAM, four dual axis accelerometers, a GPS receiver, two low power radios, lithium ion batteries with management circuits, and a solar panel. The purpose of the prototype was firstly to prove the capability of the equipment, and secondly to enable ongoing research into the capabilities of the proposed Health Card system. Figure 3-2 shows one of the four systems installed on a ballast wagon.



Figure 3-2 Health Card prototype installed on a ballast wagon

Figure 3-3 presents the arrangement of the prototype Health Card with photographs of the installed system. The processor, batteries and power management electronics were located in an enclosure mounted on the deck of the wagon, along with a solar panel.

Accelerometers resided at three corners, two of which had radios to communicate between wagons.

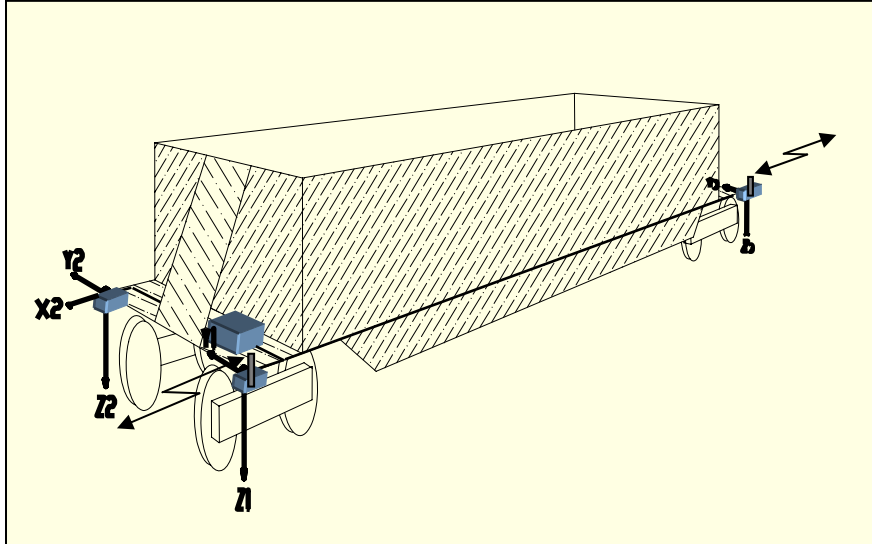


Figure 3-3 Health Card Prototype System Arrangement

3.2.1 Network Throughput Constraints

The network topology prohibited Health Cards from transmitting raw data for further analysis. The network of Health Cards was arranged in a message passing chain topology. The actual throughput of the network had not been determined in quantified terms. However, the potential for network congestion was very high, considering that freight trains can run with over one hundred wagons. Consequently, the algorithm onboard the Health Card was required to analyse and interpret the acceleration signals, reporting event codes only to the network. The network protocol for the prototype system allowed one value per degree of freedom to be transmitted from each Health Card approximately every half second. This constraint was conservative compared to the expected throughput restriction in the fully developed system when installed on a train of up to one hundred wagons in a message passing topology.

3.2.2 Processing Capability

The hardware design for the Health Card device employed a single microcontroller [20] which was required to perform the following tasks:

- continuously sample 8 channels of PWM signals at 200 samples/sec per channel
- manage sampled data in 256kB of onboard memory
- analyse the signals online
- interface with the radio modules and perform communications routines to implement the device network.

Furthermore, the device was to be powered by solar energy, therefore the power budget for the entire prototype Health Card was 0.5W, with a target of 50mW for the final version. CPU clock speed is the primary limiting factor for data processing on a microcontroller, and is directly proportional to power consumption. The clock speed for the prototype was limited to 27 MHz.

3.2.3 Sensor Location and Type

Sensing was restricted to accelerometers on the wagon body. The design of the final device was to be feasible for installation on every wagon without hindering normal operation and maintenance of the rollingstock. Therefore, sensing was restricted to the wagon body, with no sensing of suspension components. Acceleration sensors were the only viable alternative at the time of the first prototype. However, low cost rotational velocity sensors were becoming feasible toward the end of this research program. The first prototype Health Card used the Analog Devices *ADXL202/ADXL210 Low Cost $\pm 2g/\pm 10g$ Dual Axis MEMS® Accelerometers with*

Digital Output [22]. The accelerometer device used silicon structures on a silicon chip to measure instantaneous acceleration in an inertial frame of reference. The sensing capabilities included static and dynamic accelerations in two perpendicular axes. Four dual axis accelerometers were incorporated in the prototype design. These could be located in various position on the wagon body.

3.2.4 Sensing Arrangement

The sensing arrangement for the Health Card Prototype was specified as part of this research. The aim of the sensing arrangement was to capture roll, pitch, yaw, vertical and lateral accelerations of the wagon body. This was to be achieved with four dual axis accelerometers with one axis in the longitudinal direction. The hardware was also to be minimised, therefore a unit on each corner was not desirable. A compromise was reached to sense three corners and assume a rigid wagon body for the frequencies of interest.

Figure 3-4 shows the locations and sensor orientations. Two axes were measured at two corners and three axes at one corner. The system dealt primarily with relative motion in the lateral plane; however one longitudinal axis was included. Figure 3-5 shows how the measured axes are related to the motion of the wagon body. This sensing arrangement was also designed to integrate with the radio communications configuration which included radio transmitters at each end of the wagon.

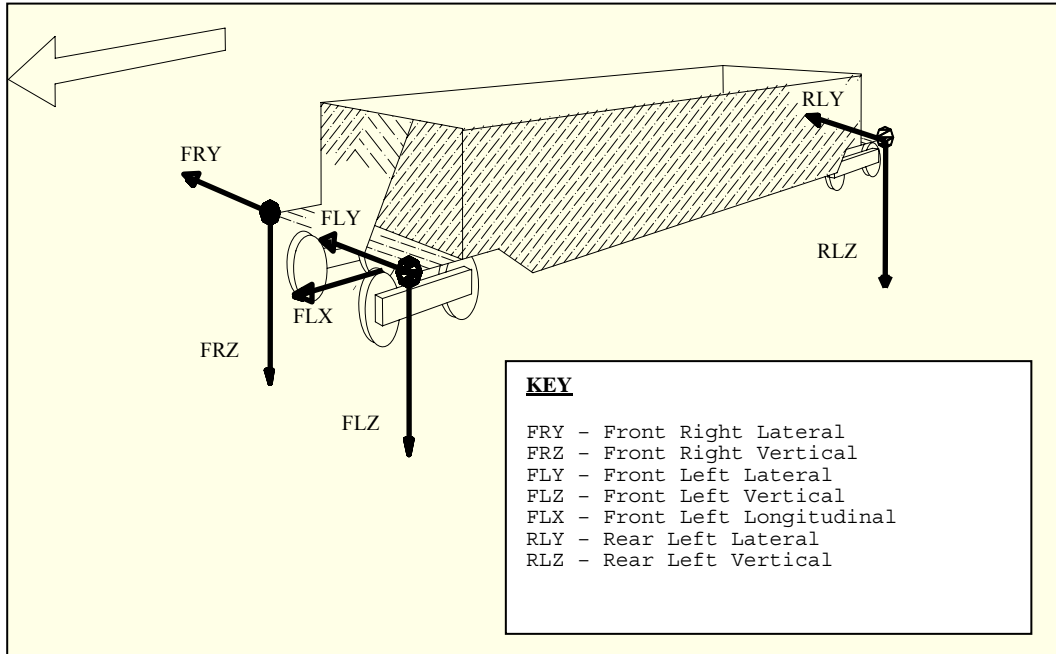


Figure 3-4 Accelerometer Locations and Axis Naming Convention

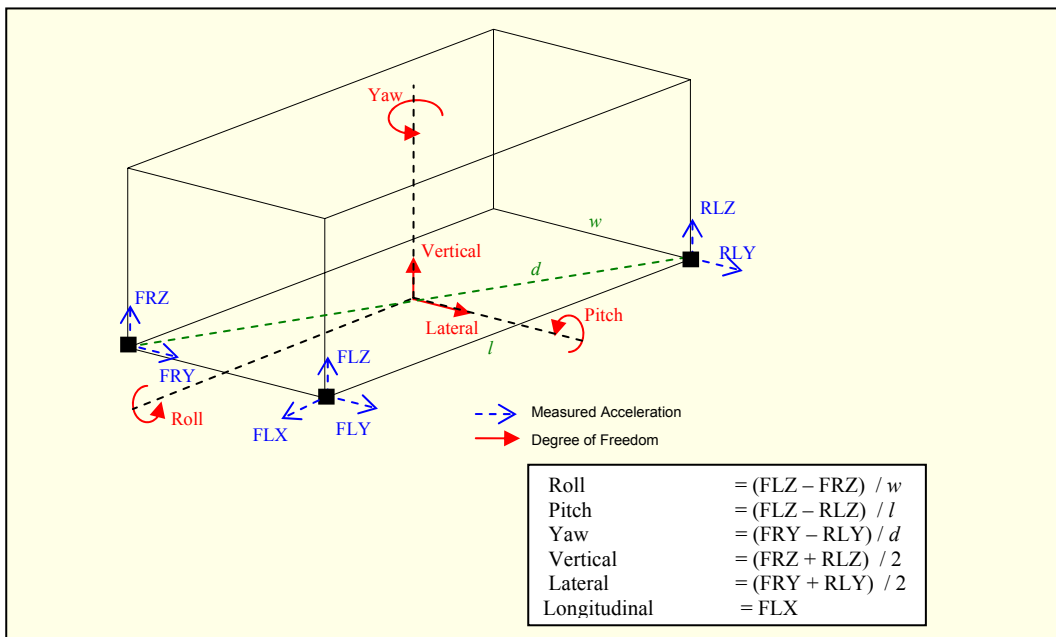


Figure 3-5 Relating corner accelerations to 5 degrees of freedom

3.2.5 Signal Pre-Processing

The signal pre-processing adopted for the first prototype Health Card is shown in Figure 3-6 for one of the eight channels. The ADXL210 accelerometers provided a choice of analog output or pulse width modulated (PWM) output. The PWM option was adopted

for the first generation prototype to eliminate the need for analog to digital conversion onboard the microcontroller.

The sensing element, anti-aliasing filter, and PWM generator resided within the accelerometer package. The anti-aliasing filter was a low pass first order RC network, with adjustable corner frequency selected by an external capacitor. The PWM generator converted the filtered analog signal to a 1 kHz PWM signal.

The PWM pulse signal was demodulated by the microcontroller using a “capture and compare” port to measure the pulse durations. An interrupt routine sampled values from the capture compare port at 200Hz per channel. The reduced sampling rate was required to minimise the processing overhead generated by the sampling interrupt routine, and to allow enough time for the routine to measure the eight incoming channels.

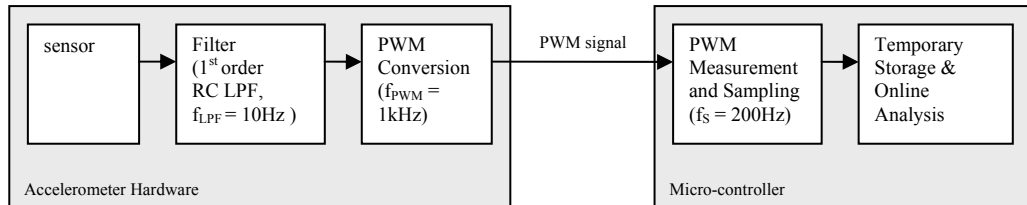


Figure 3-6 Prototype Health Card Signal Pre-Processing (one of eight axes)

3.2.6 Signal Filtering

The Nyquist sampling theorem [23], states that the minimum sampling rate must be twice the bandwidth of the signal.

$$f_s \geq 2 \times BW$$

eq. 3-1

If the Nyquist rate is not satisfied, signal aliasing will occur. Figure 3-7 illustrates signal aliasing. A sinusoidal waveform is sampled at a rate less than twice the signal frequency resulting in a false sampled waveform.

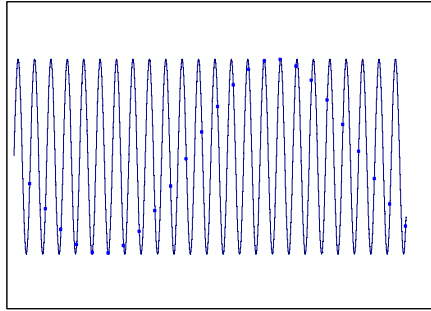


Figure 3-7 Example of Signal Aliasing

The single order low pass filter was included in the ADXL210 device to ensure that the eq. 3-1 was satisfied for the conversion to 1kHz PWM. However, in this application, the samples were to be further decimated to 200Hz at the microcontroller (c.f. Figure 3-6). Hence the Nyquist rate had to be satisfied for 200Hz sampling.

According to eq. 3-1, the signal could be filtered at 100Hz and sampled at 200Hz without aliasing. However, this assumes an ideal filter, which is represented in Figure 3-8. The ideal filter removes all content at frequencies higher than the cut-off frequency (f_c), and does not affect the signal at frequencies lower than f_c .

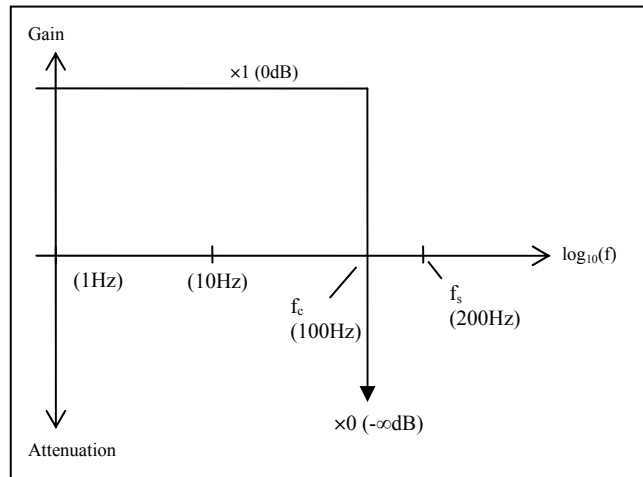


Figure 3-8 Ideal Low Pass Filter for 200Hz sampling

In practice, an ideal filter cannot be achieved. Real filters produce finite attenuation of signals above the cut-off frequency. The transition from minimum attenuation to maximum attenuation occurs across a finite frequency range. In this case, only a first order low pass filter was available in the hardware configuration and a signal range of 0 to 10Hz was to be analysed. A first order filter attenuates signal above the cut-off frequency at -20dB per decade. This meant that for a cut off frequency of 10Hz, the attenuation at 100Hz was -20dB or 1/10 signal reduction.

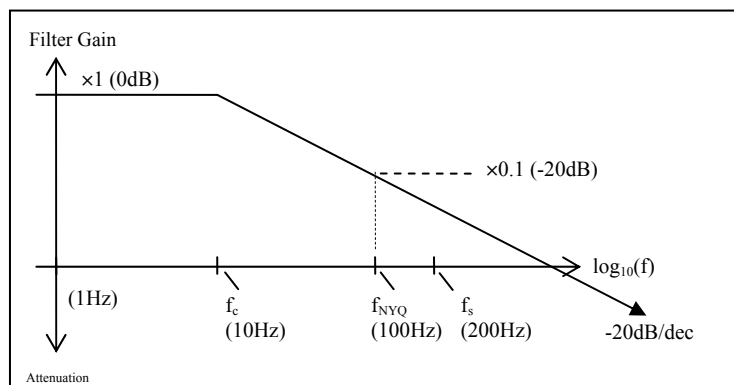


Figure 3-9 Low Pass Filtering for Prototype Health Card.

Acceleration signals are particularly dominated by high frequency content due to the derivative order of acceleration, as explained further in 4.1.2. A small vibration at 100Hz results in very large magnitude acceleration signal. Initial testing of the

prototype pre-processing arrangement was performed by comparing data with a benchmark accelerometer sampled at a much higher sampling rate. The results showed that the signal collected by the prototype was heavily aliased, i.e. the low frequency content was significantly altered compared to the benchmark signal. This identified that the single order filter in the prototype did not provide sufficient attenuation at frequencies higher than 100 Hz.

There were three options to add attenuation at 100Hz which were to:

1. Add of a higher order filter to the signal path. This was not possible because the signal was converted to PWM within the device, and the internal signal path could not be interrupted to place a filter in series.
2. Increasing the sampling rate. The sampling rate was limited by the clock speed of the microcontroller, which was limited by the 0.5W power budget of the device.
3. Introduce a mechanical filter to attenuate frequencies above the frequencies of interest. This was the only feasible option without rebuilding the electronics hardware.

A mechanical filter was achieved by mounting the enclosures on steel plates which were mounted to the wagon body on resilient mounting pads. The steel plates increased the mass m of the sensor and the resilient mounts introduced a spring-damper characteristic with spring constant K . The resulting second order system had a cut-off frequency f_c given by eq. 3-2 which further attenuated the high frequency content of the signal until signal aliasing was insignificant.

$$f_c = \frac{1}{2\pi} \sqrt{\frac{K}{m}}$$

eq. 3-2

K and m were chosen to produce a cut-off frequency of around 20Hz. This would produce an additional 40dB per decade attenuation above 20Hz.

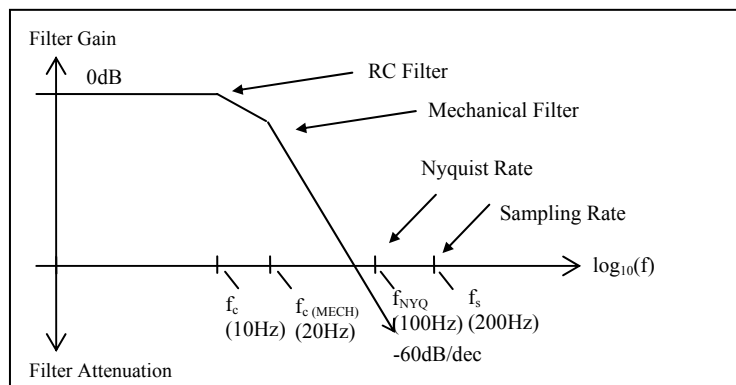


Figure 3-10 Low Pass Filtering for Prototype with Additional Mechanical Filter.

A mechanical filter is not an unusual method for eliminating high frequency content from acceleration signals. It is reported in [25] that a resilient mount was used to attach an accelerometer to an axle-box of a wagon to detect short wave rail defects.

The intention for the next generation prototype of Health Card was to adopt the analog output option on the ADXL210 accelerometer and replace the mechanical filter with a higher order electronic filter prior to A/D conversion.

3.2.7 Algorithm Requirements

Online analysis algorithm/s were required so that the Heath Card device could operate for testing and ongoing research. Chapter 6 describes the implementation of an initial algorithm that was developed for the project as part of this research. It was developed primarily to allow the prototype to run for multi wagon field testing. However, its

secondary purpose was to prove that time-frequency analysis of eight concurrent signals could be performed on a low power embedded processor. Chapter 4 introduces the theory of time-frequency analysis and Chapter 5 reports on the application of time-frequency analysis to field data. The discussions of Chapter 5 examine time-frequency analysis as a mechanism for detection of dynamic performance of the wagon-track system in the context of the Health Card system.

The final generation Health Card would require algorithms to perform detection and classification of dynamic events onboard the device without human intervention. This is discussed further in Section 6.4. Automatic signal classification is an area of research which is outside the scope of this thesis. However, some review of literature in this area was undertaken and a recommended direction for future research is detailed in Section 6.7.

3.3 CONCLUSION

This chapter has described the Health Card system concept and the initial prototype that was developed in parallel with this research and forms the context for this research. Several challenging system constraints are identified which include:

- **Sensor Type and Placement:** Sensing was limited to accelerometers that could only be placed on the wagon body.
- **Accelerometer Data Sampling Rate:** The prototype Health Card could not sample each channel faster than 200 s/sec. This resulted in a theoretical bandwidth of 100Hz, however with practical filtering issues the bandwidth was limited further to 10Hz.

- **Processing Speed and RAM:** The Health Card processor was limited to 27MHz clock speed. The memory available for data processing was limited to 256kB of RAM.
- **Network Throughput:** The prototype network would not allow more than six 16bit values (one per degree of freedom) to be transmitted from each Health Card approximately every half second.

These system constraints present a significant challenge for an embedded analysis algorithm. The algorithm would be required to analyse all of the acceleration signals to a level adequate for automatic detection of dynamic events. The next chapter examines the nature of acceleration signals and introduces time-frequency analysis as a necessary basis for online signal detection. The capabilities of time-frequency analysis are explored in Chapter 5 by application to field data taken from a hopper wagon in service. The feasibility of time frequency analysis under the constraints of the device is then proven with an implementation detailed in Chapter 6

4 Time Frequency Analysis of Acceleration Signals

Online analysis of acceleration signals onboard a low powered device is a significant challenge. Final Health Card algorithms would be required to process the acceleration signals and generate coded reports without any further analysis offline. Existing ride monitoring systems and associated standards apply RMS and peak to peak measures to create exceptions. This chapter firstly examines the RMS and peak to peak measures, and then highlights the importance of frequency based analysis in order to detect significant events. Fourier time-frequency analysis is explained and a more contemporary alternative, wavelet analysis is introduced for comparison.

4.1 ONLINE ANALYSIS OF ACCELERATION SIGNALS

The existing ride monitoring systems and associated standards identified in Chapter 2 use RMS and peak to peak measures to create exceptions. The waveforms that generated the exceptions are then stored or transmitted to land-based systems for further offline analysis. In the case of the Health Card system, network throughput prohibits transmission of waveforms. Therefore, algorithms onboard the Health Card are required to process the acceleration signals and generate coded reports without any further analysis offline.

4.1.1 Online Analysis in Existing Systems and Standards

Existing ride monitoring systems create exceptions based upon peak to peak (Pk-pk) magnitude and root mean square (RMS) magnitudes. The FRA levels [6] and maintenance indication levels applied in North American track monitoring systems [13], introduced in Section 2.3.3, are summarised in Table 4-1.

Table 4-1 Example Ride Acceleration Limits in [13] and [6]

	Level 2 (Maintenance limits)	Level 1 (FRA limits)	Filtering Requirements
Body Vertical	0.40-0.59g Pk-pk	> 0.60g Pk-pk	10 Hz filtered, 1 second widow
Body Lateral	0.25-0.49g Pk-pk	> 0.50g Pk-pk	10 Hz filtered, 1 second widow
Bogie Lateral	0.35-0.39g RMS	> 0.40g RMS	10 Hz filtered, 2 second widow

Comparable limits are included in Australian minimum requirements for rollingstock performance [16][7][9] summarised in Table 4-2. In the Australian railway standards, all acceleration signals are to be filtered to below 10Hz.

Table 4-2 Australian Ride Performance Standards

Assessment Quantity	Limit
Body vertical	0.80g (pk-pk)
	0.50g (av pk-pk)
Body lateral	0.50g (pk-pk)
	0.35g (av pk-pk)

The RMS value gives a positive valued measure of the magnitude of cyclic variation in the signal.

$$RMS\{x(n)\} = \sqrt{\frac{1}{N} \sum_{n=0}^{N-1} x^2(n)}$$

eq. 4-1

Peak to peak (Pk-pk) values give a positive valued measure of the magnitude of the extremities of the signal.

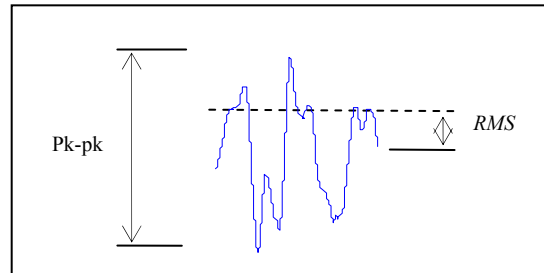


Figure 4-1 Root Mean Square (RMS) and Peak to Peak Values

RMS and Pk-pk measures do not take into account the frequencies of the oscillations in the signal. The following section examines the significance of the frequency content of signals.

4.1.2 Frequency Content of Acceleration Signals

The magnitude of acceleration signals is highly dependent on frequency of vibration. The magnitude of measured acceleration signals is typically dominated by high frequency “noise” due to structural vibrations. This is typically controlled by low pass filtering to remove the high frequency content before sampling and further analysis.

The reason for the dominating nature of high frequency noise is the fact that acceleration is the second derivative of displacement. Acceleration is the derivative of velocity $v(t)$ and the second derivative of displacement $s(t)$.

$$a(t) = \frac{dv(t)}{dt} = \frac{d^2s(t)}{dt^2}$$

eq. 4-2

Differentiation in the time domain is equivalent to multiplication by ω in the frequency domain where $\omega = 2\pi f$. (c.f.4.3 for an introduction to the Fourier transform) A proof of this property of the Fourier transform can be found in [26]

$$\frac{d}{dt}x(t) \xrightarrow{FT} (j2\pi f)X(f)$$

eq. 4-3

$$\frac{d^2}{dt^2}x(t) \xrightarrow{FT} (j2\pi f)^2 X(f)$$

eq. 4-4

Hence, the magnitude of an acceleration signal is proportional to the displacement multiplied by the frequency *squared*.

The effect is clearly demonstrated in Figure 4-2 which shows a simulated acceleration in the form of a constant magnitude frequency sweep (“chirp”) signal (1). The pk-pk amplitude of the acceleration signal is constant at 20m/s^2 (approx. 2g). However the frequency sweeps from 0 to 10Hz over a 10s period. The corresponding velocities and displacements are calculated by integration and plotted below that acceleration signal as (2) and (3) respectively. The result demonstrates that high frequency accelerations relate to very small velocities and negligible displacement, however low frequency acceleration signals *of equal pk-pk and RMS magnitude* relate to very large velocities and displacements. The significant displacements occur in the 0-5Hz range.

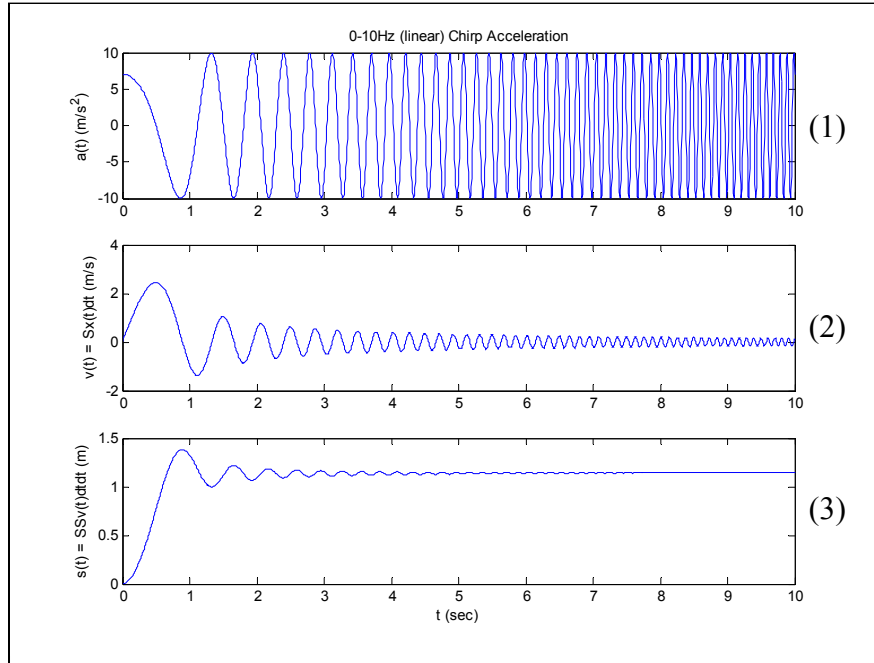


Figure 4-2 Acceleration Frequency Sweep from 0 to 10Hz (1) with Velocity (2) and Displacement (3)

The significance of lower frequency accelerations was also demonstrated by the field data acquired from a wagon as detailed in Section 5.1. An example of a large bounce that occurred during the data acquisition is shown in Figure 4-3. The signal relating to the large bounce is shown by the circle. The unfiltered vertical acceleration (1) completely hides the bounce signal in high frequency noise. The 10Hz filtered signal makes the bounce signal visible (2), however the low frequency content is the distinguishing feature, not increased magnitude. The signal was integrated offline (a process that requires careful filtering to remove integration drift) to produce velocity (3) and displacement (4). The figure shows that the magnitude of the acceleration signals highlight discontinuities rather than large magnitude displacements.

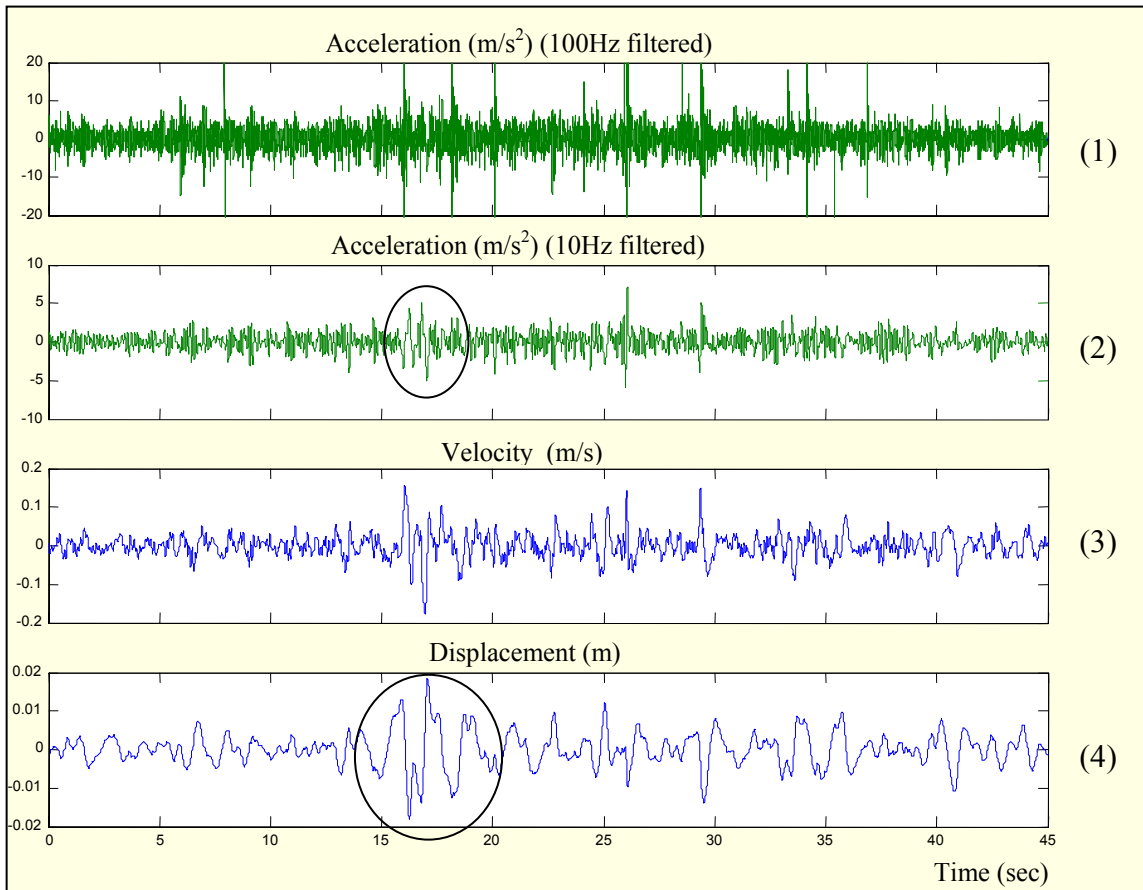


Figure 4-3 Large Bounce Site: Acceleration, Velocity and Displacement.

Discontinuities in motion of the wagon body can be induced by the non-linear elements in the suspension system, including dry friction dampers, bump stops and slack between unsprung interfaces. The field data also showed that high frequency vibrations occur at the rail joints in many locations. The dipped rail joint and non-linear “stick and bump” actions are much less important to detect than resonant behaviour, however they dominate the pk-pk and RMS magnitudes of the acceleration signals.

In the Health Card application, it is most desirable to detect large displacements in the lateral plane, and particularly cases of resonant oscillation. Resonant modes of oscillation for a railway wagon are generally quite low. The modal analysis results in Table 2-4 shows all modes for a loaded wagon are below 5Hz.

European standards for acceptable dynamic performance [27] are summarised briefly in Table 4-3. The European standards give more consideration to the frequency content of the signals than the North American and Australian standards. The behavioural limits are related to track fatigue and running behaviour, whereas the safety limit is related to derailment risk. The safety limits are filtered at lower frequencies than the behavioural limits. This approach is a significant improvement on the Australian and North American standards.

Table 4-3 European Ride Performance Standards

Axis	Limit	Behavioural	Safety
Body Vertical	0.50g Pk-pk 0.20g RMS	0.4-10Hz	0.4-4Hz
Body Lateral	0.30g Pk-pk 0.13g RMS	0.4-10Hz	6Hz
Bogie Lateral	12-($M_b/5$) Pk-pk 6-($M_b/10$) RMS	-	$f_0 \pm 2\text{Hz}$

M_b = Bogie Mass f_0 = theoretical natural oscillation frequency

(NB: In [27] the measurement referred to above as peak to peak (Pk-pk) is actually the width of the statistical interval 0.15% to 99.85% of the magnitude distribution of the signal. See [28] for more on statistical signal analysis)

In the case of Health Card, algorithms are required to analyse the signals online and report event codes. The events and behaviours that are desirable to detect are expected to be the subject of ongoing research. This section has demonstrated the importance of local frequency content when analysing acceleration signals. The following sections introduce time-frequency analysis which analyses signals according to their local frequency content.

4.2 TIME FREQUENCY ANALYSIS

Time frequency analysis is a broad term describing the assessment of a signal based upon its time-localised frequency content. Various specialised techniques exist which achieve optimal resolution in time and frequency. A comparative study of time frequency techniques in various applications is provided in [29]. The most generic technique is the Fourier spectrogram. In most cases, the spectrogram is used initially to explore a signal. Once the finer aspects of the system which the signal represents are known, more specialised techniques are used to highlight those features in the time-frequency representation.

The following sections will introduce the concept of time frequency analysis, starting with frequency analysis using the Fourier transform. Then, the more specialised technique, wavelet analysis, will be introduced for comparison throughout the field data analysis.

4.3 FOURIER ANALYSIS

4.3.1 Continuous Fourier Transform

The Fourier Transform (FT) converts a continuous time signal in the frequency domain. It does this by decomposing the signal into a sum of complex exponentials with continuously varying frequency. The amplitudes and phases of the exponential components make up the complex Fourier representation $X(f)$ which is calculated by the Fourier Transform integral shown by:

$$X(f) = \int_{-\infty}^{\infty} x(t)e^{-j2\pi ft} dt$$

eq. 4-5

Each value of $X(f)$ is the time integral of the signal $x(t)$ multiplied with the corresponding basis function $e^{-j2\pi ft}$ which is a complex exponential at the frequency f . $X(f)$ is therefore a complex decomposition of the original signal $x(t)$ into constituent exponential functions at each frequency f .

The transform is reversible such that the time signal can be reconstructed from the Fourier representation by the inverse Fourier transform given by

$$x(t) = \int_{-\infty}^{\infty} X(f)e^{j2\pi ft} df$$

eq. 4-6

The signal $X(f)$ is referred to as the “frequency domain” representation of the signal, whereas $x(t)$ is referred to as the “time domain” representation of the signal.

4.3.2 Discrete Fourier Transform

In computer systems, continuous signals are sampled at regular intervals, resulting in a sequence of discrete values. Discrete Fourier Transform (DFT) is used to convert a sampled time representation of a signal into a sampled frequency representation. The DFT is given by eq. 4-7, where k is the frequency index, n is the time index, and N is the total number of samples in the sequence.

$$X(k) = \sum_{n=0}^{N-1} x(n)e^{-j2\pi kn / N} \quad k = 1..N$$

eq. 4-7

Like the continuous FT, the DFT is also reversible. The inverse Discrete Fourier Transform (IDFT) given by eq. 4-8.

$$x(n) = \frac{1}{N} \sum_{k=0}^{N-1} X(k) e^{i2\pi kn/N} \quad k = 1..N$$

eq. 4-8

An example time signal is shown in Figure 4-4 with corresponding DFT magnitude and phase plots. The discrete time signal $x(n)$ is composed of two sinusoids at frequencies $f_1=10\text{Hz}$ and $f_2=30\text{Hz}$ sampled $\Delta t=0.001 \text{ sec}$ such that

$$\begin{aligned} x(n) &= \sin(2\pi f_1 n \Delta t) + \sin(2\pi f_2 n \Delta t) \\ &= \sin(2\pi 0.01n) + \sin(2\pi 0.03n) \end{aligned} \quad n = 1..512$$

eq. 4-9

An $N=512$ point DFT is performed on $x(n)$ resulting in $X(k)$ which consists of 512 complex values with frequency spacings given by

$$\Delta f = \frac{1}{N\Delta t} \text{ Hz}$$

eq. 4-10

The magnitudes and phases of the values are plotted in what are referred to as the *magnitude spectrum* and *phase spectrum* of the signal. Typically, only the magnitude spectrum is of interest when using DFT to analyse a signal, because the magnitude spectrum represents the energy of the signal in each frequency band Δf . However, the phases contain important information necessary to reconstruct the time signal with the IDFT.

The two magnitude peaks on the positive side of the vertical axis correspond to the two frequency components, 10Hz and 30Hz. The same information is mirrored in the negative frequencies. (Note that the DFT produces a sampled spectrum: the two peaks are of equal magnitude, however the sampling of the 30Hz peak does not coincide with

the peak. Finer sampling of the frequency spectrum can be achieved by increasing the DFT length N , as can be seen in eq. 4-10.)

The *Power Spectrum* is often used to present the distribution of signal power over the frequency spectrum. The power spectrum is simply the magnitude squared. It can be calculated by multiplying the DFT result by its complex conjugate.

$$|X(f)|^2 = X(f)X^*(f)$$

eq. 4-11

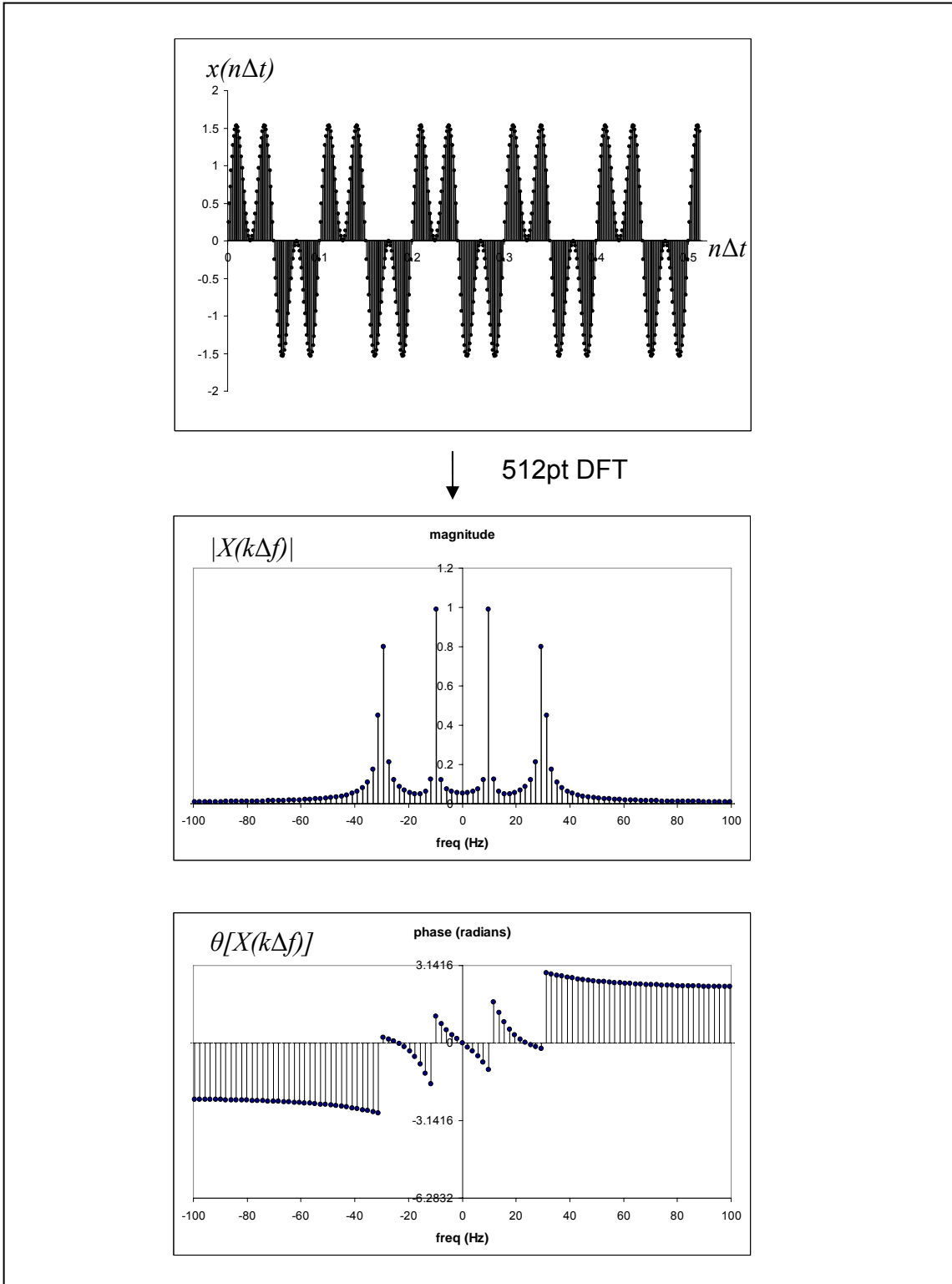


Figure 4-4 Discrete Fourier Transform Example

4.3.3 Fast Fourier Transform

To compute the DFT by eq. 4-7, the number of computations required is proportional to N^2 , thus preventing its use for online algorithms. Providentially, fast algorithms have been developed which calculate the DFT with drastically reduced computational effort. These Fast Fourier Transforms (FFT's) capitalise on the fact that it is possible to split a signal into two parts, take the DFT of each part, then combine the results. Conveniently, the combined result is the same as taking the DFT of the whole signal, but now the effort is proportional to $(N/2)^2$ instead of N^2 . By the same process, the DFT task can be broken down successively, reducing the computational effort from N^2 to $(N/2)\log_2 N$. The inverse DFT can also be calculated by a similar algorithm known as the IFFT.

To illustrate the reduction, Figure 4-5 compares the computation for FFT versus direct computation of the DFT.

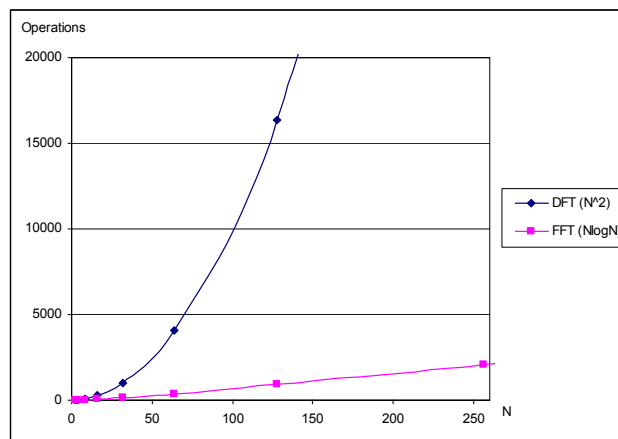


Figure 4-5 Comparison of DFT and FFT Processing Load

Many variations of FFT (and IFFT) algorithms exist which manage trade-offs between code complexity, memory use and computation. More detail on FFT algorithms can be

found in [23] and [24]. For the microcontroller used in the Health Card prototype, a library of C language FFT function calls were provided by the manufacturer [30].

4.4 ANALYSIS OF NON-STATIONARY SIGNALS

Non stationary signals are those which contain spectral information that varies with time. Vehicle ride signals are highly non-stationary with frequency content that changes with transient track excitation and lateral instability.

The Fourier magnitude or power spectrum is ideal for viewing the frequency content of a signal; however the time location at which the frequencies occur is hidden. (The information is not lost, but hidden in the phase information, where it is difficult to interpret.)

Figure 4-6 illustrates the concept of stationary and non-stationary signals and how they appear in the frequency domain. Three signals are compared with their respective power spectra. The first signal (top) is stationary, with component frequencies at 10Hz, 20Hz and 30Hz continuing throughout the signal. These frequencies are manifest in the power spectrum as three spectral peaks. The second signal (middle) is non stationary. It has three component frequencies the same as the first, but they occur sequentially in time. Note that the power spectra is almost identical in form to the first, differing only in magnitude and sharpness. The third signal (bottom) is also non-stationary. The frequency sweeps from 0 to 10Hz over a period of 20sec. Here, the power spectrum shows that frequency content existed between 0 and 10Hz, however the sequence is lost.

This loss of time location can be overcome by taking the DFT over shorter intervals of time.

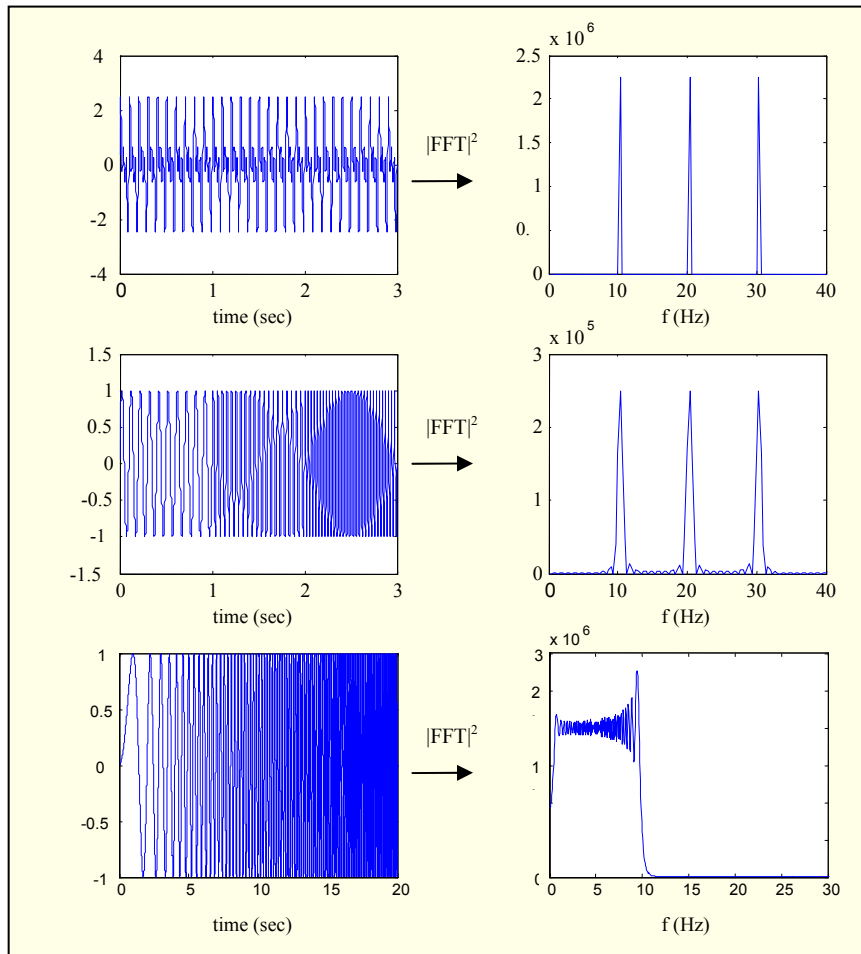


Figure 4-6 Time Signals and Corresponding Power Spectra: Sum of Sinusoids at 10, 20 and 30Hz (top); Sequence of Sinusoids at 10, 20 and 30Hz (middle); Frequency Sweep of 0-10Hz (bottom).

4.4.1 Short Term Fourier Transform and Spectrogram

When analysing the frequency content of a non-stationary signal, it is necessary to find a representation that will capture the frequency content and its time location. A natural extension of the FT for analysing non-stationary signals is the short term Fourier transform (STFT), or in the discrete case, the (STDFT).

The DFT can be taken over short time periods, within which the signal can be assumed stationary. This gives a series of localised spectra which describe the time changing frequency content. The power spectrum for each time interval can be displayed in a three dimensional plot with axes: time, frequency and magnitude. This plot is known as

a *spectrogram*. Figure 4-7 shows the spectrogram of the same three signals as Figure 4-6. In this case, the magnitudes of the spectrogram are displayed as an inverted grayscale image. (i.e. min. is white, max. is black). The vertical axis is frequency and the horizontal axis is time. On inspection, the component frequencies and their sequence in time are clearly seen.

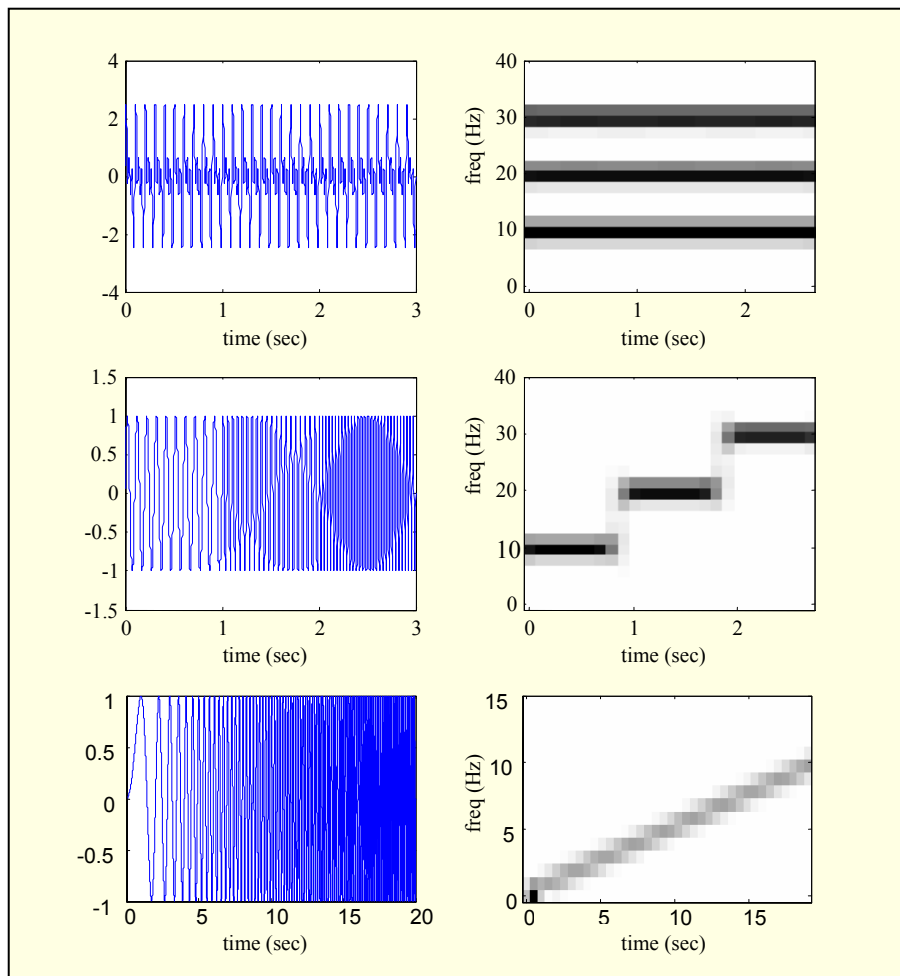


Figure 4-7 Time Signals and Corresponding Spectrogram: Sum of Sinusoids at 10, 20 and 30Hz (top); Sequence of Sinusoids at 10, 20 and 30Hz (middle); Frequency Sweep of 0-10Hz (bottom).

4.4.2 Windowing

When calculating the STDFT, it is necessary to multiply the signal by a window function. The DFT is calculated over a finite number of samples N . However, the DFT

inherently assumes that the signal is periodic, and that the N samples are one complete period, see Figure 4-8. The resulting discontinuities at the boundaries introduce frequency components to the magnitude spectrum which interfere with the true components of the signal.

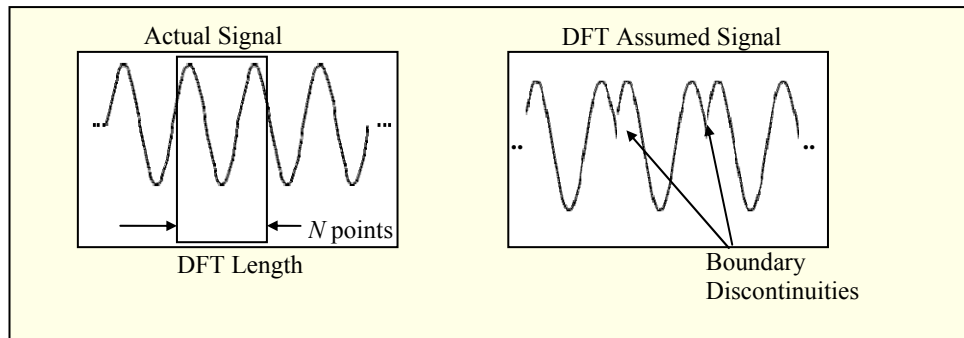


Figure 4-8 DFT Assumed Periodicity and Boundary Discontinuities

A *window* function is normally used to smooth the edges of the short term signal. Figure 4-9 illustrates the process. The signal of Figure 4-4 is analysed over a shorter period. First, the signal and its magnitude spectrum without windowing is shown (top). Note the interfering side lobes around the spectral peaks. Next, a window function is applied (middle). In this case, a *Hanning* window (raised cosine) is used. The spectrum of the Hanning window is shown to the right hand side. The first signal is multiplied with the window function to produce the windowed signal (bottom). The resulting magnitude spectrum is shown to the right. Note that the interference between the spectral peaks is reduced; however the resolution of the peaks is diminished.

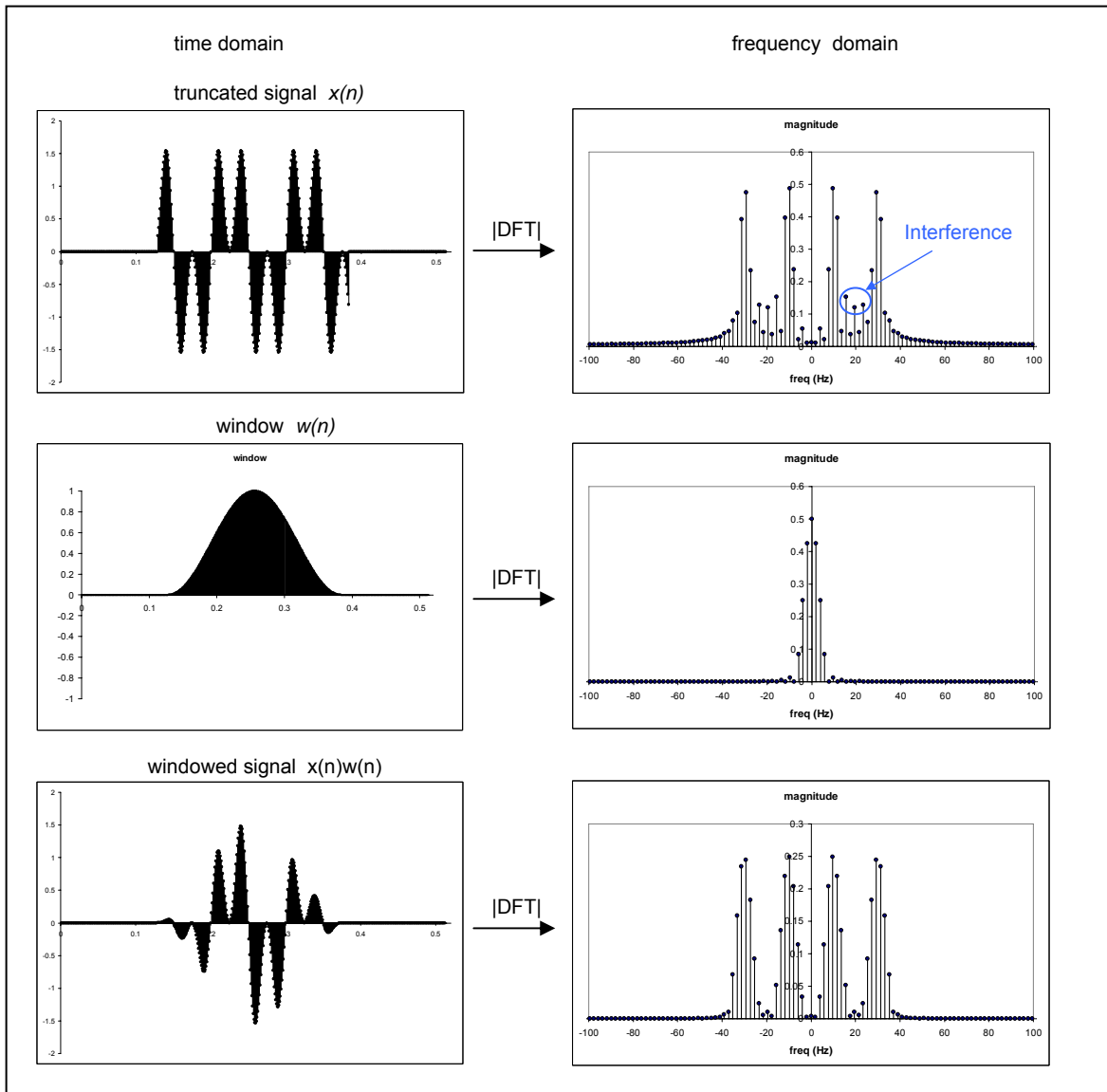


Figure 4-9 Windowing

A range of different window functions can be applied with different advantages and disadvantages [23]. When choosing a window, the predominant trade-off is main-lobe width which affects the peak resolution, versus side-lobe reduction which affects spectral interference. These properties are compared in Table 4-4 for some commonly used window types. The Hanning (raised cosine) window was adopted for the spectrogram analysis throughout this thesis.

Table 4-4 Comparison of Commonly Used Window Types (source [23])

Window Type	Peak Side-lobe Amplitude (relative)	Approximate Width of Main-lobe
Rectangular	-13	$4\pi/(N+1)$
Bartlett	-25	$8\pi/N$
Hanning	-31	$8\pi/N$
Hamming	-41	$8\pi/N$
Blackman	-57	$12\pi/N$

Besides the limitation of side-lobe interference and main-lobe widening, there is a basic limitation to the resolution that can be achieved in the time frequency plane.

4.4.3 Limitation of Time Frequency Resolution

The resolution of the time-frequency representation is limited by the *uncertainty principle* derived in [29]. The frequency of a signal cannot be determined without some finite period of time in which to observe the signal. The more time taken to observe the signal, the more precisely the frequency content can be determined. Conversely, the less time taken to observe the signal, the more precisely the time location can be determined. Therefore, it is possible to achieve a high resolution in frequency or a high resolution in time, but time and frequency cannot be resolved simultaneously beyond a theoretical limit.

This is illustrated in Figure 4-10. The frequency resolution Δf becomes less defined as the time window Δt is reduced, and more defined as the time window is increased. The time-frequency resolution is limited by the area of the rectangles. The theoretical limit of time-frequency resolution is:

$$\Delta t \Delta f \geq \frac{1}{4\pi}$$

eq. 4-12

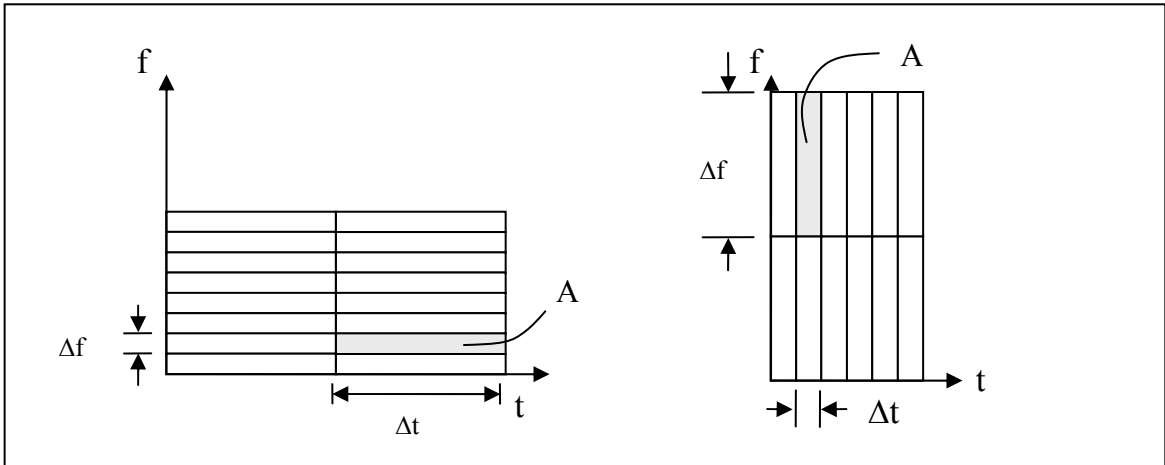


Figure 4-10 Time-Frequency Plane and Time Frequency Resolution

The Fourier Spectrogram divides the time-frequency plane uniformly for all frequencies. The practical consequence is that the location of short transient high frequency detail is diluted across Δt .

Wavelet analysis is a technique which allows the time-frequency plane to be divided in a more flexible way, such that a smaller Δt is used for higher frequencies (with the inherent loss of frequency resolution) and a larger Δt is used for lower frequencies (with the inherent gain in frequency resolution). Section 4.5 introduces wavelet analysis and discusses this topic in more detail.

4.5 WAVELET ANALYSIS

Wavelet analysis is a special form of time frequency analysis which has recently attracted experimental interest in a wide range of applications. Examples in literature include: detection of transient fault signals in power systems [31]-[56]; machine and

process fault detection [57]-[59]; vibration analysis [60]-[70]; medical signal analysis [71]-[74]; and road roughness indexing [75]. Experimental railway applications for wavelet analysis include: direct analysis of track irregularity data [76]; magnetic rail head defect detection [77]; wayside acoustic signal analysis [78]; and image processing for rail head inspection [79]. Wavelet analysis has shown good success at locating small scale features or details amongst larger scale signals. This makes it suitable for detecting transient signals such as spikes on AC power lines, and bearing fault signals on rotating machinery.

The Wavelet Transform (WT) is a technique that is relatively new compared to the Fourier transform. According to [80] the wavelet method was established by Stephane Mallat in 1988 [81]. In contrast, Fourier transform was founded by Joseph Fourier (1768-1830) in the early nineteenth century.

4.5.1 Wavelet Transform

A wavelet is, as the name suggests, a small wave. It is any waveform with a zero mean that exists for a finite amount of time. An example wavelet is shown in Figure 4-11.

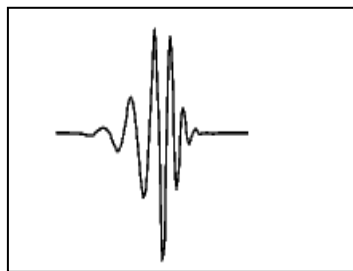


Figure 4-11 Example Wavelet

The WT is calculated by convolving the wavelet with the original signal. (i.e. shift the wavelet in time in relation to the original signal, multiply the shifted wavelet with the

original signal, then sum the result to produce a single value. Repeat for each time shift). The convolution is repeated with the wavelet scaled up, Figure 4-12(3), to capture low frequency (large scale) features, and scaled down (1) to capture high frequency (small scale) detail.

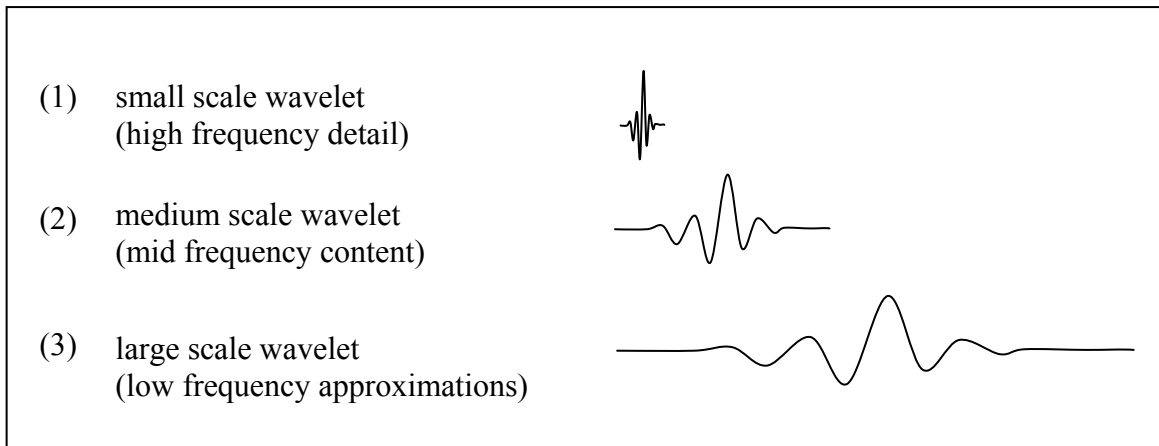


Figure 4-12 Wavelet Scaling

The continuous wavelet transform $C(a,b)$ of a signal $s(t)$ is given by eq. 4-13, where $\Psi(t,a,b)$ is the wavelet, a is the scaling factor, b is the position of the wavelet in the signal.

$$C(a,b) = \int_R s(t) \frac{1}{\sqrt{|a|}} \Psi\left(\frac{t-b}{a}\right) dt$$

eq. 4-13

The relationship between Fourier analysis and Wavelet analysis can be seen by comparing eq. 4-13 with the Fourier integral of eq. 4-14

$$X(f) = \int_{-\infty}^{\infty} x(t) e^{-j2\pi ft} dt$$

eq. 4-14

The Fourier transform uses a complex exponential $e^{-j2\pi ft}$ as the basis function with variable frequency f . Whereas, the Wavelet transform uses a wavelet $\Psi(t,a,b)$ as the basis function with variable time shift b and scale a .

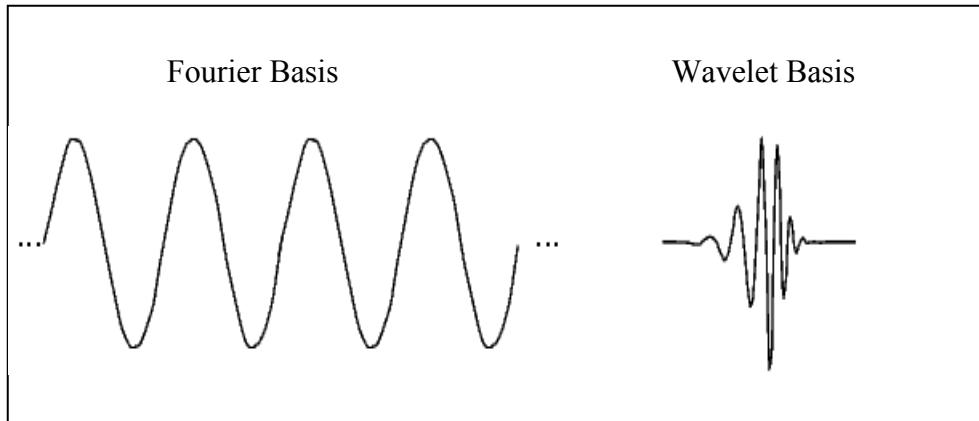


Figure 4-13: Fourier Basis Function (left) vs Wavelet Basis Function (right)

The WT is not strictly a time-frequency representation, but rather, a *time-scale* representation of the signal. However, WT can give a time-frequency analysis if the centre frequency of the wavelet is estimated for each scale. In comparison to the STDFFT time frequency distribution of Figure 4-10 which is divided uniformly across all frequencies, the WT produces a non-uniform distribution as represented in Figure 4-14.

WT exploits the natural tendency for high frequency content to be more transient than low frequency content. Therefore, the higher frequencies are better represented with finer time and broader frequency resolution. Conversely, lower frequency content tends to change more slowly, so it is represented with broader time and finer frequency resolution. Note that the time-frequency resolution, given by the area of the rectangles, does not change. This area is ultimately limited by the uncertainty principle described in 4.4.3. The choice of wavelet will determine how closely this limit is approached.

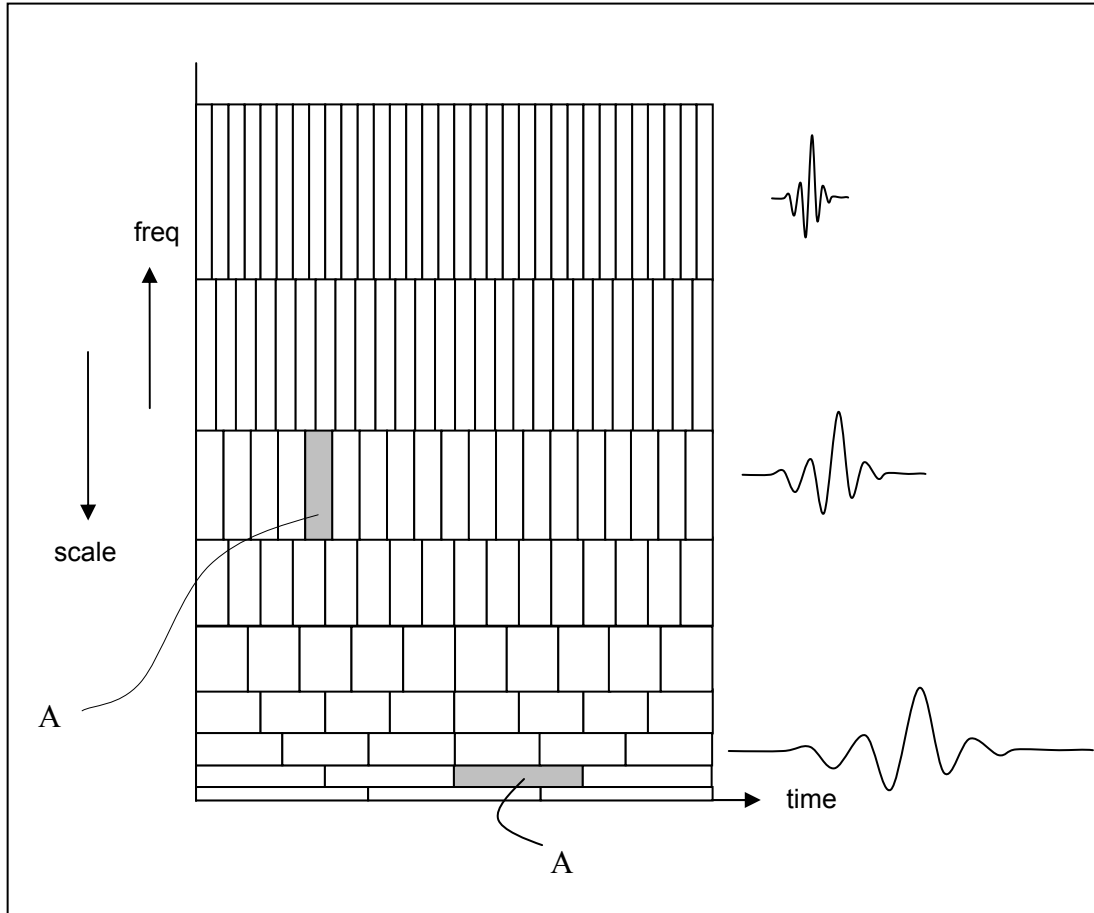


Figure 4-14: WT Time-Freq Relationship

Any finite length function with zero average magnitude can be used as the wavelet basis function. A practical comparison of the commonly used wavelets and their respective properties is given in [80]. Some wavelets can be implemented with a fast algorithm using a bank of filters. The following section introduces filter bank implementation of wavelet analysis in more detail.

4.5.2 Fast Wavelet Algorithm

The continuous wavelet transform (CWT) is a processor-hungry operation, which convolves the signal with the wavelet for every scale. In fact, the CWT produces a large redundancy of information. A reduction in processing can be achieved by the Discrete Wavelet Transform (DWT) which scales the wavelet in powers of two in

process referred to as *diadic* scaling. Figure 4-15 illustrates this. The reduction in calculation yields no loss of information from the original signal.

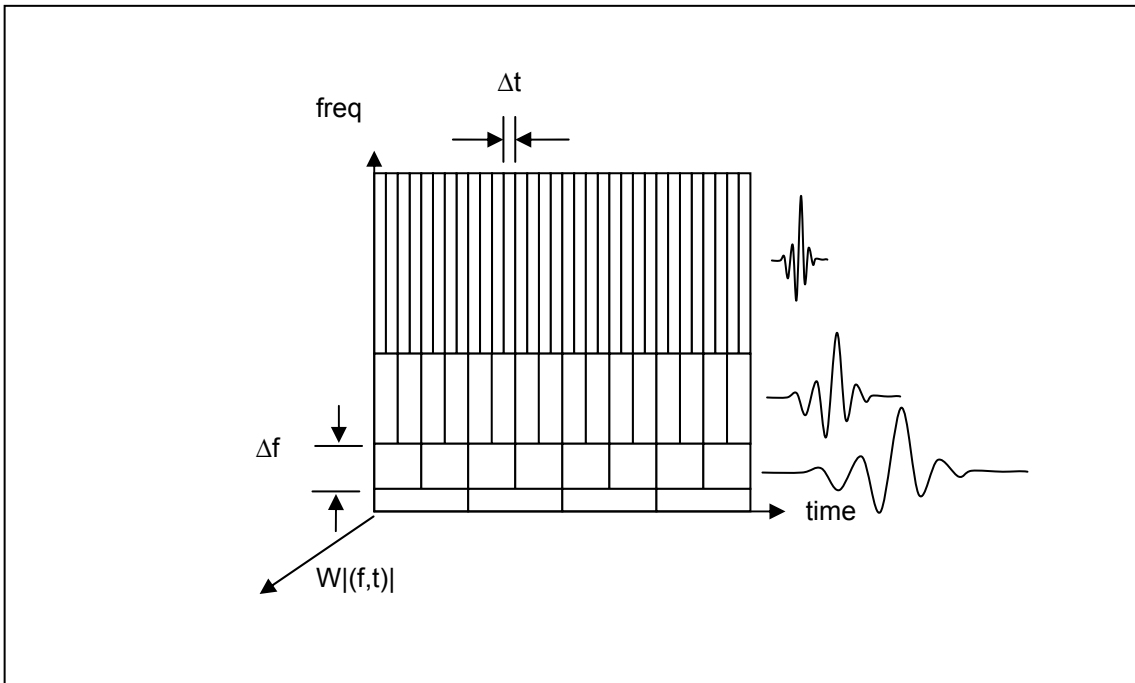


Figure 4-15 Diadic (powers of 2) Scaling

Diadic scaling reduces the computational effort to a large extent, however true gains in efficiency are achieved by a fast algorithm developed by Mallat [81]. The DWT can be implemented online using a bank of digital filters as shown in Figure 4-16.

The process of fast wavelet analysis is as follows: The digital input signal $S(n)$ is passed through a high-pass filter H and down-sampled to remove every second sample, yielding the first level of detail $D1$. Simultaneously, $S(n)$ is passed through a low pass filter L and down-sampled to produce the first signal approximation $A1$. The down-sampling reduces the redundant samples produced by simultaneous filtering. The process is repeated for $A1$ to produce $D2$ and $A2$. $A2$ is then decomposed further into $D3$ and $A3$. $D1$, $D2$, $D3$ and $A3$ form the coefficients of the time-scale representation

of the signal. Figure 4-16 shows a three level decomposition, however more levels can be added to yield larger scale detail and approximation.

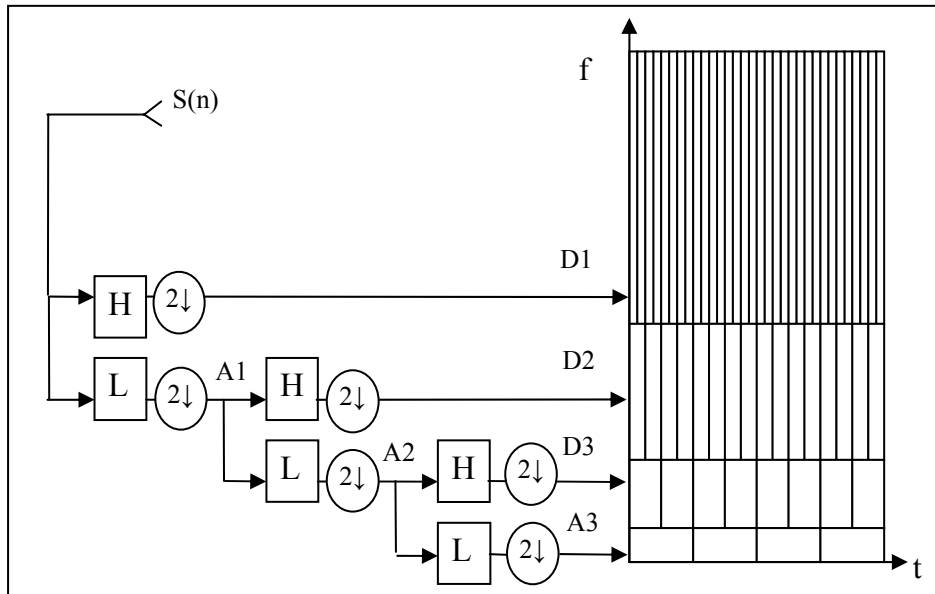


Figure 4-16: Fast Wavelet Analysis Transform

The wavelet shape itself is “created” from the coefficients of the filters, and can be viewed by successively convolving and up-sampling the high pass filter coefficients. By this process, many new and interesting wavelet shapes have been created.

If perfect signal reconstruction is required, special filters called Quadrature Mirror Filters must be used. There is detailed literature available on this topic [80][82]. However, signal reconstruction is not necessary in this research application, which is only concerned with signal analysis.

An example diadic wavelet analysis is shown in Figure 4-17. The analysed signal is produced by a simulation package modelling a wagon running over a vertical track irregularity. The transient signal, as each bogie runs over the irregularity, has a sharp impact spike followed by a resonant oscillation. Scales 512 and 256 show the overall

presence of the transient. Scale 128 corresponds with the resonant oscillation. Scales 64, 32 and 16 reveal the time location of the impact spikes.

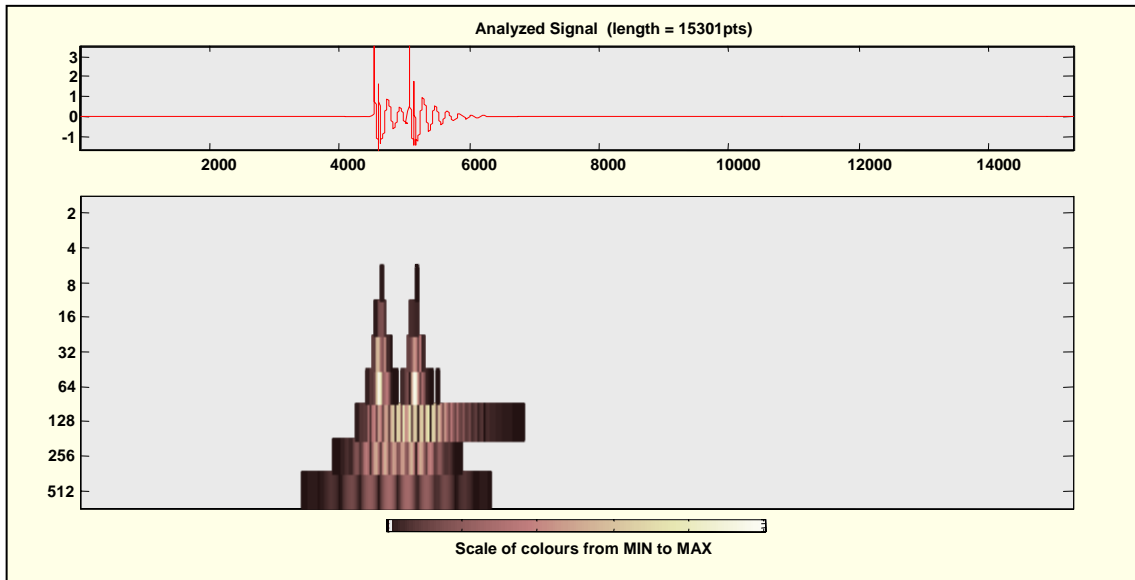


Figure 4-17 Diadic Wavelet Analysis of a Transient Signal

4.5.3 Wavelet Type Selection

The simplest wavelet arising from a filter bank is the Haar wavelet which is the square wave shown in Figure 4-18.

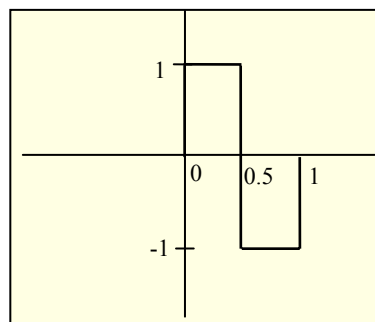


Figure 4-18 Haar Wavelet

A comparison of properties of the various wavelets is given in [80]. Many of the discerning properties of the wavelet types are associated with other applications of wavelets including signal compression and signal smoothing. The wavelet properties that are important in this application are

1. it can be implemented with a filter bank, and
2. it achieves a good time-frequency resolution.

The Haar wavelet fulfils both of these properties and was therefore adopted for the signal analysis in Chapter 5.

4.5.4 Relating Scales to Frequencies

As mentioned previously in Section 4.5.1, wavelet analysis produces a time-scale representation of the signal. In order to relate this to a time-frequency representation, the wavelet scales must be converted to equivalent frequencies. If the centre frequency f_c of the wavelet is estimated by best fit with a sinusoid, see Figure 4-19, the estimated frequency at scale a with a sampling rate Δt is calculated by

$$f_a = \frac{\Delta t f_c}{a}$$

eq. 4-15

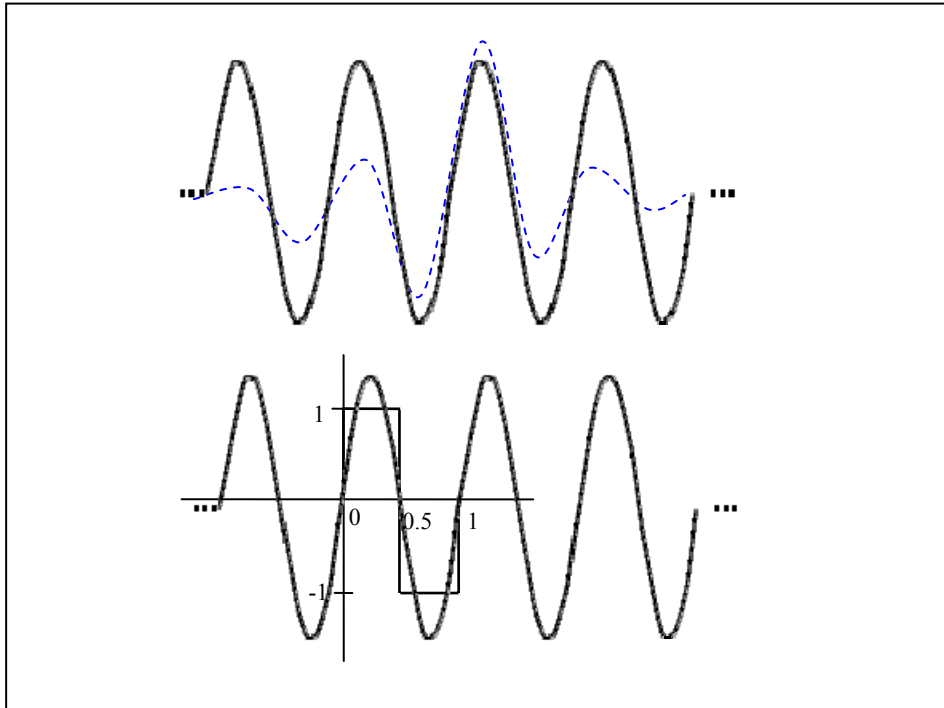


Figure 4-19 Approximating the Centre Frequency of a Wavelet with a Best Fit Sinusoid

4.5.5 Example of Wavelet Analysis vs Fourier Spectrogram

Figure 4-20 compares an FFT spectrogram with a Haar wavelet analysis at diadic scales with estimated wavelet centre frequencies (f_c) covering the 0.5 to 10Hz range. Note that, as the scale decreases, centre frequency (f_c) increases, and frequency step (Δf_c) increases.

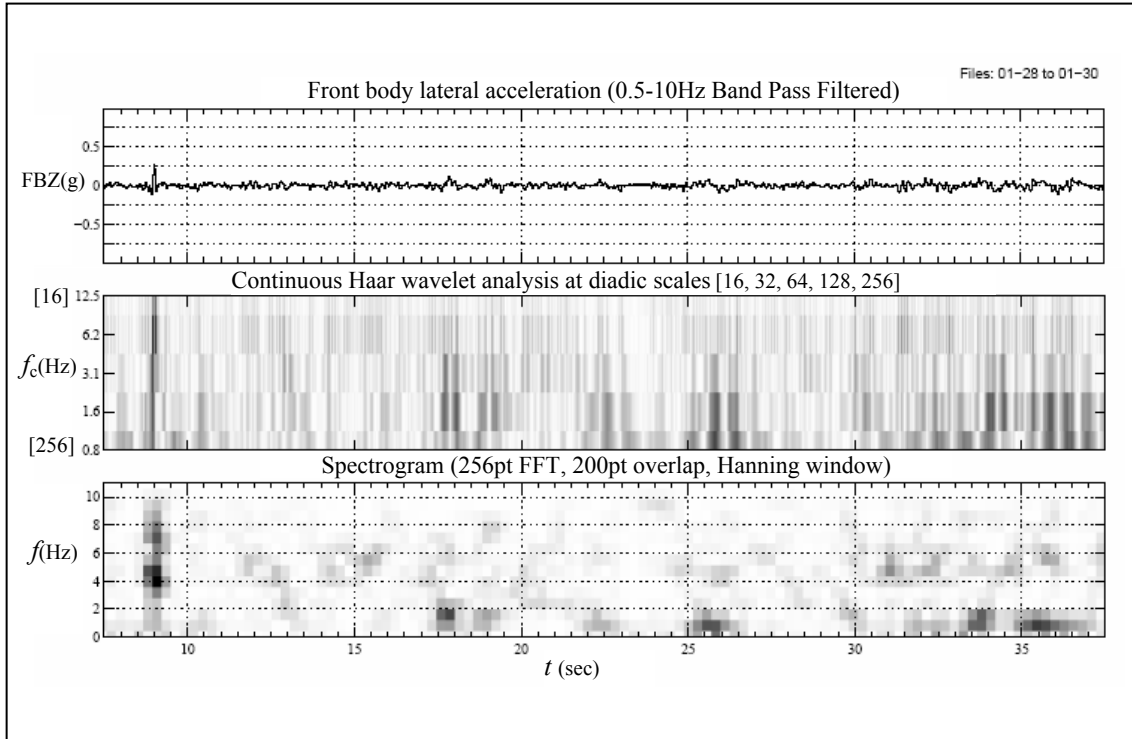


Figure 4-20 Lateral Wagon Body Acceleration with Wavelet and FFT Spectrogram Compared.

The wavelet analysis highlights the exact time location of the transient spike however it does not accurately measure the frequency of the spike. Conversely, the lower frequencies on the right hand side are less resolved in time and more clearly resolved in frequency.

The FFT spectrogram divides the time frequency plane uniformly. The high frequency content of the spike appears less sharp in time but the frequency is measured with peaks at 4, 5 and 7Hz. The low frequency content on the right hand side is also adequately resolved.

More comparison of wavelet analysis and spectrogram can be seen in Chapter 5 with their application to the field data analysis.

4.6 CONCLUSION

This chapter firstly demonstrated the importance of the frequency content of acceleration signals when using them to analyse physical motion of a wagon body. Large resonant motions were shown to produce small magnitude acceleration signals compared with less consequential high frequency discontinuities. The strong dependency of signal magnitude on frequency content demands that signal analysis algorithms for Health Card monitor frequency content as well as signal magnitude.

Time frequency analysis was introduced in the form of the Short Term Discrete Fourier Transform (STDFT) which can be implemented on a low power processor using Fast Fourier Transform (FFT) algorithms. Wavelet Analysis was also introduced as an alternative to be compared throughout the offline data analysis. The following chapter describes the application of these techniques to field data collected from a hopper wagon in service.

5 Time Frequency Analysis of Field Data

This chapter presents the application of Fourier and wavelet time-frequency analysis to acceleration signals collected from the body corners and bogie sideframes of a wagon. The purpose of the analysis is to assess the content of the signals, and the capabilities of time-frequency analysis as a basis for detection of dynamic behaviour. In particular, detection of lateral instability, severe vehicle track interaction, and changes in wagon parameters are considered.

This chapter describes the data acquisition that was undertaken, the offline analysis that was performed, and the significant results that were obtained. Results of STDFT spectrogram, wavelet analysis and standard RMS and peak to peak techniques are compared throughout. Results for the entire journey are included on the attached compact disk, CD01, and results that represent significant findings are presented and discussed in the chapter.

5.1 FIELD DATA ACQUISITION

Data was collected from a ballast wagon travelling north from station A to just north of station B with a full load of ballast, and returning with an empty load. Figure 5-1 shows the test wagon and acquisition system. Dual axis accelerometers were fitted to each corner of the body and each side frame. The wagon was coupled in a test train with a QR test car which is normally used primarily for locomotive testing. The accelerometers were wired back to the testing car which carried the data acquisition equipment. The data acquisition system was an industrial PC running a Labview application with a National Instruments data acquisition card.



Figure 5-1 Field Data Acquisition

5.1.1 Purpose

The purpose of the data acquisition was to provide real data that represented the signals available to the Health Card device. The data was to be used to test and demonstrate the effectiveness of signal analysis techniques and facilitate the development of an online analysis algorithm. Additional data was also collected from the sideframes to give the accelerations of the unsprung masses.

5.1.2 Test Wagon

The test wagon was a ballast hopper wagon. It was a two bin hopper wagon with doors that open longitudinally to unload rock ballast onto the track between and beside the rails during track maintenance. Details of the test wagon are shown in Figure 5-2. The wagon had conventional three piece bogies spaced 10.97m apart. The wheelsets were spaced 1.675m apart within each bogie and wheels had a diameter of 850mm. The

wagon was constructed of steel, with an unloaded (tare) mass of 18.8 tonnes, and designed to carry a payload of up to 52.2 tonnes with a capacity of 24m³ (level).

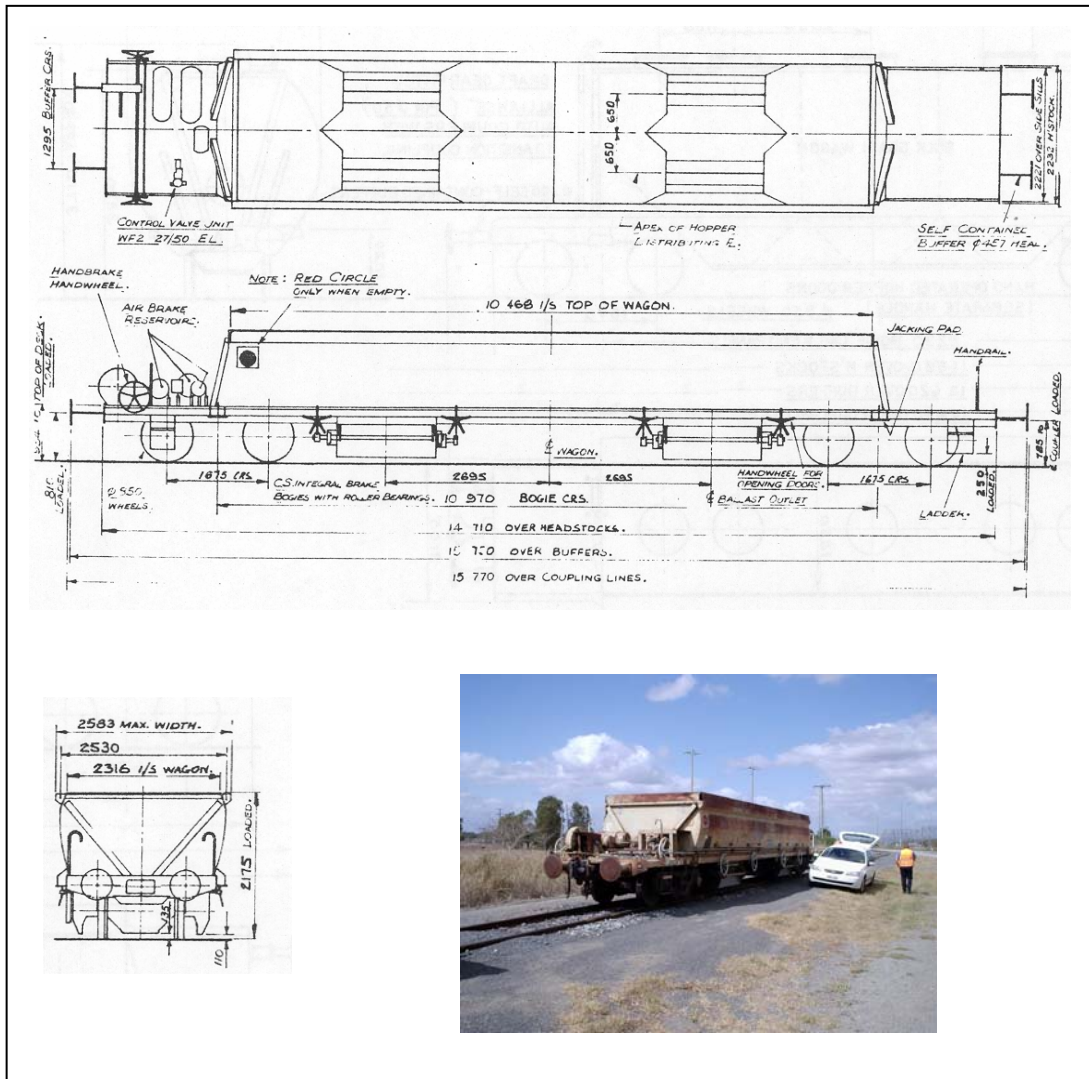


Figure 5-2 ballast hopper wagon used for signal acquisition

5.1.3 Test Track

The test track section was chosen to provide an interesting level of excitation to the suspension of the test wagon. The track construction was a mix of 31 and 47 kg/m rail on timber sleepers with some steel sleepers interspersed at a ratio of 1 in 4 on various sections. The rail was welded and joined in various lengths. The track was rated for a

maximum allowable axle load of 15.75 tonnes per axle, and the maximum allowable speed was between 50 km/h and 80 km/h.

5.1.4 Test Journey

The test run was a normal ballast laying operation, starting with a full load of ballast, travelling to the maintenance site, dropping the ballast on the track, and returning empty via the same route. Data was collected during the journey north from station A to just north of station B with a full load of ballast, during the ballast drop, and during the return journey with an empty load. This gave opportunity to compare the ride signal characteristics for the wagon in both loaded and empty states over the same track sections at similar speeds.

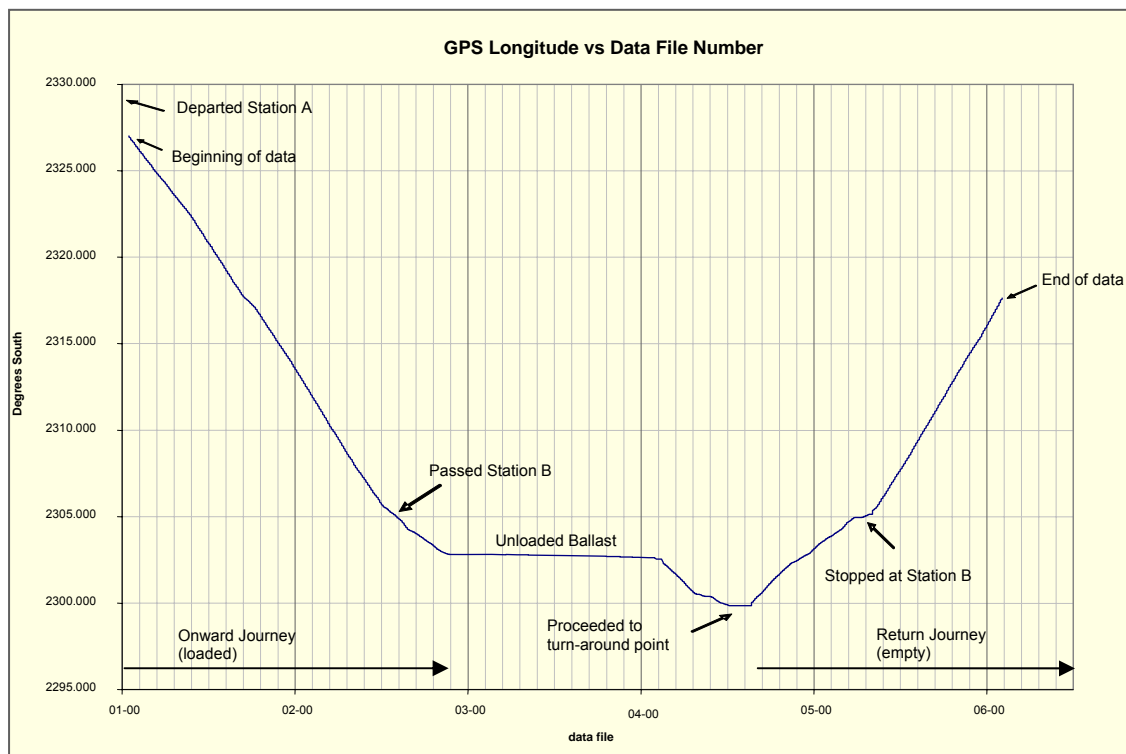


Figure 5-3 Journey Description from GPS Locations

5.1.5 Data Acquisition Equipment

The data acquisition system was designed, manufactured, tested and installed on the test train by CQU technical staff. The accelerometer devices were the same devices that were used in the prototype Health Card, however to interface with the National Instruments Data Acquisition Card, the analog output was chosen rather than the PWM feature. The chip required some supporting circuitry and additional signal conditioning to provide a signal suitable for the PC based data acquisition system. These circuits were assembled and encapsulated in resin filled enclosures as shown in Figure 5-4

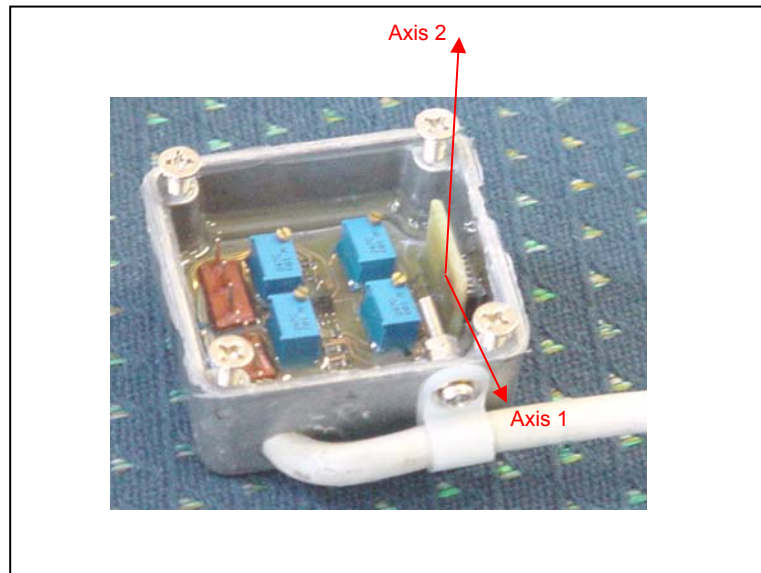


Figure 5-4 Accelerometer units used for data acquisition

The assemblies were adhered with epoxy resin to four corners of the wagon body and to the four side frames of the wagon. The mounting locations and orientations of measurement axes were specified as part of this thesis work.

5.1.6 Sensing Arrangement

The data acquisition system had 16 analog input channels. Figure 5-5 shows the sensing arrangement and axis directions and Table 5-1 lists the channel names. A dual

axis accelerometer was placed on each corner of the wagon and on each sideframe. All of the axes measured in the vertical and lateral directions.

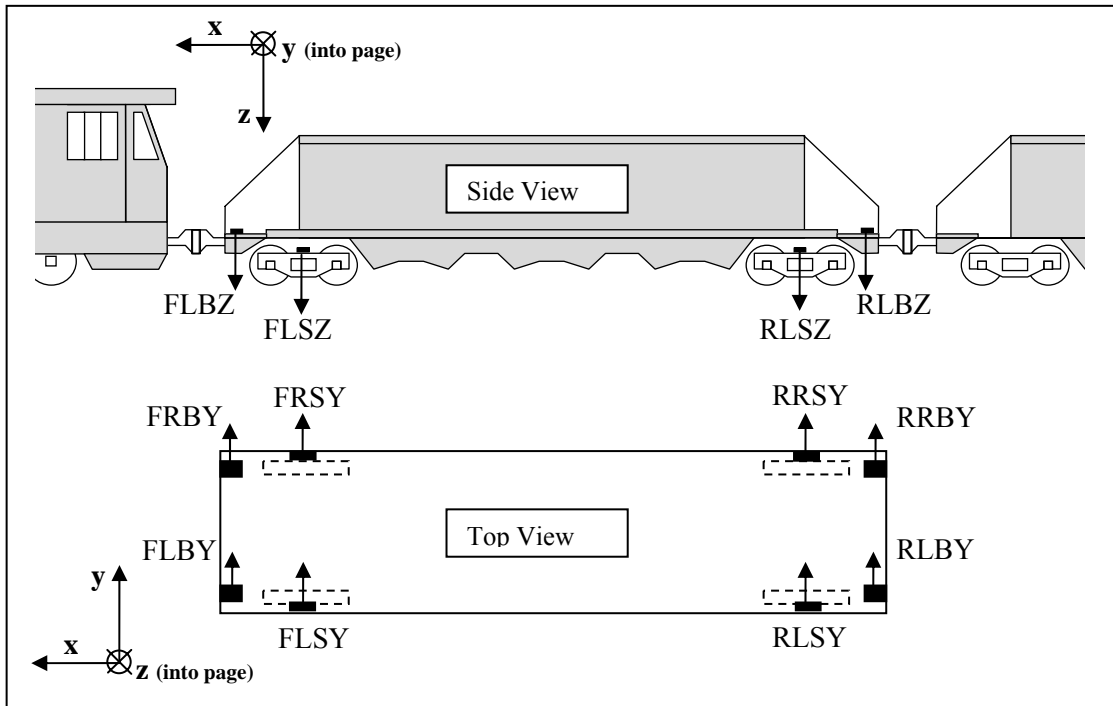


Figure 5-5 Accelerometer locations and xyz coordinate system

Table 5-1 Channel Names

FLBZ	Front Left Body Vertical
FLBY	Front Left Body Lateral
FLSZ	Front Left Sideframe Vertical
FLSY	Front Left Sideframe Lateral
RLBZ	Rear Left Body Vertical
RLBY	Rear Left Body Lateral
RLSZ	Rear Left Sideframe Vertical
RLSY	Rear Left Sideframe Lateral
RRBZ	Rear Right Body Vertical
RRBY	Rear Right Body Lateral
RRSZ	Rear Right Sideframe Vertical
RRSY	Rear Right Sideframe Lateral
FRBZ	Front Right Body Vertical
FRBY	Front Right Body Lateral
FRSZ	Front Right Sideframe Vertical
FRSY	Front Right Sideframe Lateral
Total:	16 Channels

The sensing arrangement was chosen to discern five degrees of freedom in the wagon body, i.e. roll, pitch, yaw angular accelerations, vertical and lateral translational accelerations. (Longitudinal accelerations were considered to be outside the scope of this work which is only concerned with responses to track excitation.) Measuring vertical and lateral accelerations at each corner of the wagon body allowed the rotations and translations of the body to be determined, according to Figure 5-6. The additional sideframe accelerations were measured to indicate the suspension excitation simultaneously to the body responses.

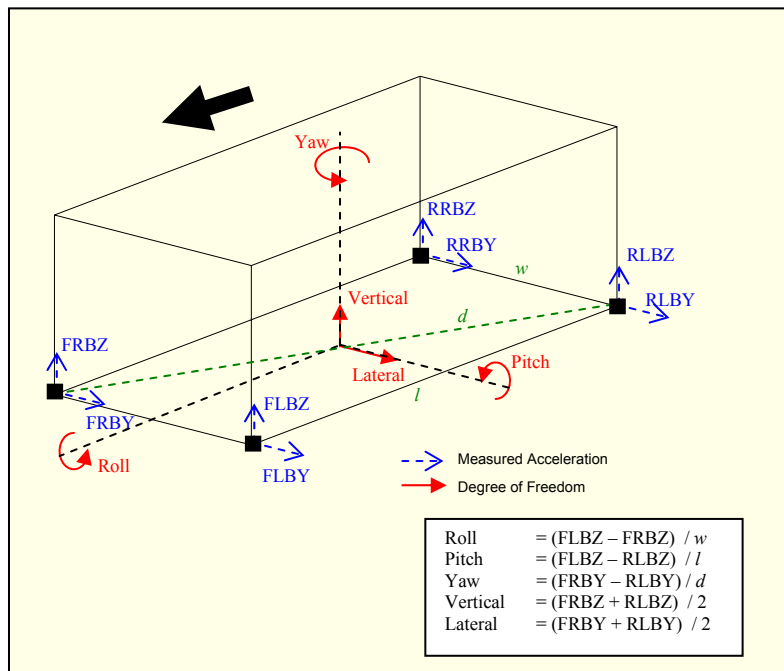


Figure 5-6 Relating corner accelerations to 5 degrees of freedom

5.1.7 Signal Conditioning, Sampling and Storage

The signal processing block diagram for each channel is shown in Figure 5-7. The ADXL2010 includes a first order anti-aliasing filter with a corner frequency set by an external capacitor. The cut off frequency was set to 100Hz for the data acquisition. Preliminary lab testing showed that the signal required heavier attenuation to eliminate

high frequency content, so an additional 2nd order filter was added. Each filtered analog signal was sampled at 1KHz by a National Instruments data acquisition card. The sampled data was stored on a local hard drive. The acquisition and file storage was handled by a Labview application running on Microsoft Windows 98 operating system. The data was successfully acquired and stored in files of 5000 samples, i.e. 5 seconds of data.

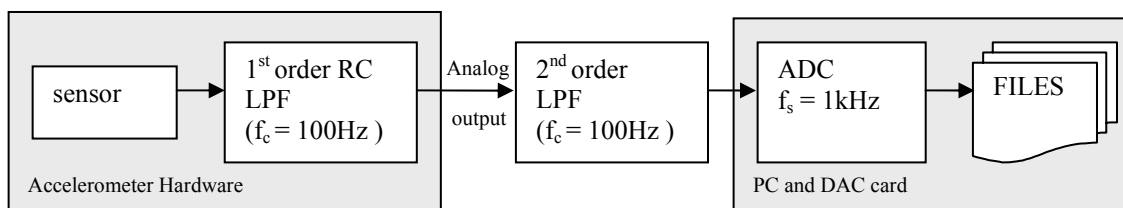


Figure 5-7 - Signal Processing for Data Acquisition using PC and DAC Card

Figure 5-8 shows an example of the simultaneous side frame and body signals collected. Vertical accelerations at four corners are shown. The figure shows signals for the same track location collected on the onward journey loaded (left) and return journey empty (right). The track section shows a transition from rough corrugation to relatively smooth with dipped rail joints. The effect of the load is clearly seen in the transfer of excitation from the sideframes (bottom) to the body (top).

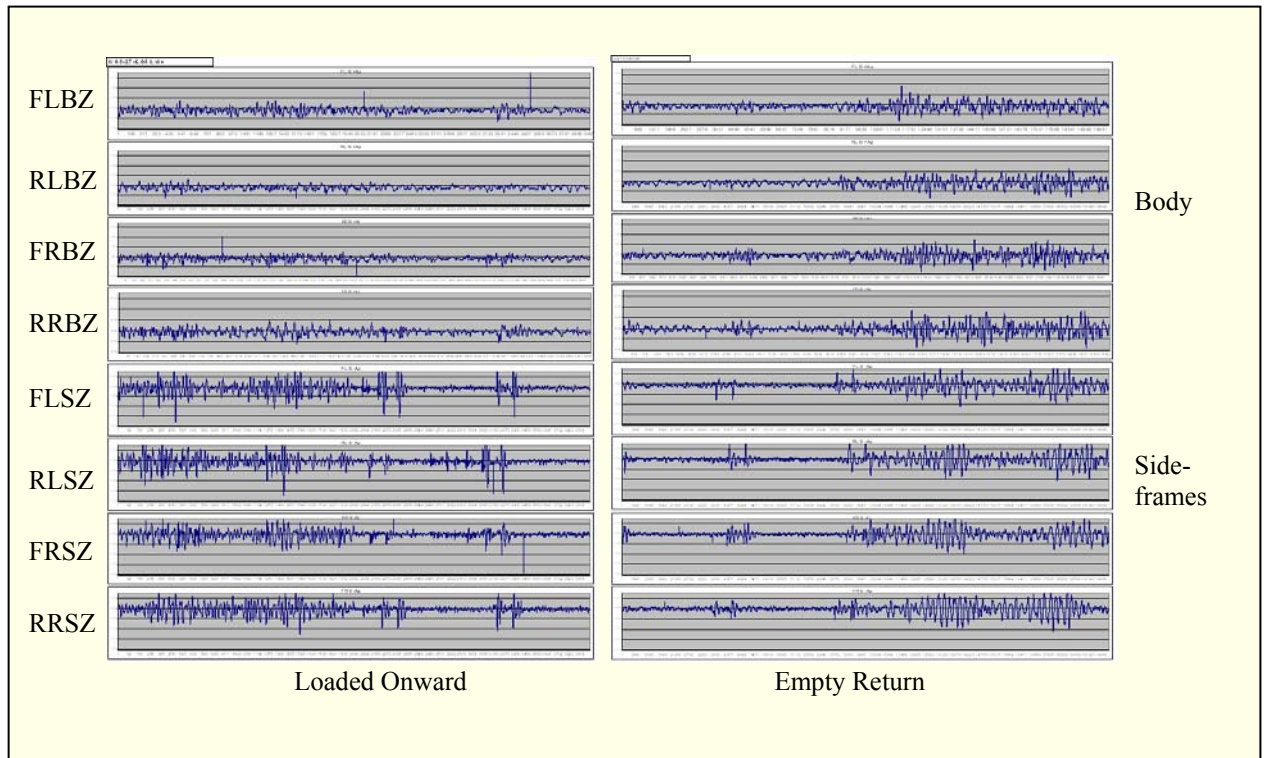


Figure 5-8 Wagon Body and Sideframe Accelerations in the Loaded and Empty Case

5.2 OFFLINE ANALYSIS OF DATA

It was necessary to establish a basis of comparison for the results. Wheel force measurements were not possible in the scope of the research. However, a significant attempt, reported in the paper by Xia and Bleakley [83], was made to estimate wheel forces from the sideframe and body acceleration data using an inverse modelling approach. If refined adequately, this would have allowed estimated wheel contact forces to be aligned with the time-frequency analysis. However, the method was not refined adequately within the time frame of this research..

An alternative approach was adopted which was to compare the results with the criteria for lateral and vertical accelerations specified in Australian Standards for acceptance of new and modified rollingstock [16][7][9]. The limits and filtering requirements are summarised in Table 5-2. In the standard, measurements were to be taken from the

floor level of the rail wagon, as close as possible to the bogie centre. All signals were to be filtered to below 10Hz.

Table 5-2 Australian Ride Performance Standard

Assessment Quantity	Limit
Body vertical peak-to-peak	0.80g
Body vertical mean peak-to-peak	0.50g
Body lateral peak-to-peak	0.50g
Body lateral mean peak-to-peak	0.35g

The limits are specified for peak to peak and average peak to peak values. The standards do not specify the time window of observation for the two values. For this analysis, the peak to peak values are calculated over a 1sec sliding window, and the average peak to peak value is calculated over a 30sec period overlapping by 20sec. North American standards, Table 4-1, specify 2 second RMS values for lateral accelerations to detect bogie hunting. This assessment quantity was also included in the data analysis.

It should be noted here that the track used for the data acquisition was particularly rough, and the track was under maintenance at the time (hence, the ballast laying operation). The track section was selected because it provided an interesting level of vehicle-track excitation. Therefore, the acceleration levels experienced on this track exceeded standard limits in many locations. This track should not be taken as an indication of the quality of the rail network in Queensland. Neither should the ride levels be taken as an indication of the quality of ballast wagons in Queensland.

5.3 DATA ANALYSIS IN MATLAB™

Program code was developed in MATLAB™ to read the data files, pre-process the data, perform the analyses, and plot the results to standard A4 pages. A file range could be selected and the analysis was performed on the files in overlapping windows. This allows transient signals to be seen moving across the page as the viewer scrolls from one page to another. The MATLAB™ code for an example analysis is included in Appendix B. Figure 5-9 is an example page from page 5 of CD01:\FBY(01-04 to 06-08).pdf

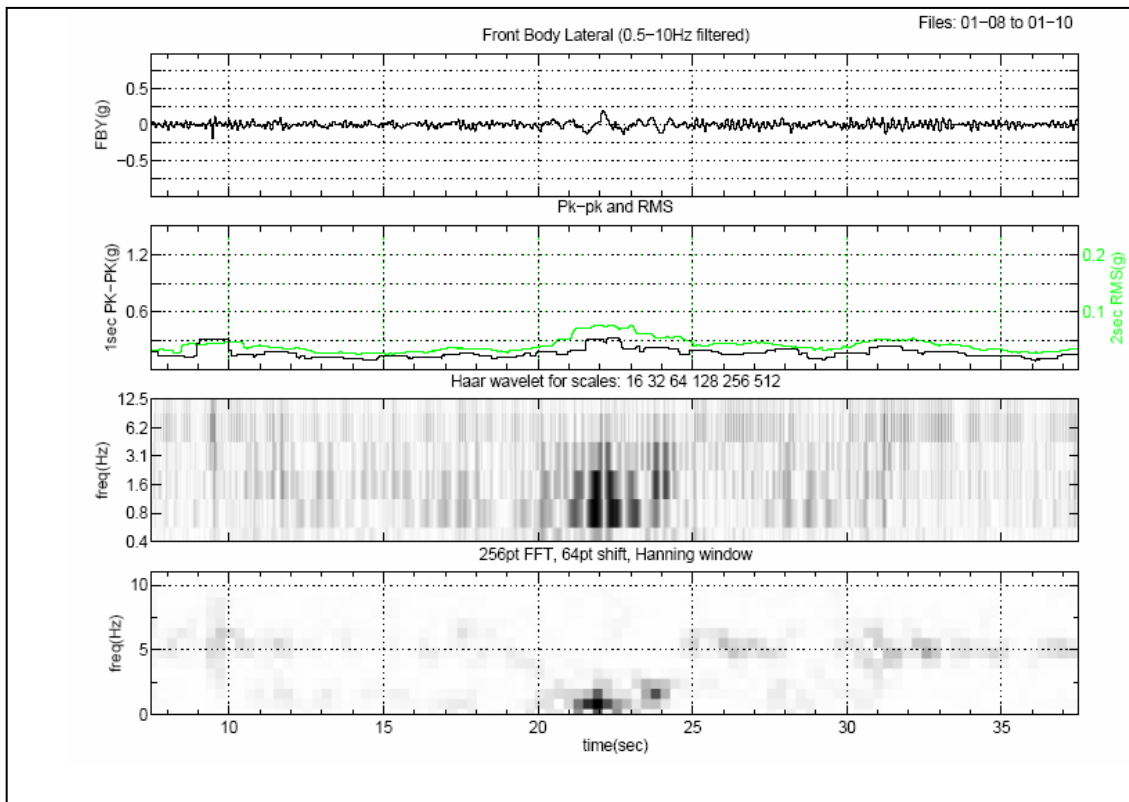


Figure 5-9 Example Data Analysis Page (source - CD01:\FBY(01-04 to 06-08).pdf page 5)

The top line of Figure 5-9 is the acceleration signal in the axis nominated in the title. The signal has been band-pass filtered to remove the static and low frequency content below 0.5 Hz and the high frequency noise above 10Hz. The filtering is done in the

frequency domain by taking the FFT for the entire signal length with a Hanning window, clearing coefficients above 10Hz and below 0.5Hz and then taking the IFFT. The signal is down-sampled from 1kHz to 200Hz to match the Health Card sampling rate.

The second line is the root mean square (RMS) and peak to peak (Pk-pk) accelerations calculated from the filtered signal. The RMS value is calculated over a 2 second period in steps of 1 sample. The Pk-pk value is calculated by subtracting the minimum value from the maximum value over a 1 second period also in steps of 1 sample.

The third plot is a Haar wavelet transform calculated at diadic scales. The Haar wavelet plot was produced using the function `cwt` (provided in [80]). The scales were related to frequencies using `scal2frq` command. The magnitude of the wavelet coefficients is displayed as a grayscale image where white is the minimum value in the plot and black is the maximum.

The fourth plot is a spectrogram of the filtered signal. In this case, the spectrogram is calculated using the function call `specgram` (provided in [84]) with a 256pt FFT, 64pt shift and 256pt Hanning window. Only the 0 to 11Hz range is plotted. Like the wavelet plot, the magnitude of the spectrogram is also a grayscale image where white is minimum and black is maximum.

Note that in both the wavelet and the spectrogram plots, the image is scaled to the data in view. The absolute magnitude of the signal is given by the Pk-pk and RMS values.

(The initial algorithm implementation on Health Card in Chapter 6 used 128pt shift. This introduces a complication which is explained in Appendix C. For this offline analysis, a smaller shift of 64pts was adopted)

5.4 RESULTS

Each analysis was performed for the entire length of the data set. The results files are included in the attached compact disk CD01. The files are compatible with Adobe Reader™ which is available for download free of charge from [85].

Table 5-3 CD01 File Names and Descriptions

File	Description
CD01:\FBY(01-04 to 06-08).pdf	Front Body Lateral Acceleration for files 01-04 to 06-08 (entire data length)
CD01:\FBZ(01-04 to 06-08).pdf	Front Body Vertical Acceleration for files 01-04 to 06-08 (entire data length)
CD01:\FSY(01-04 to 06-08).pdf	Front Sideframes Lateral Acceleration for files 01-04 to 06-08 (entire data length)

To view the analysis results for the entire length of the data:

1. open the file in Adobe Reader™
2. set the view to “fit page”
3. use scroll up or down to progress through the data

Figure 5-10 can be used as an index to the data.

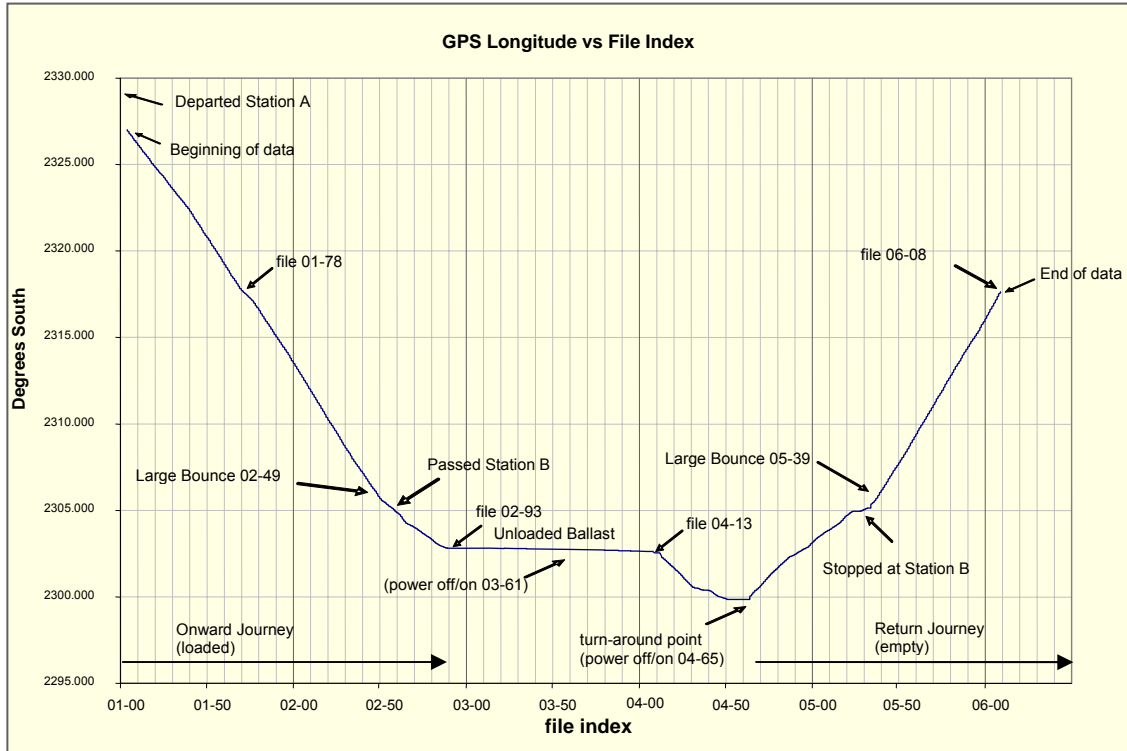


Figure 5-10 Journey Description with File Locations

5.5 DISCUSSION OF RESULTS

5.5.1 Detection of Bogie Hunting

Section 2.2.1.3, discussed whether bogie lateral oscillation could be reliably detected from the wagon body. The data shows consistently that periodic lateral accelerations measured at the bogie was accompanied by an equal or larger magnitude oscillation at the wagon body. An example for the unloaded case is shown in Figure 5-11 and the loaded case in Figure 5-12. This was consistent throughout the data in loaded and unloaded states.

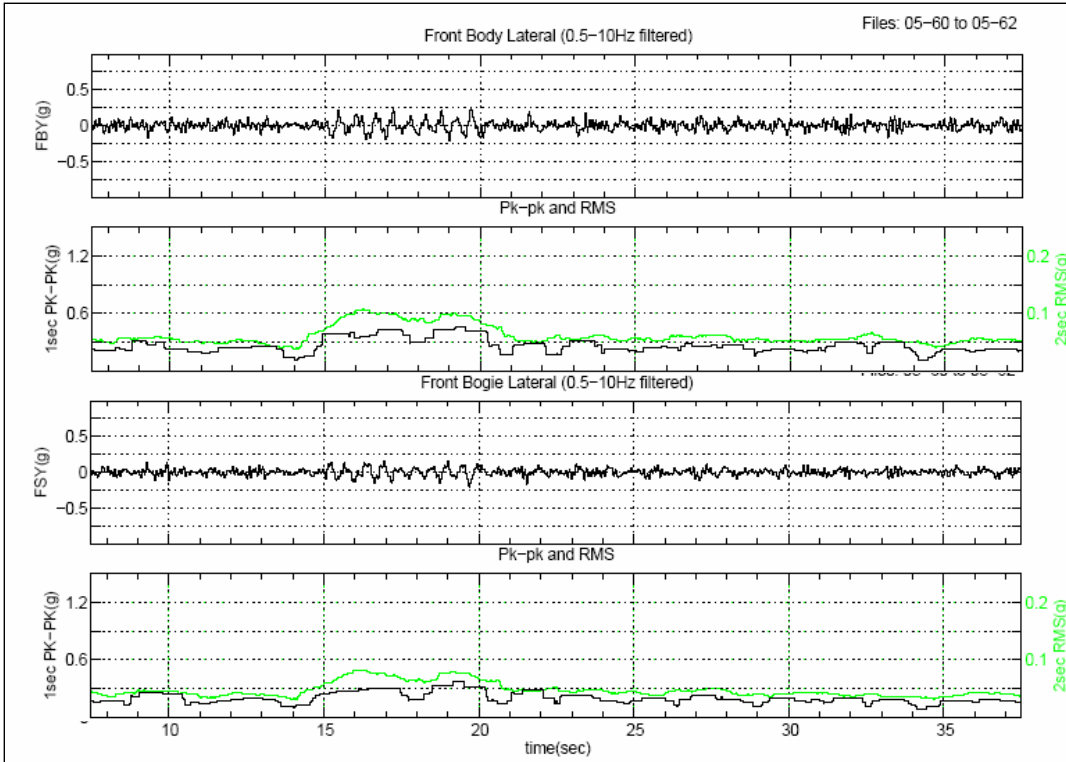


Figure 5-11 Body Lateral (top) vs Bogie lateral (bottom) during lateral oscillation of an empty wagon

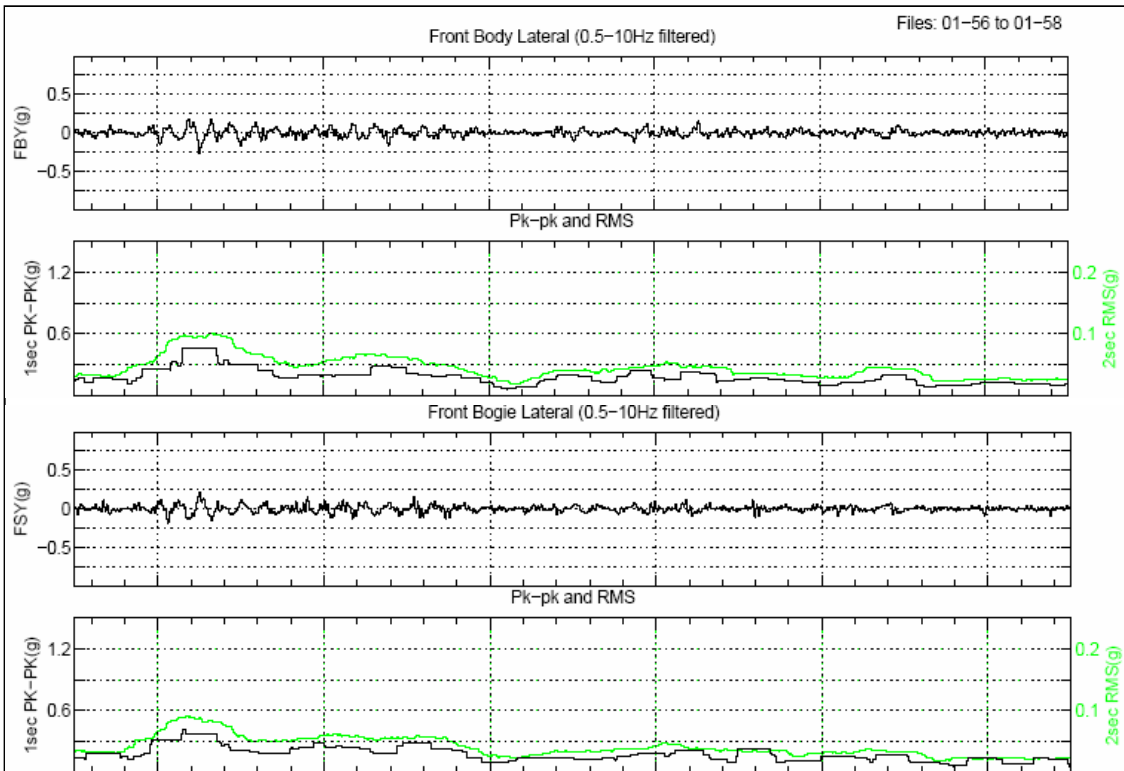


Figure 5-12 Body Lateral (top) vs Bogie lateral (bottom) during lateral oscillation of a loaded wagon

The standards vehicle acceptance tests, defined in [7] and [9], used accelerometers on the wagon body to detect instances of unacceptable bogie hunting. Unacceptable hunting was defined as “*Sustained lateral sinusoidal acceleration of frequency greater than 0.5 Hz, producing average peak accelerations at the bogie centre in excess of +/- 0.35g over a period of at least 10 seconds.*” with 10Hz filtering. This equates to a lateral peak to peak value of 0.7g sustained for more than 10 seconds. There were no instances in the data of bogie hunting under this definition. However, there were many instances of lateral oscillation at lower levels and durations.

For the empty wagon, there were two clear modes of lateral oscillation throughout the data. One was between 1.5Hz and 2.0Hz. The other was between 5Hz and 6Hz. The higher frequency mode was not sustained for long periods. As discussed in Section 4.1.2, the lateral displacements for a low frequency waveform are very large compared to high frequency vibrations. The lower frequency oscillation is certainly the more serious artefact that relates to hunting.

Figure 5-13 is an example location where peak or RMS measures would not be sufficient to discern between the oscillation that relates to hunting (right) and higher frequency vibrations (left). The RMS and peak levels are equivalent in each case. However the time frequency representation of the signal clearly reveals the difference between the two sections of the signals in their local spectra.

The lower frequency hunting signal could be detected by first filtering the signal at, for example, 4 Hz before measuring RMS or peak levels. However, the higher frequency content may still be of interest. In the case of Figure 5-14, the high frequency information at the start of the oscillation indicates that the oscillation was initiated by a

sharp lateral irregularity. Thus, the time location of the higher frequency, relative to the lower oscillation may also reveal useful information. Pre-filtering the signal to a lower frequency would have removed this information.

Filtering at a lower level may also eliminate detection of other modes of bogie hunting. As mentioned in Section 2.2.1.2, there are generally two modes of lateral instability. One involves vehicle body oscillation, the other involves oscillation of bogie components at higher speeds. The time-frequency analysis maintains the flexibility to detect and discern different modes of oscillation.

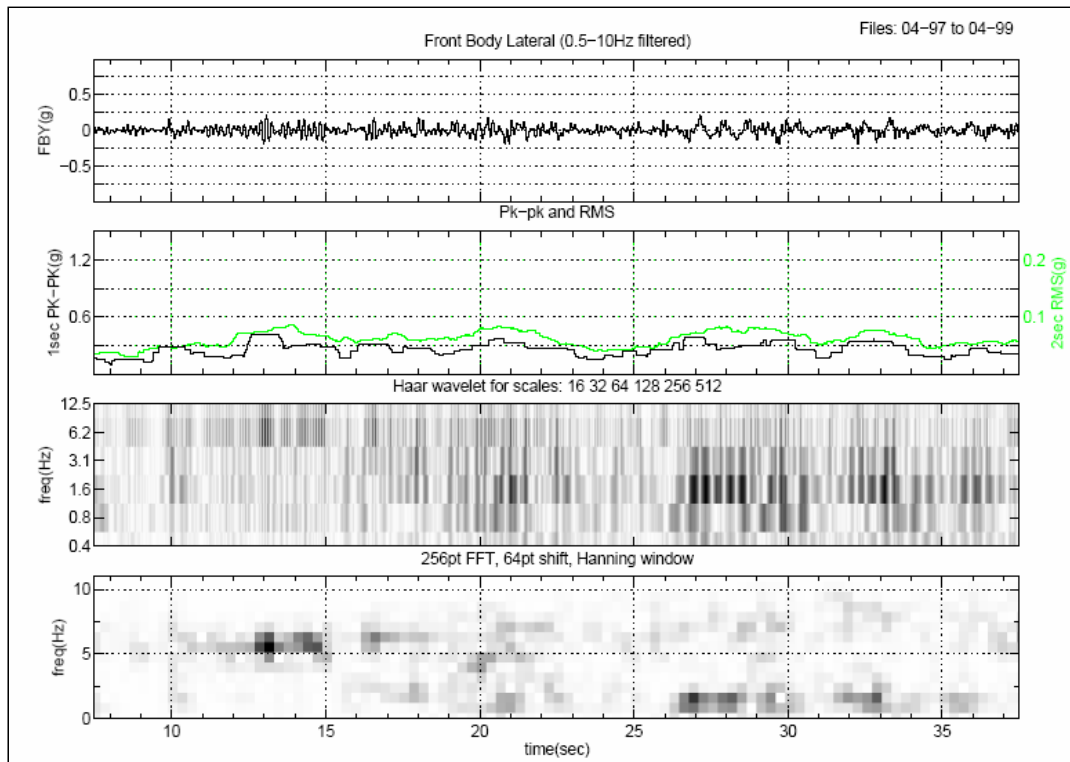


Figure 5-13 Discerning Hunting from Other Lateral Oscillations

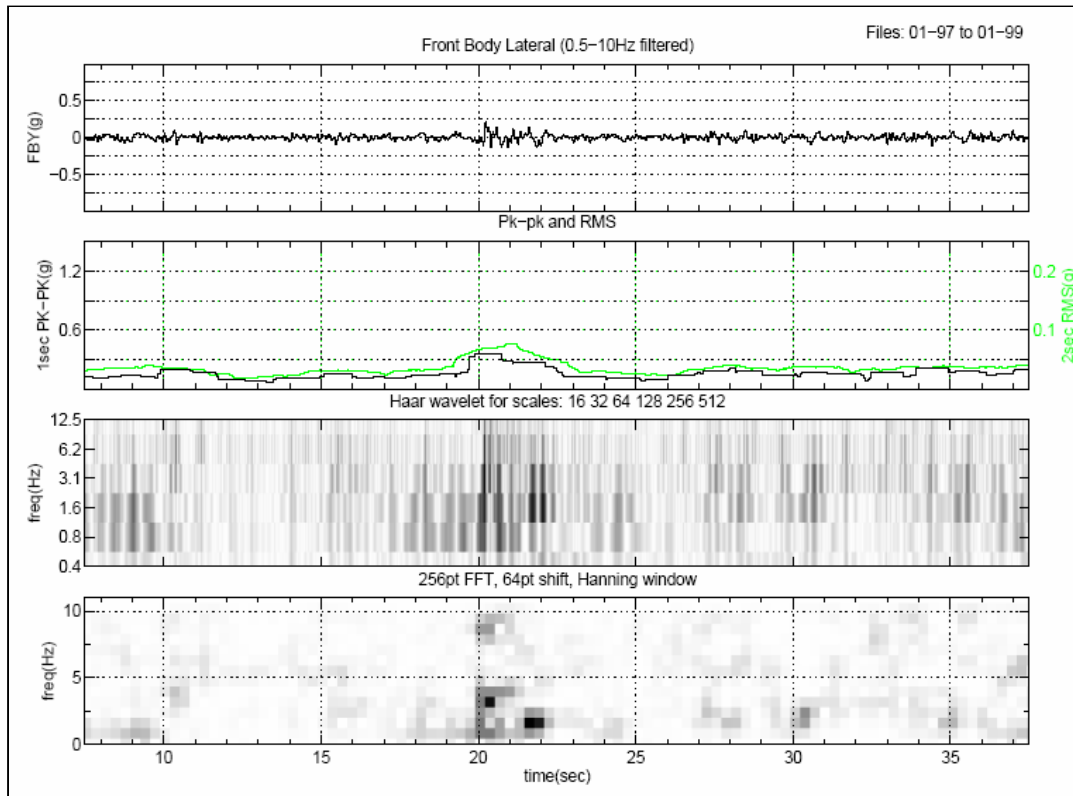


Figure 5-14 Hunting Initiated By Irregularity

5.5.2 Detection of Severe Vehicle-Track Interaction

There was one outstanding case of severe vehicle-track interaction that occurred on the data acquisition. It is not likely that this was caused by resonant interaction because equally poor ride was experienced on the neighbouring test equipment car which had significantly different geometry and suspension characteristics. This ‘large bounce’ site was used in Section 4.1.2 to introduce the need for frequency based analysis of acceleration signals. Figure 4-3 compared the acceleration signal with velocity and displacement signals produced by integration.

In Figure 5-15 below, the vertical acceleration at the front centre of the wagon is analysed. In the spectrogram, the large ‘spot’ beginning at 16sec is the time-frequency feature caused by the large bounce event. The signals at 26sec and 29sec are less severe events. The RMS and Pk-pk levels show very little difference between the three

locations. However, in the time-frequency plane, the events are clearly differentiated. The same site on the return journey with an empty wagon is shown in Figure 5-16.

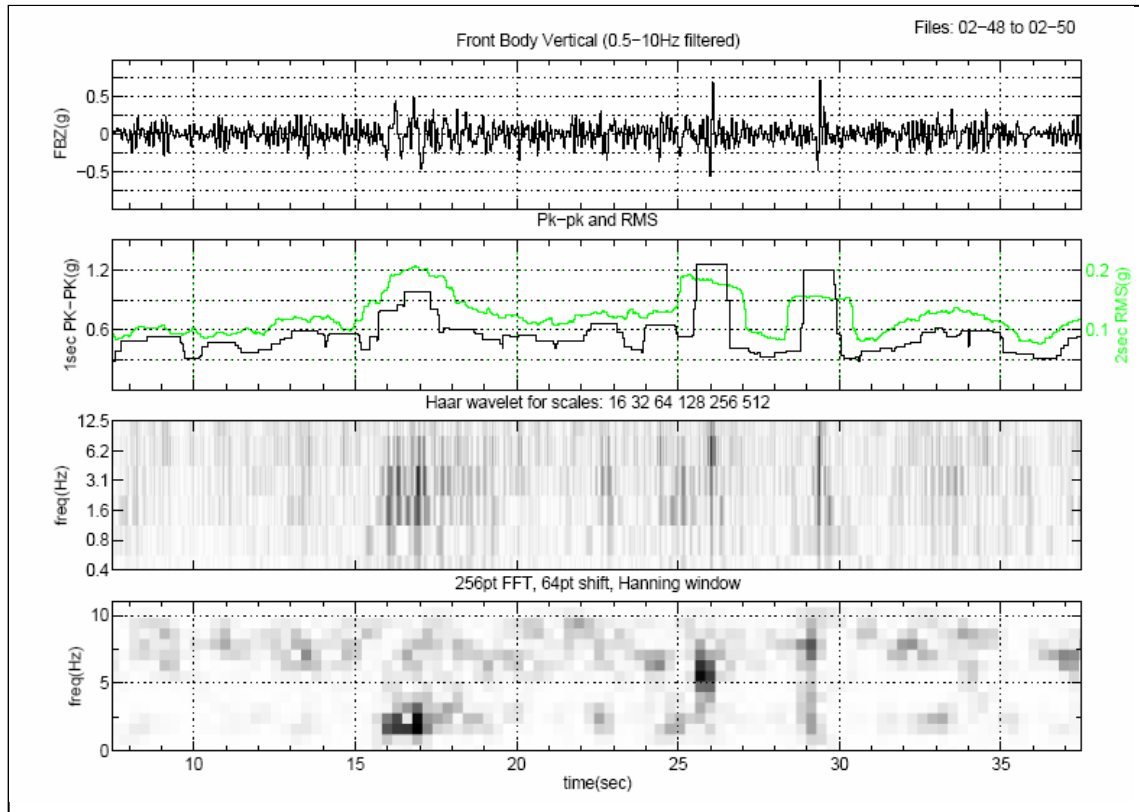


Figure 5-15 “Large Bounce” Site, Onward Journey, Loaded

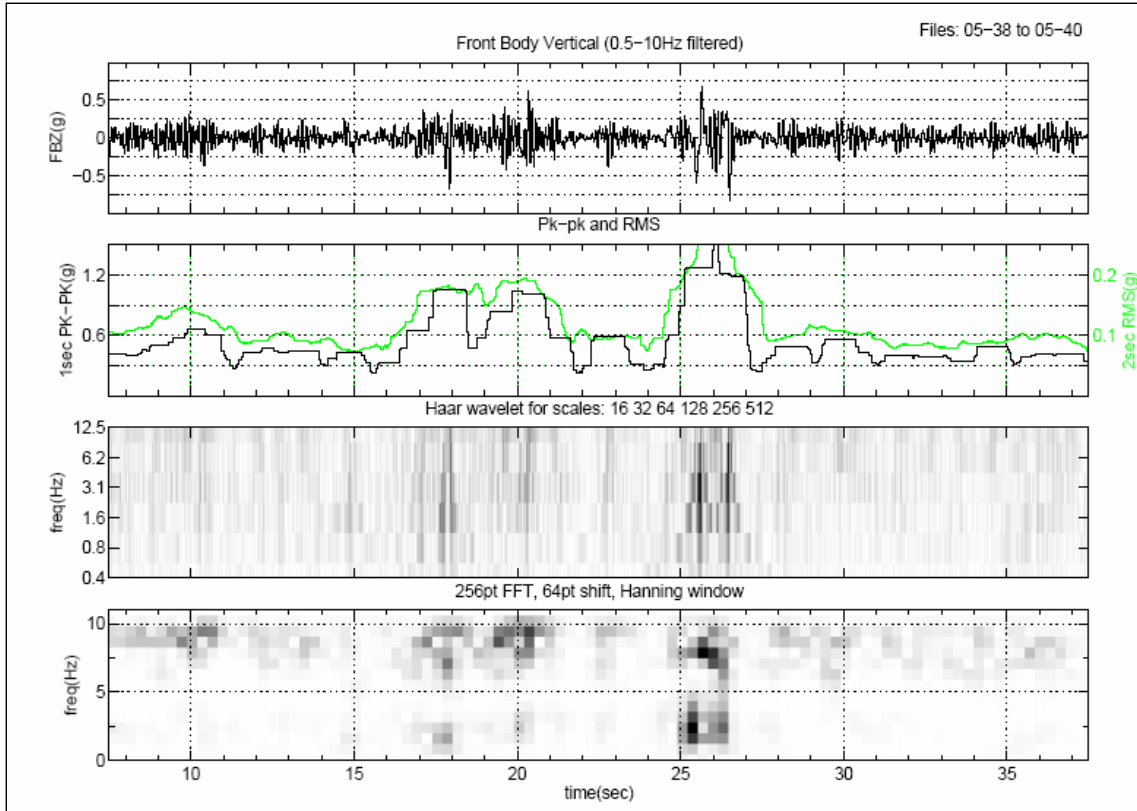


Figure 5-16 “Large Bounce” Site, Return Journey, Unloaded

5.5.3 Deficiencies in Australian and North American Standard Measures

Some deficiencies in the North American and Australian standards were identified in Sections 4.1.1 and 4.1.2 and confirmed in the results of this chapter. The standard acceleration limits applied to vehicle acceptance in the Australian Standard and ride monitoring in the North American standard are specified as 0.5-10Hz filtered RMS and peak acceleration levels.

Section 4.1.2 established that the lower frequency oscillations will produce small magnitude accelerations even with large displacements. On the other hand, higher frequency oscillations will produce large magnitude acceleration signals even though the displacements are small. The Australian and North American standard RMS and peak measures give equal weighting to all frequencies in the 0.5-10Hz range.

Sections 4.1.2 and 5.5.2 showed that cases of severe vertical interaction create signals in the lower frequencies that are hidden in the 0.5-10Hz filtered peak and RMS measures. The lower frequency accelerations relate to larger lateral displacements and are more likely to relate to wheel unloading for periods long enough to derail a wheelset.

The results in Section 5.5.1 demonstrated that there are two predominant modes of lateral oscillation which contribute equally to the RMS magnitude and occur at different frequency bands in the 0.5-10Hz range. The lower frequency mode is most likely to increase derailment risk because it increases lateral forces for longer periods, whereas the higher frequency mode will increase bogie component wear and wheel-rail wear. The lower frequency mode, hidden by the 0.5-10Hz RMS magnitude, is clearly the more serious behaviour.

This means that the Australian and North American standard measures could fail to detect some dangerously large dynamic events. This finding suggests that the Australian and North American standards need to be reviewed with more careful consideration given to the lower frequency oscillations.

The European Standards [27], summarised in Table 4-3, apply separate limits for Safety and Maintenance, with different filter cut-off frequencies specified. The Safety limits have lower filtering cut-off frequencies than the maintenance (behavioural) limits. This approach is more consistent with the findings of this research.

5.5.4 Detection of Loading State from Spectral Average

The data acquisition was performed with a loaded wagon for the onward journey, and an empty wagon for the return journey. It would be useful for Health Card to be able to detect whether the wagon is unloaded or loaded from the acceleration signals.

According to Table 2-4 on page 22 the resonant modes frequencies of the wagon body should exhibit a shift in frequency. This should be reflected in the general overview of the local spectra.

Figure 5-17 and Figure 5-18 show the analysis of the roll signal for the full wagon and the empty wagon respectively travelling over the same section of track in opposite directions at the same speed. This analysis page allowed a longer selection of files in one page. An estimate of the average frequency content was obtained by averaging each vertical lines of the spectrogram over the period of time covered by the analysis page. The top plot is the 0-10Hz filtered signal. The second plot is the RMS and Pk-pk values. The third plot is the spectrogram with the same parameters as before. The last plot is the average spectrum (solid line) and the standard deviation (dashed line).

The first peak in the roll signal shows a change in frequency from 1.5Hz in the loaded state, to 2.5Hz in the unloaded state. The change is not as clear as 1.237Hz to 5.426Hz predicted in Table 2-4. The other distinction is the magnitude of the spectral peaks (note the scaling). There is a tenfold increase in magnitude of the peaks relative to the baseline magnitude.

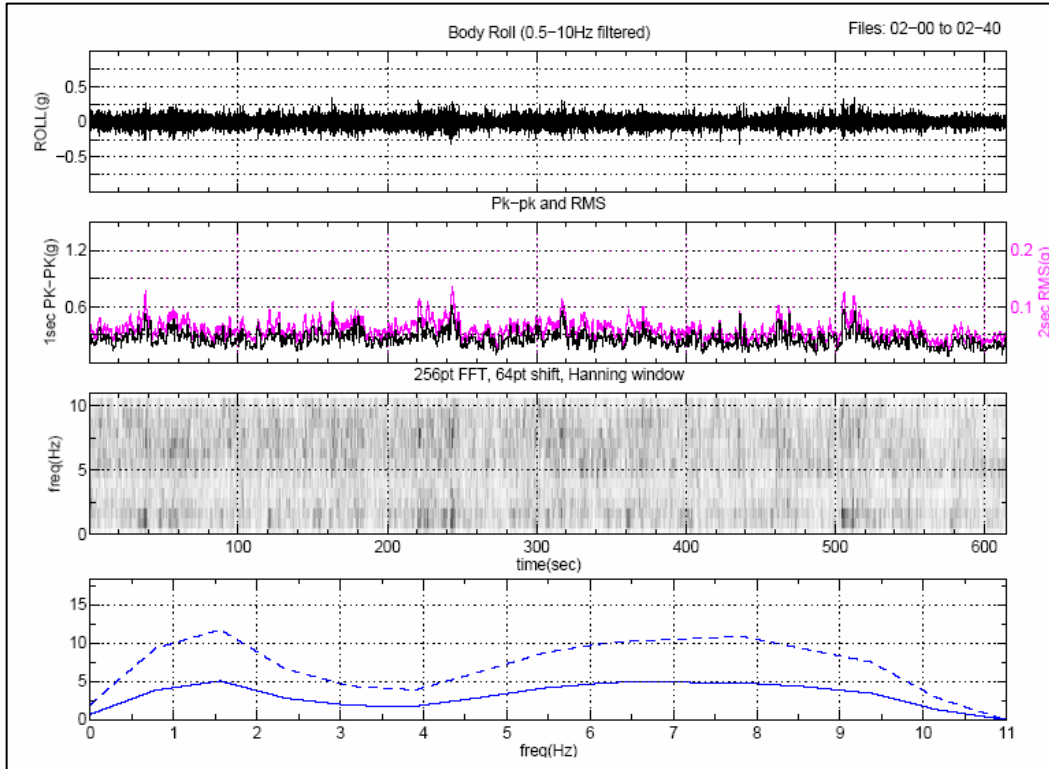


Figure 5-17 Average of Local Spectra for Loaded Wagon on Onward Journey

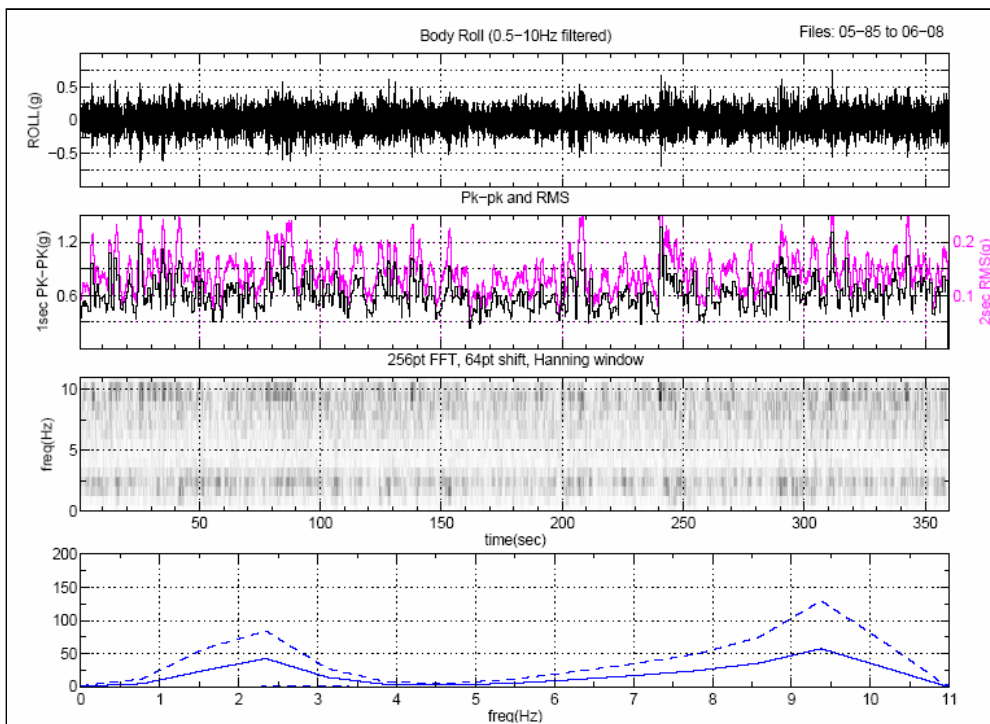


Figure 5-18 Average of Local Spectra for Empty Wagon on Return Journey

These results demonstrate how a change in load mass is reflected in the average spectrum. It follows that, if load mass is constant or known, then a change in another wagon parameter would also produce a detectable change in the average spectrum. Section 2.3.1 identified that wagon performance can be affected by a number of variable factors in the wagon, including wheel profile, bogie rotation resistance, and suspension characteristics.

5.5.5 Comparison of Wavelet and Fourier Time-Frequency Analysis

Fourier and wavelet analysis are compared throughout the data analysis results on CD01. Although the majority of literature comparing the two techniques promoted wavelets over Fourier analysis, the benefits in this application are not clear.

Fourier analysis revealed a lot of information in the 5 - 10Hz frequency region which is less clear in the wavelet analysis. This can be seen in Figure 5-15. Note that the 5 to 10Hz region is analysed by a single wavelet scale centred around 6.2Hz. The Fourier analysis divides the region into 7 bands. The Fourier analysis would appear to be more useful in detecting characteristic conditions that can be traced to bogie component oscillation frequencies that occur in the 5 to 10Hz region.

The wavelet analysis performed better than Fourier at locating sharp signals exactly in time. This is evident in Figure 5-14 where the wavelet analysis detects the precise location of the sharp spike at the initiation of the damped oscillation. This is consistent with the majority of the literature where wavelets have been very successful in detecting the exact time location of higher frequency transient signals superimposed on lower frequency periodic signals. This is particularly useful in applications such as detecting fault transients on fixed frequency a.c. waveforms.

In the case of a railway wagon running on track, sharp transient vibrations occur at every rail joint, and are the most normal signal present. As developed in Chapter 2, the behaviours that are most desirable to detect are periodic oscillations and low frequency vibrations. In these cases, it is the periodic frequencies, not the sharp transients, which are desirable to detect.

Fourier time-frequency analysis is adequate for the application at this stage of the research. In the literature, wavelets have been applied to many established fields and highly controlled experiments showing notable benefits over the conventional Fourier time-frequency analysis. However, understanding in these fields has been established using Fourier time-frequency analysis. Health Card research has not reached the stage of refinement that these other fields have reached. It therefore may be valuable to re-introduce wavelets at a later stage for specific detection of some known specific fault signals.

5.6 CONCLUSION

A field data acquisition on an in-service ballast wagon has been presented and time-frequency analysis has been applied to the acquired data. STDFT spectrogram and Haar Wavelet analysis has been applied and compared with RMS and peak measures specified in relevant Australian and North American standards. The results demonstrate a number of findings.

The results prove that bogie lateral oscillation can be reliably detected from the wagon body. Although no instances of the standard definition of hunting occurred during the data acquisition, many instances of lateral oscillation did occur. Throughout the data, the magnitude of lateral oscillations was equal or larger in the body than in the bogies.

The results demonstrate the advantage of time frequency analysis over the standard 0.5-10Hz filtered RMS and peak to peak levels. There are clearly two predominant modes of lateral oscillation in the data, which contribute equally to the RMS magnitude. The time frequency analysis clearly discerns the features of the signal based upon its frequency content. Furthermore, cases of severe wagon-track interaction can be detected clearly in the time-frequency plane by observing the lower frequencies, where little distinction is seen in the 0.5 -10Hz Pk-pk and RMS measures.

This chapter has also highlighted some deficiency in the measures specified in the Australian and North American standard measures which could fail to detect some dangerously large dynamic events. This finding suggests that the standards need to be reviewed with more careful consideration given to the lower frequency oscillations. A strategy similar to the European Standard should be adopted where safety related limits are specified with lower frequency cut-offs.

The results show that it is possible to detect loading state from the time-frequency information. Averaging the vertical lines of the spectrogram yielded an average spectral content in the signal. The difference between a loaded wagon and an empty wagon is clearly in the peaks of the spectral average. This measure could be used to detect whether the wagon is loaded or unloaded. It is postulated that, if the wagon mass is known, changes in other wagon parameters could be detected in the same way.

Fourier and Wavelet analysis were compared throughout the results. The benefits of wavelet analysis over Fourier analysis are not clear in this application. Fourier analysis revealed a lot of information in the 5 - 10Hz frequency region which is represented by a single coefficient in the wavelet analysis. The wavelet analysis performed better than

Fourier at locating sharp signals exactly in time. However it is not the location of sharp transients but rather the presence of periodic oscillations that are characteristic of lateral bogie instability and resonant interaction between the wagon and the track. Fourier time-frequency analysis is adequate for the application at this stage of the research however it may be valuable to re-introduce wavelets at a later stage for detection of some known specific fault signals.

This chapter has shown significant advantage for using time-frequency analysis as a basis for signal analysis onboard the Health Card device. The next chapter proves that STDFT spectrogram analysis is feasible given the constraints of the Health Card device by implementing it on the prototype.

6 Implementing Short Term Fourier Analysis on Health Card

A signal analysis algorithm was required for the prototype Health Card system to run for initial testing. This section describes the online algorithm developed and specified as part of this research. The algorithm description is given in the same level of detail specified to the device programmer.

6.1 PURPOSE

The purpose of this algorithm was to allow four Health Cards to run in a multi wagon network for an initial proof of concept test and ongoing testing of the capabilities of the integrated system. A secondary purpose was to verify that STDFT time-frequency analysis was feasible given the processing constraints of the prototype system.

6.2 REQUIREMENTS

The algorithm was required to measure six degrees of freedom from the eight accelerometer axes and provide single values to represent motion in each degree of freedom. The network protocol, also under development, allowed for a maximum of one 16bit value per degree of freedom to be transmitted approximately every half second.

6.3 IMPLEMENTATION OF STDFT ANALYSIS

The algorithm read the acceleration signals taken from the wagon body and related them into 6 degrees of freedom (DOF): Roll, Pitch, Yaw, Vertical, Lateral, and Longitudinal, according to Figure 3-5 in Section 3.2.4. A 256pt FFT with 128pt shift was calculated on each of the 6 DOF signals every 640msec.

The PWM signals were measured using a capture and compare port to count the duration of the pulses. An interrupt driven routine sampled the 8 signals and refreshed 8 input buffers every 5msec. Once a sweep of the input channels was complete, the data was placed into eight 256 x 16 bit cyclic buffers, one buffer per channel. Each buffer was organised into two blocks of 128 16 bit values. The current location in each buffer was maintained by an 8 bit pointer. When the buffer pointer reached 128, or rolled over to 0, the last block of 128 values to be written became ready to process. At a sampling rate of 200 s/s, the blocks became ready to process every 640ms.

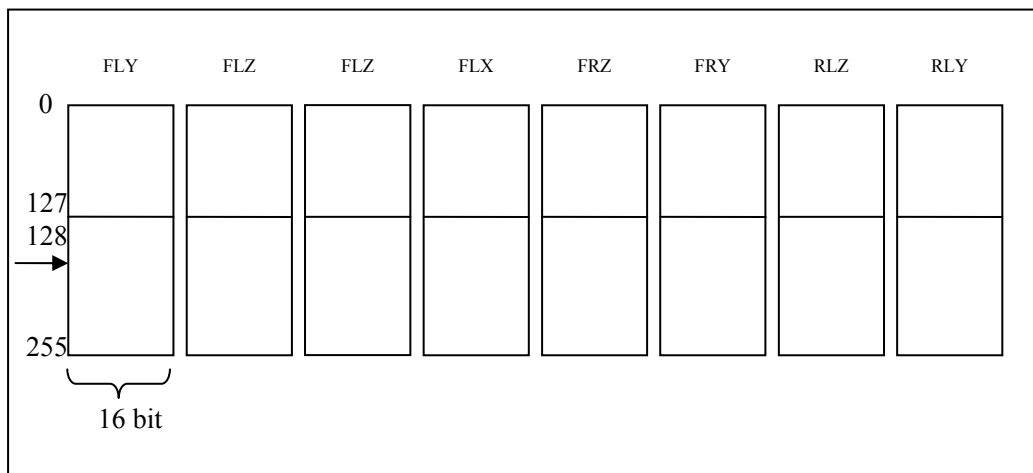


Figure 6-1 Raw Data Buffers – 8 Channels

When each block of 128 16 bit values became ready to process, the following tasks were executed:

The quasistatic component was estimated by an accumulated average. Each block of 128 values was averaged to produce \bar{x}_{128} . The results of the current average and the previous accumulated value were averaged to obtain the current value.

$$\bar{x}_{\text{accumulated}} = (\bar{x}_{\text{accumulated}} + \bar{x}_{128}) / 2$$

$$\text{where } \bar{x}_{128} = \left(\frac{1}{128} \sum_{i=1}^{128} x_i \right)$$

(The divide by 2 and divide by 128 were done efficiently by right-shifting the binary result).

7 blocks were used to calculate accelerations in 6 degrees of freedom (DOF): Roll, Pitch, Yaw, Vertical, Lateral, and Longitudinal according to Figure 3-5 in Section 3.2.4.

The scaling factors w , l and d were ignored here. These factors may not be powers of two, and thus could not be divided efficiently. Rather than perform an integer divide on every sample, it was much more efficient to scale the final detection thresholds in the master device. The quasistatic values were also removed from the signals at this stage.

$$\text{ROLL} = \text{FLZ} - \text{average}(\text{FLZ}) - \text{FRZ} + \text{average}(\text{FRZ})$$

$$\text{PITCH} = \text{FLZ} - \text{average}(\text{FLZ}) - \text{RLZ} + \text{average}(\text{RLZ})$$

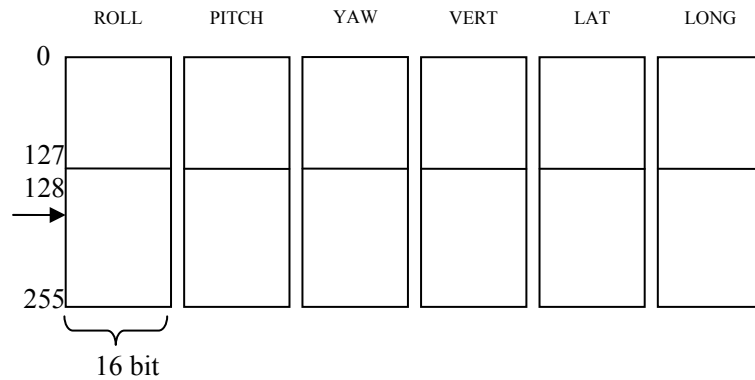
$$\text{YAW} = \text{FRY} - \text{average}(\text{FRY}) - \text{RLY} + \text{average}(\text{RLY})$$

$$\text{VERT} = [\text{FRZ} - \text{average}(\text{FRZ}) + \text{RLZ} - \text{average}(\text{RLZ})]/2$$

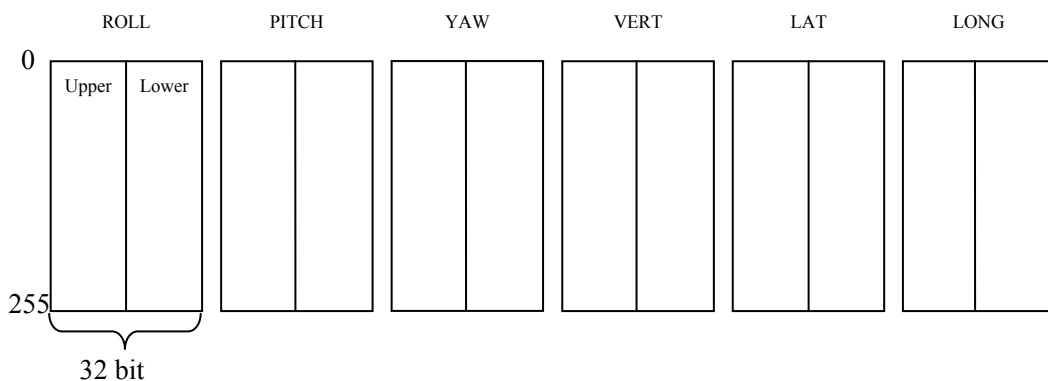
$$\text{LAT} = [\text{FRZ} - \text{average}(\text{FRZ}) + \text{RLZ} - \text{average}(\text{RLZ})]/2$$

$$\text{LONG} = \text{FLX} - \text{average}(\text{FLX})$$

The results were placed in six 256 x 16bit buffers which are organised into two blocks of 128 values, such that the oldest block was always overwritten.



Once the pointer reached 128 or rolled over to 0, the six 256 value blocks were copied into six 256 x 32 bit FFT buffers. During the copy operation, the blocks of 128 were rearranged into time sequential order. In the FFT buffers the upper 16 bits contained the input values and the lower 16 bits were set to zero. The FFT function was then called for each of the 6 blocks. The FFT function read the input from the buffer, performed the FFT with a Hanning window and wrote the result back into the same location. The upper 16 bits became the real component of the result and the lower 16 bits became the imaginary component. The Power Spectrum function was then called for each buffer. The Power Spectrum function took the 16bit complex values and returned 32bit real values in their place.



After the FFT and Power Spectrum functions executed, each buffer contained the 256 pt $|FFT|^2$ of one DOF as 32bit values, which constitutes one vertical line of the spectrogram of the signal.

6.4 OUTPUT VARIABLE

The network protocol allowed a maximum of one 16bit value per degree of freedom every half second. To achieve the required data reduction with STDFT analysis, the fully developed Health Card algorithm would require a pattern recognition stage as shown in Figure 6-2 below.

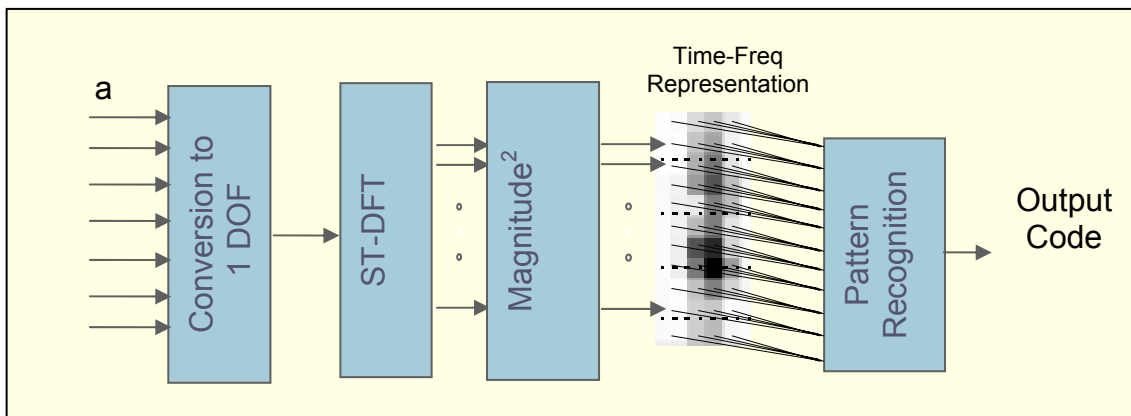


Figure 6-2 Concept of Time Frequency Analysis with Pattern Recognition to Achieve Health Card Requirements

Automatic pattern recognition is an area of research which is outside the scope of this thesis. However, some literature review was undertaken and a recommendation for automated detection of time-frequency signatures is detailed in Section 6.7.

For the purpose of testing the prototype system, an output variable comparable to existing standard limits was acceptable. The standard limits identified in Section 4.1.1 are specified in terms of peak and RMS values. Peak values cannot be obtained directly

from the frequency domain coefficients without applying an inverse FFT; however RMS values can be obtained directly from the FFT coefficients.

According to Parseval's theorem detailed in [28], the mean square (MS) value of the time domain signal can be calculated in the frequency domain by eq. 6-1 where the right hand side is known as the *spectral energy*

$$\frac{1}{N} \sum_{n=0}^{N-1} x^2(n) = \sum_{k=0}^{N-1} |X(k)|^2$$

eq. 6-1

The RMS value is simply the square root of the MS value. The MS value for the 0.5-10Hz component of the signal can be calculated by summing the coefficients that cover that frequency range. (Note: the result is scaled by the MS value of the applied window function.)

The output variable chosen for this algorithm was the right hand side of eq. 6-1 for 0.5-10Hz region of the signal. The scaling and square-root operation to calculate the RMS was left for the master system to save processing power on Health Card.

The algorithm first related the acceleration signals into 6 degrees of freedom (DOF): Roll, Pitch, Yaw, Vertical, Lateral, and Longitudinal, using the linear relationships identified in Figure 3-5. A 256pt FFT with 128pt shift was then calculated on each of the six degree of freedom signals every 640msec. A mean-square energy level was calculated on each local spectra over the 0.5-10Hz range. The value for each DOF was transmitted via the network to the master device every 640msec. Figure 6-3 is a graphical representation of the process for one degree of freedom, which in this case is

roll acceleration. The output variable was then calculated by adding first 13 coefficients to get the 0.5-10Hz energy value.

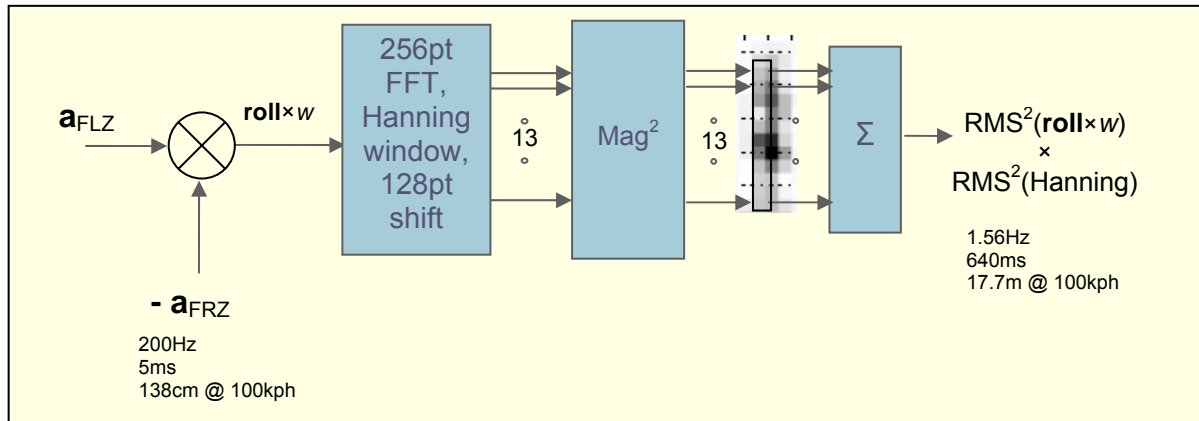


Figure 6-3 Overview of Algorithm for One Variable (roll)

Calculating the mean square or root mean square value from the FFT coefficients means that the signal can be assessed or adjusted in the frequency domain. Figure 6-4 is an example output of the equivalent algorithm applied offline to the body lateral signal in MATLAB. Here the frequency spectrum is summed over the 0.5-10Hz range and the variable follows the 0.5 -10Hz RMS.

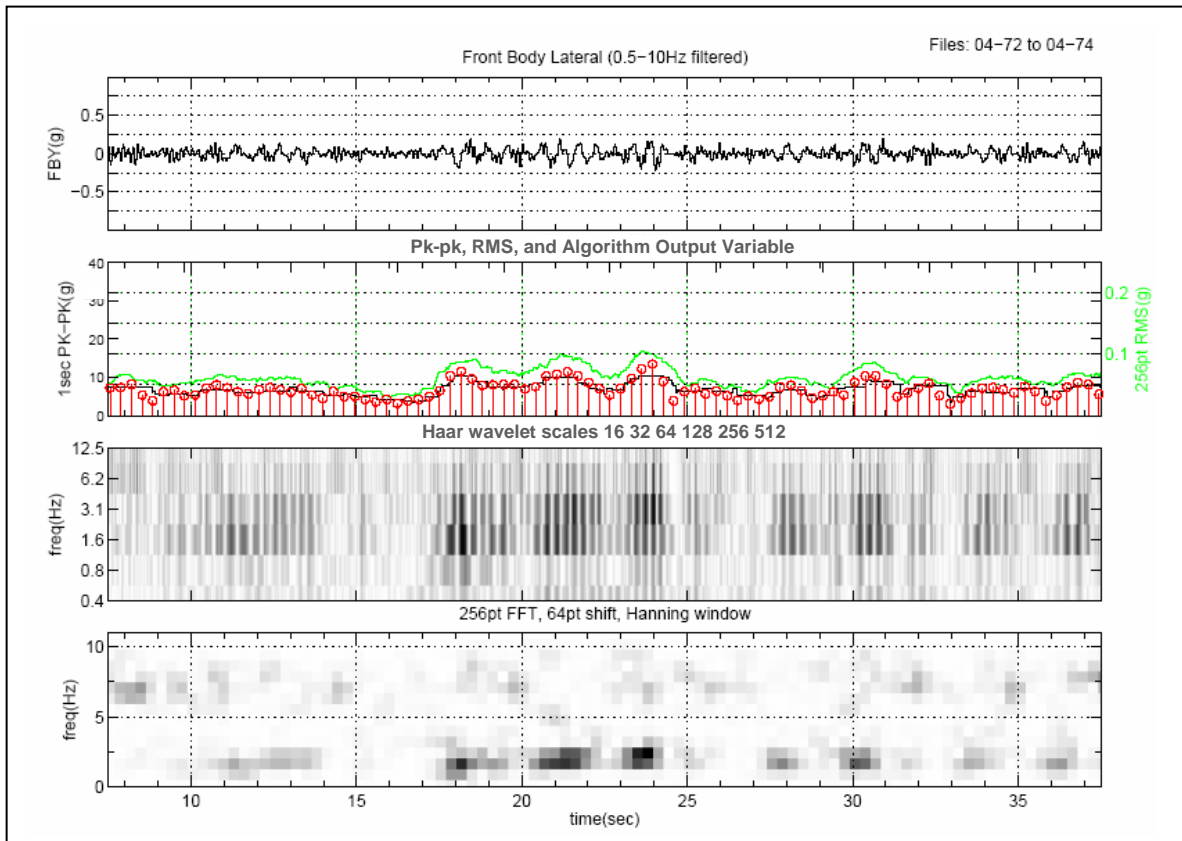


Figure 6-4 Algorithm Output Variable (0-10Hz) Lateral

Any weighting function can be chosen and multiplied with the local spectra. Narrower frequency bands can also be targeted, like those of Table 4-3 specified in European bogie wagon ride standards. Figure 6-5 is the same signal with the FFT coefficients summed over the 0-4Hz range. Similarly in Figure 6-7 the large bounce event that was analysed in Section 5.5.2 is clearly highlighted by limiting the energy to the 0-4Hz range.

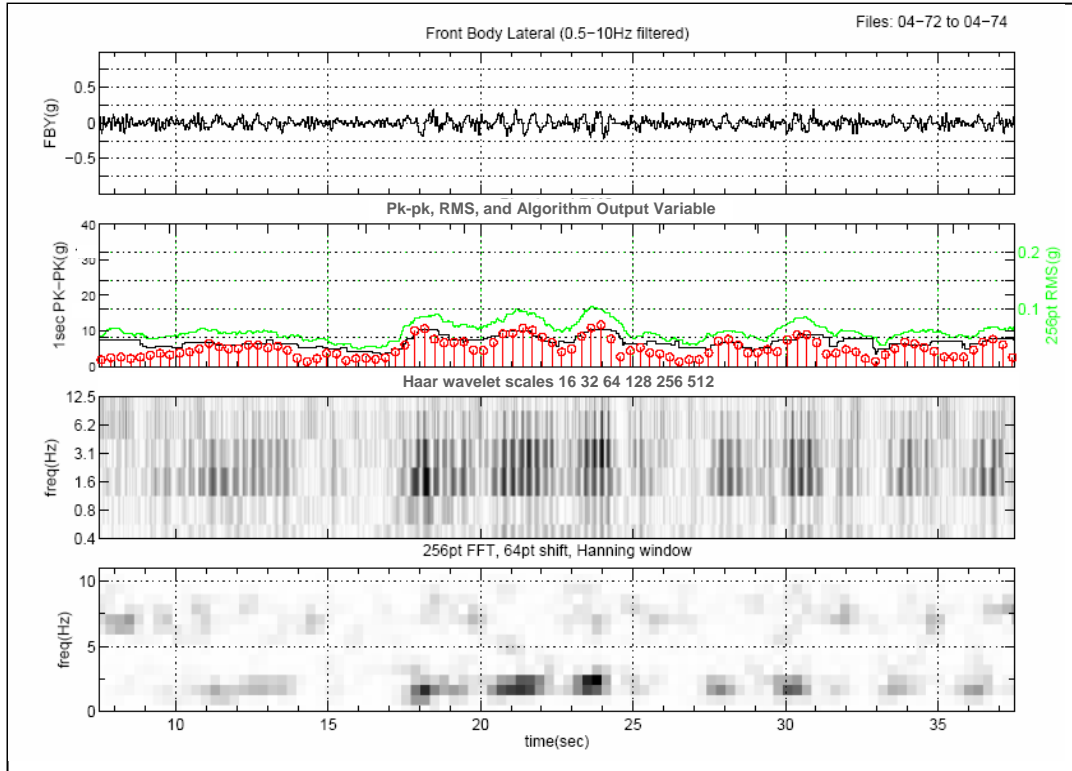


Figure 6-5 Algorithm Output Variable (0-5Hz) Lateral

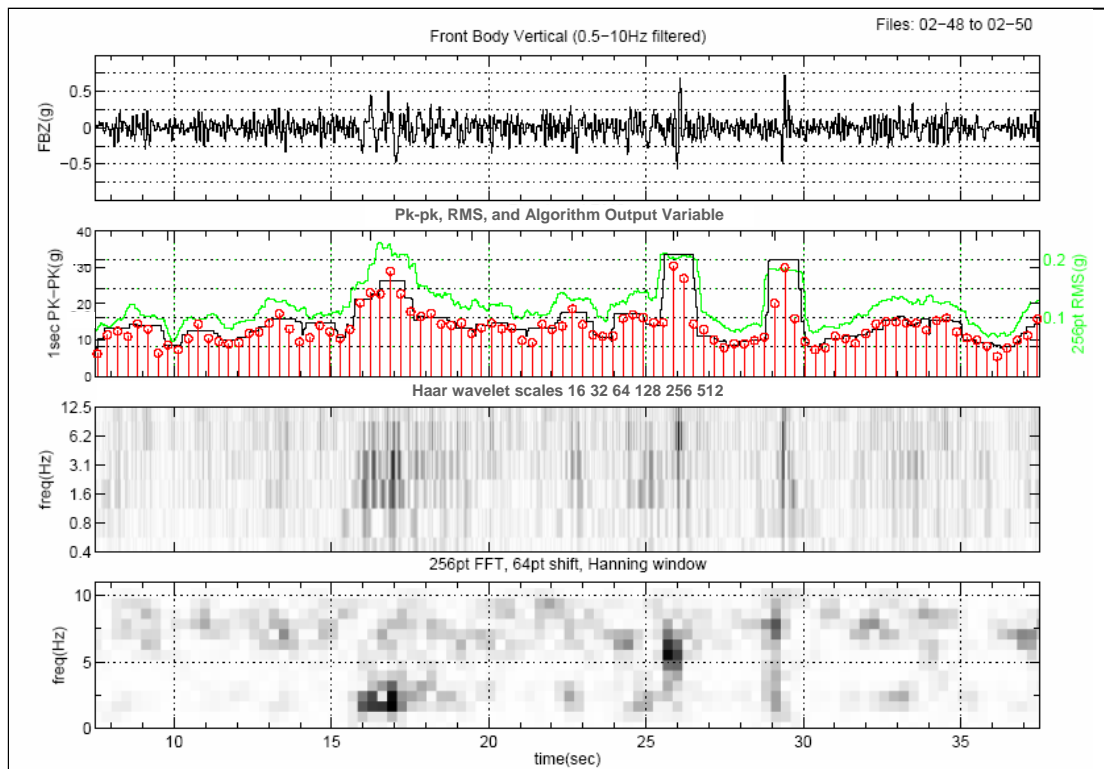


Figure 6-6 Algorithm Output Variable (0-10Hz) Vertical

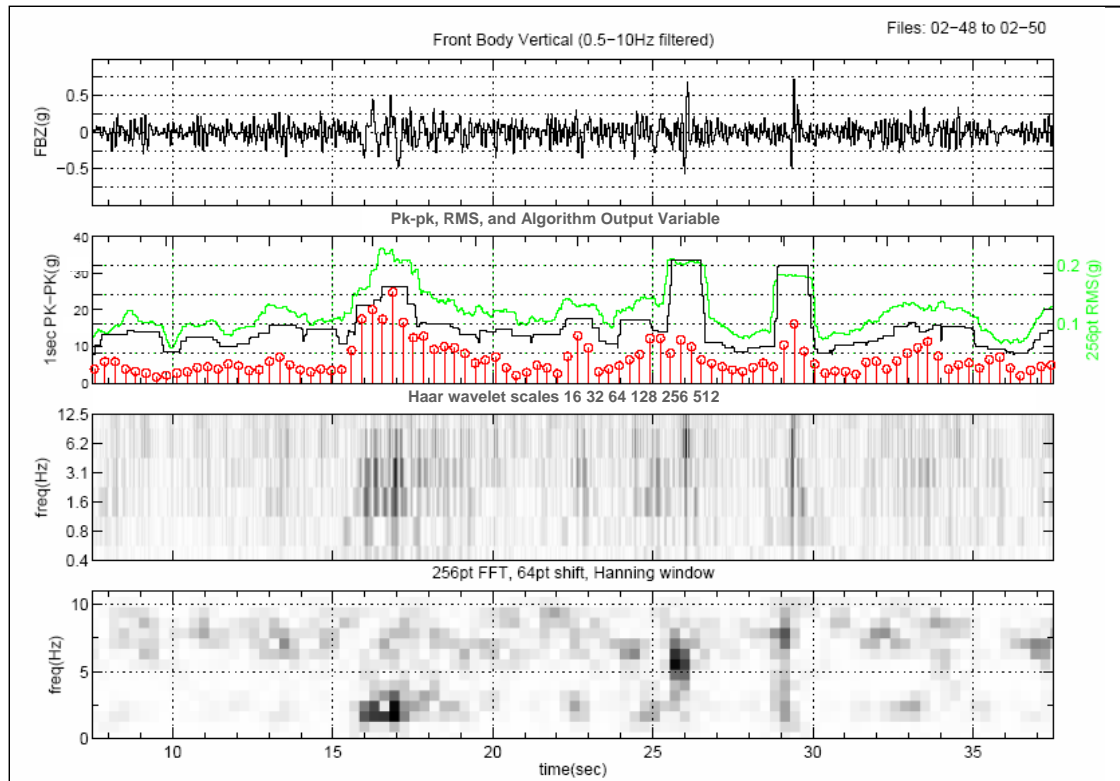


Figure 6-7 Algorithm Output Variable (0-4Hz) Vertical

Section 4.1.2 established that acceleration is related to velocity by $1/\omega$ and displacement by $1/\omega^2$. It is therefore possible to multiply the local spectra by $1/\omega$ or $1/\omega^2$ before summing the coefficients will give respective velocity signal energy or displacement signal energy. Taking the square root and dividing by a known scale factor for the window function will give the RMS values.

6.5 DISPLAY METHOD FOR THE MASTER DEVICE

The master device was emulated on a laptop computer. The program read data packets from the serial port which was linked to the Health Cards via a low power radio link. The program assembled the data into a scrolling display that showed the roll, pitch, yaw, bounce, lateral and longitudinal values as colour-scaled pixels.

6.6 DEMONSTRATION IN LABORATORY

The analysis code failed to run for the initial field test due to a compilation problem, therefore the working system could only be demonstrated in the laboratory. (Further field testing of algorithms was intended; however field tests were subject to several external factors. These included access to test wagons for installation of equipment, and the availability of a test car to carry personnel and test equipment during the test. Due to scheduling constraints and high rollingstock demand, further field tests did not eventuate within the time-frame of this research.)

The algorithm was tested by mounting the Health Card hardware on a coal wagon in the heavy testing laboratory at CQU. Figure 6-8 shows one of the three remote accelerometer units mounted which were mounted on the corners of the wagon. Figure 6-9 shows the battery powered Health Card unit wired to the remote units on the wagon. A radio transmitter in one of the accelerometer units was transmitting signal to the laptop computer on the bench. (Note: The system beside the laptop computer is the field data acquisition described in Chapter 5 and was not involved in this test.)

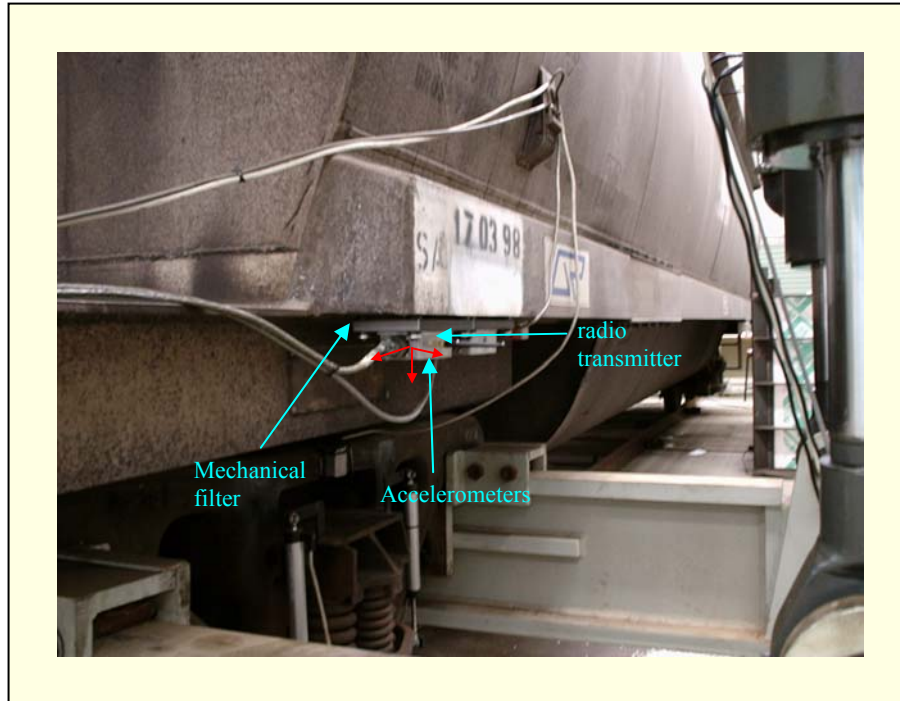


Figure 6-8: Health Card Accelerometer and Transmitter Mounted on a Wagon in the Laboratory

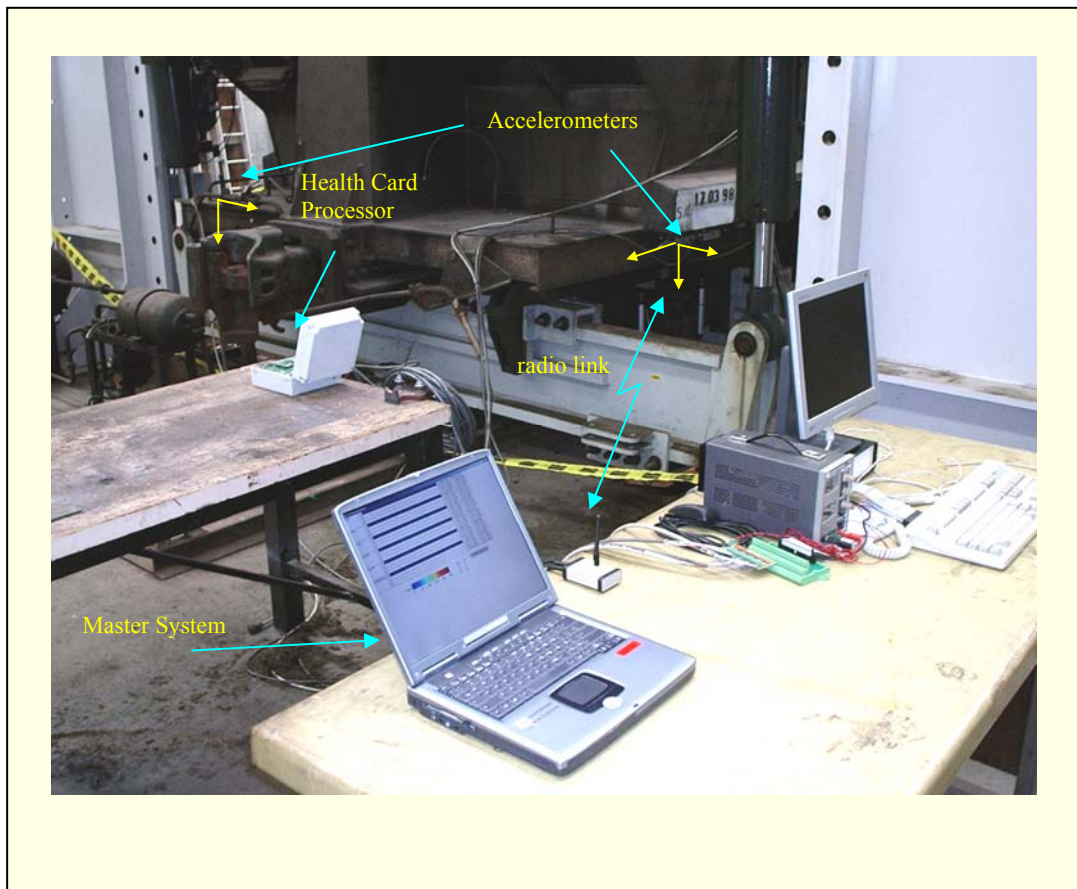


Figure 6-9 Master System on Laptop Receiving Health Card Data via Radio Link

The display on the laptop computer was designed for the in-train testing of four consecutive Health Cards to show the relative dynamics of the wagons. Figure 6-10 is a screen-shot of the display generated by manually exciting the roll mode on the wagon in the laboratory with a human body weight only. Approximately one minute of data is shown, as the data flows from right to left. The row numbers 1,2,3 & 4 are the outputs from the four wagons (only one wagon was active in the laboratory test). The major rows show the output variables for roll, pitch, yaw, vertical, lateral, and longitudinal modes respectively.

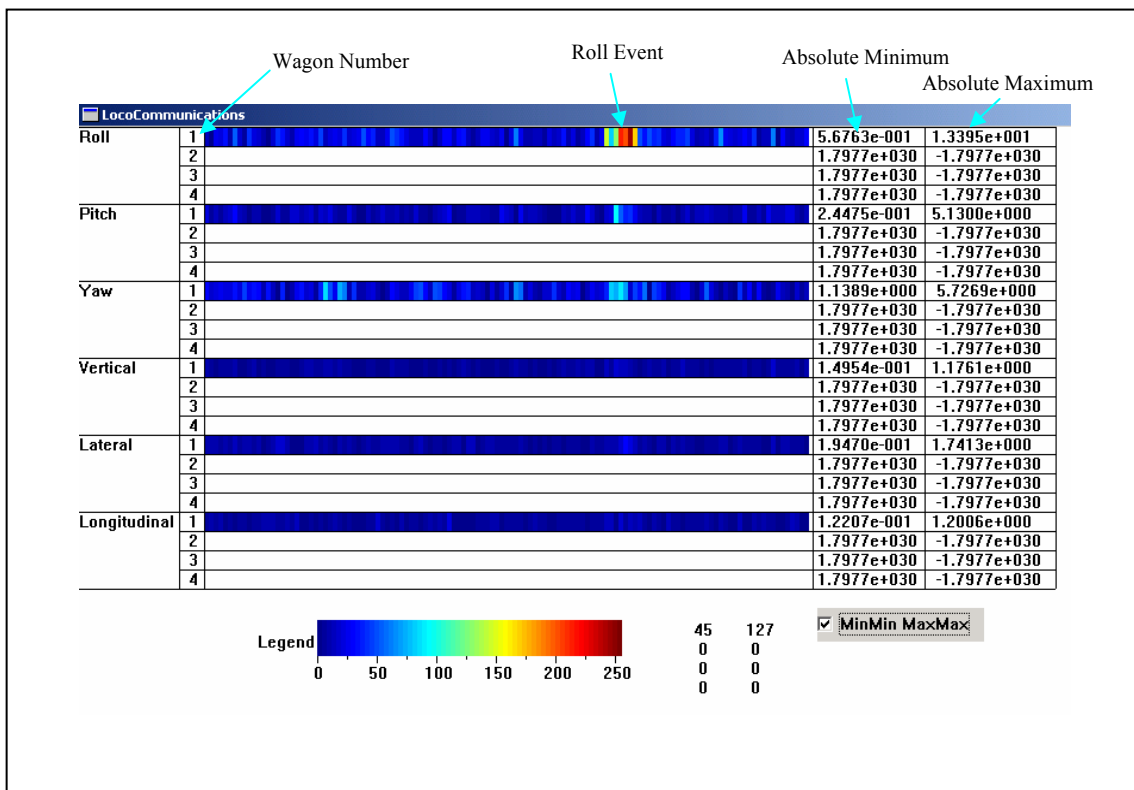


Figure 6-10 Master Display Showing (0.5-10Hz) Energy in Each DOF. (roll action excited, one wagon only)

The colours on the display gave a visual sense of the relative magnitudes occurring in each mode. The numbers alongside the bands are the absolute minimum and absolute maximum values over the period covered by the display. Figure 6-11 is a fabricated

output illustrating an expected result had the algorithm been working for the in-train test. Four consecutive wagons of the same type with equivalent suspension characteristics should experience the similar excitation, resulting in a diagonal correlation. Wagons with different characteristics would exhibit less correlation. The angle of the diagonal away from vertical should be proportional to the train speed.

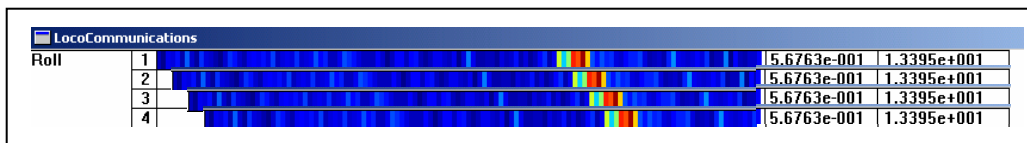


Figure 6-11 Expected Result for Four Wagons with Equal Characteristics (fabricated result)

This visual representation was designed to allow test engineers to see what was happening during the initial test. For a working automatic system, recognition of abnormal wagons could be automated by performing a correlation on the output streams.

6.7 RECOMMENDATION FOR AUTOMATED DETECTION OF TIME-FREQUENCY SIGNATURES

A range of literature was reviewed which presented the use of time-frequency analysis, including wavelet analysis, as the feature extraction stage of artificial neural network (ANN) based detection systems, c.f. Figure 6-2. Many of these were applied to electrical power system fault detection. It was consistent throughout the literature that the techniques were applied to relatively simple, well controlled experiments, with known inputs and outputs. It was very difficult to find literature that detailed how to implement the schemes that they presented. A refreshing exception was a text chapter

on detection and classification by ANNs and time-frequency distributions [86]. The chapter identified some basic requirements for extraction of features from transient signals for input to a neural network. These are outlined here as follows.

The feature extraction stage should produce a representation of the signal which:

1. reveals the significant characteristics of the signal
2. discriminates well between different signals
3. remains the same as the signal moves across the window of observation

An extension to the FFT spectrogram was presented which fulfilled these requirements. The method was to first construct the spectrogram, then take the FFT of each frequency band in the spectrogram with respect to time and return the result back into the same horizontal line as in the original spectrogram. The result is a representation that is dependant upon the frequency content, *and duration* of the time-frequency feature, but does not shift as time “rolls on”. It only changes as features enter or leaves the observation window of the complete spectrogram.

Figure 6-12 demonstrates the technique applied to some offline data. The figure is divided into five rows of sequential data with $1/3^{\text{rd}}$ shift in time from one row to the next. The top image on each row is the spectrogram. The lower image on each row is the result of the process described above. The time-frequency features can be seen moving across the window of observation in the spectrogram. Note that the lower image reflects the frequency content of the signal and the duration of that frequency content in the signature. The representation does not change as the feature “slides” through the window.

When applied as a feature extraction stage for an ANN classification system, the method was reported to achieve very good results with minimal training. Furthermore, the feature extraction stage used FFT algorithms to achieve a “very fast” implementation, making it suitable for an embedded application such as Health Card. This extension of the time-frequency analysis technique presents a promising direction for ongoing research into detection of unique vibration signatures from the acceleration signals.

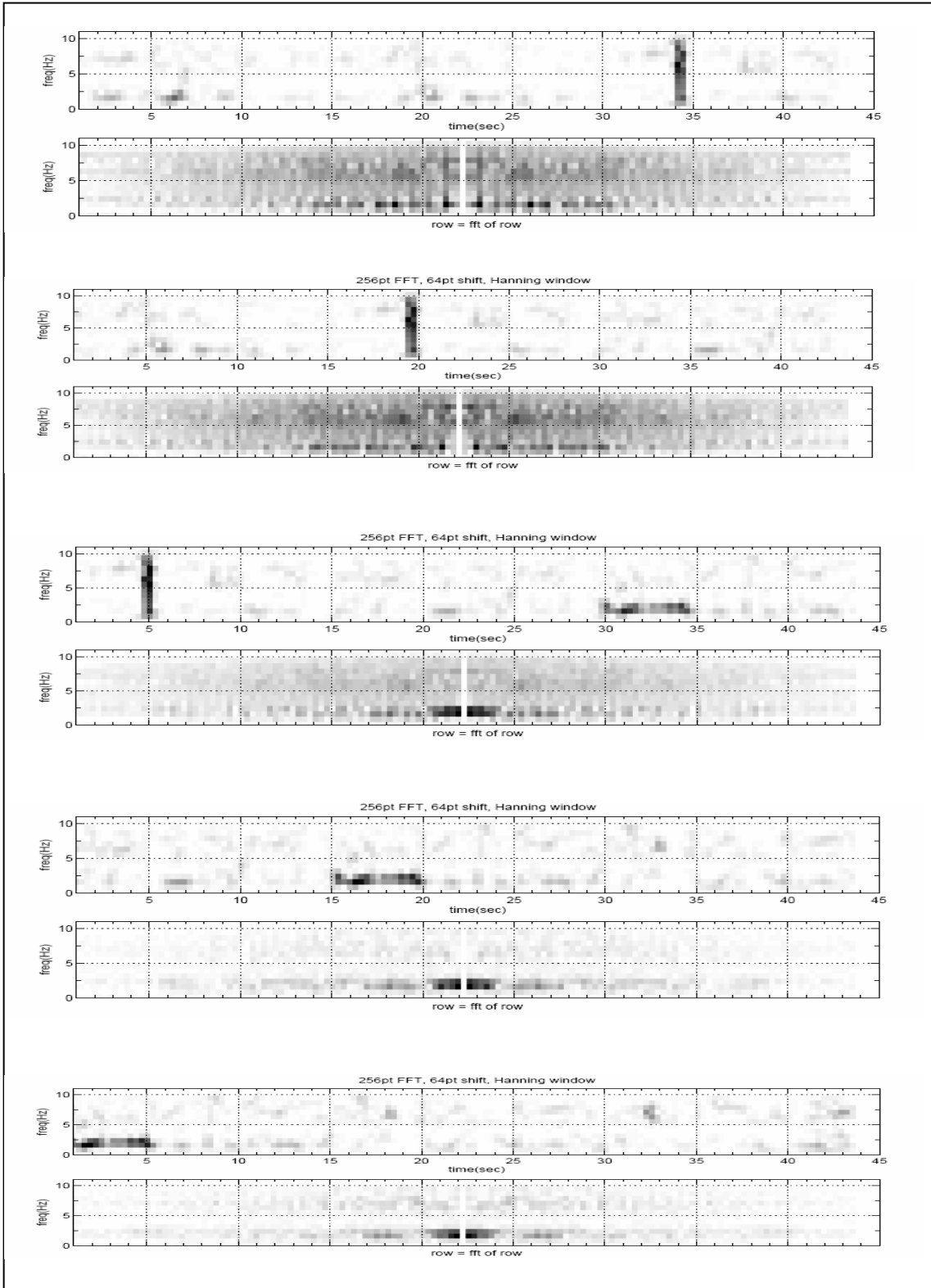


Figure 6-12 Spectrogram of Moving Signal (upper) and FFT of the Spectrogram Rows (lower)

6.8 CONCLUSION

A signal analysis algorithm was required for the prototype Health Card system to run for initial testing of the hardware and device network. This chapter has described the online algorithm that was developed by the researcher to meet the requirements of the development project, and to verify that STDFT time-frequency analysis is feasible within the constraints of the device. The algorithm has produced an output comparable with existing standards, and which also provided the flexibility to select different frequency ranges, or apply a weighting function based upon knowledge of the target behaviour.

Although the time-frequency information was not able to be transmitted to the master device for display, the results proved that the online time-frequency analysis was running and producing the expected output. This verified that the FFT based time-frequency analysis is viable under the processing constraints of the prototype device, and could be used as a basis for signal analysis onboard the fully automated device. A significant recommendation has been made for the use of FFT analysis as a feature extraction stage of an ANN signal classification system.

7 Conclusion

This research was required to examine the application of time-frequency techniques to the online analysis of wagon body acceleration signals. The application utilised a novel wagon and track health monitoring system that would measure accelerations at the wagon body of every wagon in the fleet. A prototype device was developed, and algorithms constructed for that device to operate for field testing and ongoing development.

The research outlined in this thesis has laid a foundation that did not exist before. A substantial review of the relevant literature resulted in an understanding of the application which will enable future development of the concept system. As part of this review it was important to determine the key phenomena that need to be detected by the monitoring system. Lateral bogie oscillation and resonant wagon-track interaction were identified as key indicators of the performance of the wagon-track system. This thesis has also identified existing ride monitoring systems and standards and presented these for comparison with the proposed “Health Card” system.

The signal characteristics for this application are quite unique and an understanding of the characteristics of the signals has been developed as part of this research. The theory of time-frequency analysis has been introduced as a necessary set of tools in the context of the application. Two major forms of time-frequency analysis are presented and compared throughout the thesis to determine the most appropriate approach for this application. The Fourier spectrogram and Wavelet analysis are applied to field data and the results demonstrate that Fourier analysis is most suitable for detecting the behaviour

of interest. Wavelet analysis may become more useful as Health Card research matures and specific event signatures are identified that require its advantages.

Time-frequency analysis was also compared with RMS and peak measures specified in relevant standards. The Fourier spectrogram and Wavelet analysis clearly resolved signatures of lateral bogie oscillation and severe wagon-track interaction, both of which were concealed in the RMS and peak measurements. Results also showed a strong possibility that Health Card algorithms could detect a change in wagon parameters from the time-average of the spectrogram. The results demonstrated the merits of using time-frequency analysis as a basis for online signal analysis on Health Card. They also highlighted a potential limitation in the Australian and North American ride monitoring standards that should be addressed.

Implementation of Fourier spectrogram analysis has been demonstrated on the prototype device. The algorithm implemented on the device fulfils the technical requirements of the prototype system, allowing it to run for proof of concept and ongoing research into the capabilities of the integrated system of devices. The output produced is comparable to standard RMS and peak to peak levels, but with added flexibility to weight the signal based upon frequency content. A visual display output has been implemented that allows system development engineers to view the relative motions of consecutive wagons. Although time frequency information was not transmitted as an output, the implementation proved that the device can support Fourier time-frequency analysis across several concurrent channels. A variant of Fourier time-frequency analysis has been shown in literature to be highly effective as a feature extraction stage to an

Artificial Neural Network and is recommended as a promising direction for future research.

Significant contributions were made as part of this research towards the development of the Health Card system. These contributions include:

1. strategic placement of four dual axis accelerometers for the Health Card prototype to capture six degrees of freedom in the vehicle body
2. determination of requirements for signal filtering and data sampling within the prototype device
3. conversion of raw data into measurement of six modes of vehicle body motion including longitudinal, vertical, lateral, pitch, yaw and roll
4. a time frequency analysis algorithm reporting energy levels in each mode while providing a means for frequency dependent detection
5. several informed recommendations for ongoing research and future algorithms for the Health Card device

The knowledge and tools developed in this thesis form a foundation that did not exist at the outset of this research. It is the hope of the researcher is that this foundation will be used to develop the “Health Card” concept into a working reality.

References

- [1]. Esveld, C., 2001, *Modern railway track*, 2nd ed., The Netherlands : MRT Productions, c2001. ISBN: 9080032433.
- [2]. Heeler, C.L., 1979, *British Railway Track: Design Construction and Maintenance*, 5th Edition, The Permanent Way Institution, Derry and Sons Limited, Nottingham, 1979
- [3]. Garg, V. K., R. V. Dukkipati, 1984, *Dynamics of railway vehicle systems*, Academic Press, ISBN 0-12-275950-8
- [4]. True, H., 1994, "Does a Critical Speed for Railroad Vehicles exist?" *Proceedings of the 1994 ASME/IEE Joint Railroad Conference*, 1994.
- [5]. Kaas-Petersen, C., H. True, 1985, "Periodic, Biperiodic and Chaotic Dynamical Behaviour of Railway Vehicles", 9th IAVSD Symposium, 1985, 208-221
- [6]. FRA 49 CFR Part 213, 1998, "Track Safety Standards; Final Rule", Federal Railroad Administration, Department of Transportation, Federal Register/Vol. 63, No.119, Washington DC, June 22, 1998
- [7]. Queensland Rail Safety Standard STD/0077/TEC Civil Engineering Track Standards Version 2. Module CETS 9 – Track Geometry
- [8]. DOTRS, 2002, "RCP-2201: Performance acceptance requirements", Code of practice for the defined interstate rail network, Volume 5, Rollingstock, Part 2: Common requirements, Section 2 – Commissioning and Recommissioning, Department of Transport and Regional Services, Australia (AROU V1 Consultative Draft, issued Nov 2002)
- [9]. Rail Infrastructure Corporation, 2002, "RSU 288: Common Interface Requirements: Ride Performance Test", RSS 001: Minimum Operating Standards for Rolling Stock, Version 2, 2002
- [10]. McClanachan, M., M. Dhanasekar, D. Skerman, J. Davey, 2002, "Monitoring The dynamics of Freight wagons", *CORE2002*, Wollongong.
- [11]. Code of practice for the defined interstate rail network, Volumes 1,2,3,&4, issue 3, Jan 2003, Department of Transport and Regional Services, Australia
- [12]. Mau, F., P. Olsen, A. O'Brien, 2001, "Vehicle - track interaction", *7th International Heavy Haul Conference*, 2001.
- [13]. Ackroyd, P., S. Angelo, B. Nejikovsky, J. Stevens, 2002, "Remote Ride Quality Monitoring of Acela Train Set Performance", *Proceedings of the 2002 ASME/IEEE Joint Rail Conference*, Washington, DC, April 23-225, 2002
- [14]. McClanachan, M., B.Scown, D. Roach, D. Skerman, B.Payne, 2001, "Autonomous Detection of Severe Wagon-Track Interaction Dynamics" , *7th International Heavy Haul Conference*, 2001
- [15]. Cole, C., D. Roach, 1996, "Dynamic Response of Coal Wagons During Normal Operation", *World Conference on Rail Research*, Colorado Springs

- [16]. ROA, “Road worthiness acceptance standards for rail freight vehicles”, Manual of engineering standards and practices, Vol 1, Section 3, issued Sept 1992
- [17]. McAnaw, H.E. 2001, “System That Measures The System”, *Railway Engineering 2001, proceedings of the 4th international conference*, London UK, 30 April – 1st May 2001
- [18]. RideMon, AEA Technologies <http://www.aeat.co.uk/rail/> (accessed 4-3-04)
- [19]. Remote RideMeter™, <http://www.ensco.com/products/rail> (accessed 4-3-04)
- [20]. Rabbit 3000 processor user’s manua006C, (accessed 5-3-04) <http://www.rabbitsemiconductor.com/products/rab3000/docs.shtml>
- [21]. FRA, 2002, “Track Safety Standards Compliance Manual”, Federal Railroad Administration, Department of Transportation, Washington DC, Jan 1, 2002
- [22]. Analog Devices, Inc., 1999, *ADXL202/ADXL210 Low Cost $\pm 2g/\pm 10 g$ Dual Axis MEMS® Accelerometers with Digital Output*, Device Data Sheet, Revision B, One Technology Way, Norwood, MA, U.S.A. (World Wide Web Site: <http://www.analog.com>)
- [23]. Oppenheim, A. V., R. W. Schaffer, 1989, *Discrete-Time Signal Processing*, Prentice Hall, ISBN 0-13-216292-X
- [24]. Grover, D., J. Deller, 1999, *Digital Signal Processing and the Microcontroller*, Motorola University Press, ISBN: 0-13-081348-6
- [25]. Kryniski, K., 1998, *A pre-study of the DSP techniques for detecting track and rail irregularities*, The Marcus Wallenberg Laboratory for Sound and Vibration Research, Department of Vehicle Engineering, Royal Institute of Technology, Stockholm, Sweden.
- [26]. Haykin, S., B. Van Veen, 1999, *Signals and Systems*, John Wiley & Sons, Inc, ISBN 0-471-13820-7
- [27]. UIC Leaflet 518, “Testing and approval of railway vehicles from the point of view of their dynamic behaviour – Safety – Track fatigue – Ride quality” International Union of Railways, Paris, France, April 2003
- [28]. Newland, D.E., 1993, *An introduction to Random Vibrations, Spectral and Wavelet Analysis*, 3rd Edition, Longman, ISBN 0-582-21584-6
- [29]. Hammond, J. K., P. R. White, 1996, “The Analysis of Non-Stationary Signals using Time-Frequency Method”, *Journal of Sound and Vibration* 190(3), 1996, 419-447
- [30]. Rabbit Semiconductor TN201 022-0048 Rev C, *Fast Fourier Transforms on the Rabbit 2000 and the Rabbit 3000*, http://www.rabbitsemiconductor.com/support/techNotes_whitePapers.shtml (last accessed 28-02-05)
- [31]. Huang, J. S., Negnevitsky, M. Nguyen, 1999, “Wavelet Transform based Harmonic Analysis”, *Australasian universities power engineering conference (AUPEC) and IEAust electric energy conference*, Darwin, 1999, 152-156

- [32]. Phung, B. T., Z. Liu, T. R. Blackburn, R. E. James, 1999, "Wavelet Transform Analysis of Partial Discharge Signals", *Australasian universities power engineering conference (AUPEC) and IEAust electric energy conference*, Darwin, 1999, 275-280
- [33]. Cheok, L. W., T. K. Saha, Z. Y. Dong, 2002, "Power Quality Investigation with Wavelet Techniques", *Australasian universities power engineering conference (AUPEC)*, Melbourne, 2002
- [34]. Nguyen, D.T., T.A. Hoang, 1999, "Detection of Disturbances on Electricity Supply Using Wavelets", *Australasian universities power engineering conference (AUPEC) and IEAust electric energy conference*, Darwin, 1999, 184-189
- [35]. Yeo, K. S., D. T. W. Chan, 2002, "Application of Wavelet Analysis for Generator Stator Fault Detection", *Proc. Australasian Universities Power Engineering Conference (AUPEC)*, Australia, Sep/Oct 2002.
- [36]. Hong, C., L. P. Chiang, S. Elangovan, 1999, "Wavelet Packets Analysis and Artificial Intelligence Based Adaptive Fault Diagnosis", *Australasian universities power engineering conference (AUPEC) and IEAust electric energy conference*, Darwin, 1999, 190-195
- [37]. Styvaktakis, E., *On feature extraction of voltage disturbance signals*, Thesis for the Degree of Licentiate of Engineering, Technical Report No.340L
- [38]. Yoon, W., M. J. Devaney, 2000, "Reactive Power Measurement Using the Wavelet Transform", *IEEE Transactions on Instrumentation and Measurement*, Vol.49, No.2, April 2000, 246-252
- [39]. Yoon, W., M. J. Devaney, 1998, "Power Measurement Using the Wavelet Transform", *IEEE Transactions on Instrumentation and Measurement*, Vol.47, No.5, Oct 1998, 1205-1210
- [40]. Hoang, T. A., D. T. Nguyen, 2000, "Appropriate Processing for the Classification of Power Quality Disturbances", *Proceedings of AUPEC 2000*, Brisbane, 196-201
- [41]. Ringrose, M.J., M. Negnevitsky, 1999, "Automatic Disturbance Recognition in Power Systems", *Journal of Electrical and Electronics Engineering*, Australia, Vol.19, No.1-2, June 1999, 83-90
- [42]. Santoso, S., E. J. Powers, W. Mack Grady, A. C. Parsons, 2000, "Power Quality Disturbance Waveform Recognition Using Wavelet-Based Neural Classifier-Part 1: Theoretical Foundation", *IEEE Transactions on Power Delivery*, Vol.15, No.1, Jan 2000, 222-228
- [43]. Santoso, S., E. J. Powers, W. Mack Grady, A. C. Parsons, 2000, "Power Quality Disturbance Waveform Recognition Using Wavelet-Based Neural Classifier-Part 2: Application", *IEEE Transactions on Power Delivery*, Vol.15, No.1, Jan 2000, 229-235
- [44]. Santoso, S., E. J. Powers, W. Mack Grady, J. Lamoree, S. C. Bhatt, 2000, "Characterization of Distribution Power Quality Events with Fourier and

- Wavelet Transforms”, *IEEE Transactions on Power Delivery*, Vol.15, No.1, Jan 2000, 247-254
- [45]. Mao, P. L., R. K. Aggarwal, 2001, “A Novel Approach to the Classification of the Transient Phenomena in Power Transformers Using Combined Wavelet Transform and Neural Network”, *IEEE Transactions on Power Delivery*, Vol.16, No.4, Oct 2001, 654-660
- [46]. Ye, H., S. X. Ding, G. Wang, 2002, “Integrated Design of Fault Detection Systems in Time-Frequency Domain”, *IEEE Transactions on Automatic Control*, Vol.47, No.2, Feb 2002, 384-390
- [47]. Karimi, M., H. Mokhtari, and M. R. Iravani, 2000, “Wavelet Based On-Line Disturbance Detection for Power Quality Applications”, *IEEE Transactions on Power Delivery*, Vol.15, No.4, Oct 2000, 1212-1220
- [48]. Gaouda, A. M., M. M. A.Salama, M. R. Sultan, A. Y. Chikhani, 1999, “Power Quality Detection and Classification Using Wavelet-Multiresolution Signal Decomposition”, *IEEE Transactions on Power Delivery*, Vol.14, No.4, Oct 1999, 1469-1476
- [49]. Angrisani, L., P. Daponte, M. D’Apuzzo, 2001, “Wavelet Network-Based Detection and Classification of Transients”, *IEEE Transactions on Instrumentation and Measurement*, Vol.50, No.5, Oct 2001
- [50]. Borrás, D., M. Castilla, N. Moreno, J. C. Montano, 2001, “Wavelet and Neural Structure: A New Tool for Diagnostic of Power System Disturbances”, *IEEE Transactions on Industry Applications*, Vol.37, No.1, Jan/Feb 2001, 184-190
- [51]. Dash, P. K., B. K. Panigrahi, D. K. Sahoo, G. Panda, 2003, “Power Quality Disturbance Data Compression, Detection, and Classification Using Integrated Spline Wavelet and S-Transform”, *IEEE Transactions on Power Delivery*, Vol. 18, No.2, Apr 2003, 595-600
- [52]. Angrisani, L., P. Daponte, M. D’Apuzzo, A. Testa, 1998, “A Measurement Method Based on the Wavelet Transform for Power Quality Analysis”, *IEEE Transactions on Power Delivery*, Vol.13, No.4, Oct 1998, 990-998
- [53]. Nguyen, D. T., T. A. Hoang, 2000, “Analysis of Power Transient Disturbances using Wavelet Transform Modulus Maxima Technique” *AUPEC 2000*, 2000, 190-195
- [54]. Mokhtari, H., M. Karim-Ghartemani, M. R. Iravani, 2002, “Experimental Performance Evaluation of a Wavelet-Based On-Line Voltage Detection Method for Power Quality Applications” *IEEE Transactions on Power Delivery*, Vol.17, No.1, Jan 2002, 161-172
- [55]. Poisson, O., P. Rioual, M. Meunier, 2000, “Detection and Measurement of Power Quality Disturbances Using Wavelet Transform”, *IEEE Transactions of Power Delivery*, Vol.15, No.3, July 2000, 1039-1044
- [56]. Kang, P.u, D. Birtwhistle, 2001, “Condition Assessment of Power Transformer On-Load Tap-Changers Using Wavelet Analysis”, *IEEE Transaction on Power Delivery*, Vol.16, No.3, July 2001, 394-400

- [57]. Lada, E. K., J. Lu, J. R. Wilson, 2002, "A Wavelet-Based Procedure for Process Fault Detection", *IEEE Transactions on Semiconductor Manufacturing*, Vol. 15, No.1, Feb 2002, 79-90
- [58]. Li, X., S. K. Tso, J. Wang, 2000, "Real-time Tool Condition Monitoring Using Wavelet Transforms and Fuzzy Techniques", *IEEE Transactions on Systems, Man, and Cybernetics – Part C: Applications and Reviews*, Vol.30, No.3, Aug 2000
- [59]. Kim, K., A. G. Parlos, 2002, "Induction Motor Fault Diagnosis Based on Neuropredictors and Wavelet Signal Processing", *IEEE/ASME Transactions of Mechatronics*, Vol.7, No.2, June 2002
- [60]. Feron, E., M. Brenner, J. Paduano, A. Turevskiy, 1998, "Time-Frequency Analysis for Transfer Function Estimation and Application to Flutter Clearance", *Journal of Guidance, Control, and Dynamics*, Vol.21, No.3, May-June 1998
- [61]. Xu, P., A. K. Chan, 2002, "Fast and Robust Neural Network Based Wheel Bearing Fault Detection with Optimal Wavelet Features" *IJCNN '02. Proceedings of the 2002 International Joint Conference on Neural Networks*, Vol.3, 12-17May , 2002, 2076 – 2080
- [62]. Yen, G. G., K. Lin, 2000, "Wavelet Packet Feature Extraction for Vibration Monitoring", *IEEE Transactions on Industrial Electronics*, Vol. 47, No.3, June 2000 p. 650-667.
- [63]. Ruzzene, M., A. Fasana, L. Garibaldi, B. Piombo, "Natural Frequencies and Dampings Identification using Wavelet Transform: Application to Real Data", *Mechanical Systems and Signal Processing*, 1997, Vol 11, No.2, 207-218
- [64]. Gurley, K., T. Kijewski, A. Kareem, 2003, "First and Higher-Order Correlation Detection Using Wavelet Transforms", *Journal of Engineering Mechanics*, Feb 2003, 188-201
- [65]. Newland, D. E., 1997, "Practical Signal Analysis: Do Wavelets Make Any Difference?", *Proceedings of 1997 ASME Design Engineering Technical Conferences*, Sept 14-17, 1997, Sacramento, California
- [66]. Torrence, C., G. P. Compo, 1998, "A Practical Guide to Wavelet Analysis", *Bulletin of the American Meteorological Society*, Vol. 79, No.1, January 1998
- [67]. Kijewski, T., A. Kareem, 2003, "Wavelet Transforms for System Identification in Civil Engineering", *Computer-Aided Civil and Infrastructure Engineering*, Vol.18, 2003, 339-335
- [68]. Kareem, A., T. Kijewski, 2002, "Time-frequency analysis of wind effects on structures", *Journal of Wind Engineering and Industrial Aerodynamics*, Vol.90, 2002, 1435-1452
- [69]. Lind, R., K. Snyder, M. Brenner, 2001, "Wavelet Analysis to Characterise Non-linearities and Predict Limit Cycles of an Aeroelastic System", *Mechanical Systems and Signal Processing*, 2001, Vol. 15(2), 337-356
- [70]. Doyle, J. F., 1997, "A Wavelet Deconvolution Method for Impact Force Identification", *Experimental Mechanics*, Vol 37, No. 4, December 1997

- [71]. Afonso, V. X., W. J. Tompkins, T. Q. Nguyen, S. Luo, 1996, "Multirate Processing of the ECG using Filter Banks", *IEEE Computers in Cardiology* 1996, 245-248
- [72]. Afonso, V. X., W. J. Tompkins, T. Q. Nguyen, S. Luo, 1996, "Filter Bank-Based ECG Beat Detection", *18th Annual International Conference of the IEEE Engineering in Medicine and Biology Society*, Amsterdam 1996, 4.2.8: Time-frequency Analysis of Various Signals II.
- [73]. Afonso, V. X., W. J. Tompkins, T. Q. Nguyen, S. Luo, 1999, "ECG Beat Detection Using Filter Banks", *IEEE Transactions of Biomedical Engineering*, Vol. 46, No.2, Feb 1999 192-202
- [74]. Afonso, V. X., W. J. Tompkins, T. Q. Nguyen, S. Trautmann, S. Luo, 1995, "Filter Bank-Based Processing of the Stress ECG", *1995 IEEE-EMBC and CMBEC Theme 4: Signal Processing*
- [75]. de Pont, J.J., A. Scott, 1999, "Beyond road roughness – interpreting road profile data", *Road and Transport Research*, Vol. 8, No.1, March 1999
- [76]. Machado, G. R., 2000, *Wavelet Analysis and Its Application for Detection of Track and Rail Irregularities*, MSc Thesis, TRITA-FKT 2000:04, ISSN 1103-470X, ISRN KTH/FKT/FR—00/04—SE, Dept. of Vehicle Engineering, Royal Institute of Technology, Stockholm, 2000
- [77]. Abbaszedah, K., M. Rahimian, H.A. Toliyat, L.E. Olson, 2002, "Rail Defect Diagnosis using Wavelet Packet Decomposition", *Industry Applications Conference*, 2002. 37th IAS Annual Meeting, Vol.1, 13-18 Oct. 2002 478-484
- [78]. Choe, H.C., Y. Wan., A.K. Chan, 1997, "Neural pattern identification of railroad wheel-bearing faults from audible acoustic signals: Comparison of FFT, CWT, and DWT features", *Proceedings of the SPIE - The International Society for Optical Engineering*, 1997, vol.3078, 480-96
- [79]. Mandrioto, CI, E. Stella, M. Nitti, N. Ancona, A. Distanto, 2001, "Rail Corrugation Detection by Gabor Filtering", *International Conference on Image Processing*, Vol.2, 7-10 Oct 2001 626-628
- [80]. Misiti, M., Y. Misiti, G. Oppenheim and J. Poggi, 2000, *Wavelet Toolbox User Guide Version 2*. The MathWorks, Inc, Natick, MA
- [81]. Mallat, S., 1989, "A theory of multiresolution signal decomposition: the wavelet representation," *IEEE Pattern Anal. and Machine Intell.*, vol. 11, no.7, p. 674-693
- [82]. Strang, G., T. Nguyen, 1996, *Wavelets and filter banks*. MA: Wellesley-Cambridge Press. 490.
- [83]. Xia, F., Bleakley, S., "The Estimation of Wheel-Rail Interaction Forces from Wagon Acceleration", *Advances in Applied Mechanics*, Proceedings of the 4th Australasian Congress on Applied Mechanics (ACAM2005), Melbourne, Australia, 16-18 Feb 2005, pp333-338
- [84]. The Mathworks Inc, 1998, *Signal Processing Toolbox For Use With MATLAB Users Guide Version 4*. The MathWorks, Inc, Natick, MA

- [85]. <http://www.adobe.com>
- [86]. Malkoff, D.B., 1992, "Detection and Classification by Neural Networks and Time-Frequency Distributions", Chapter 14 of *Time-Frequency Signal Analysis, Methods and Application*, Longman Cheshire, ISBN: 0 582 71286 6, p. 324-348.

Bibliography

- AS 2606-1983, “Vibration and Shock – Vocabulary”, Standards Australia, Homebush, NSW, 1983
- AS 2670.4-2001, “Guidelines for the evaluation of the effects of vibration and rotational motion on passenger and crew comfort in fixed-guideway transport systems”, Standards Australia, Homebush, NSW, 2001
- AS 2775-2004, “Mechanical vibration and shock- Mechanical mounting of accelerometers” Standards Australia, Homebush, NSW, 2001
- AS 2972-1987, “Vibration and shock– Isolators- Procedure for specifying characteristics” Standards Australia, Homebush, NSW, 2001
- Ballinger, D. R., 1992, “Inspection, monitoring and measurement of track condition”, *Cost-effective maintenance of railway track*, Institution of civil engineers, London 25-26 June 1992.
- Bleakley, S., Senini, S., “Autonomous Time Frequency Analysis of Wagon Body Accelerations”, 5th Asia-Pacific Industrial Engineering and Management Systems Conference, Gold Coast, Australia, 2004
- Boashash, B., 1992, *Time-Frequency Signal Analysis, Methods and Application*, Longman Cheshire, ISBN: 0 582 71286 6
- Bruni, S., F. Cheli, A. Collina, F. Resta, 1999, “Road Test Data Procedures for Evaluating the Hunting Instability Threshold of a Railway Vehicle from On Board Measurements”, *Vehicle System Dynamics Supplement 33*, pp. 168-179
- Cole, C., 1998, “How Accurate is Your Train Simulator? A Discussion of Simulation and Validation Techniques”, *CORE98*, Rockhampton
- Cole, C., D. Roach, M. McClanachan, B. Scown, 1999, “An Investigation of the Effect of Bogie and Wagon Pitch Associated with Longitudinal Train Dynamics”, *IAVSD*, Pretoria, South Africa, 1999
- Derailment of Coal Train EG37 , Connors Range, 1 July 2001, Public Report, Oct 2001, ISBN 0 7345 2512 5, (Accessed 24-2-04)
[http://www.transport.qld.gov.au/qt/LTASinfo.nsf/ReferenceLookup/BlackMTN_Derailment_report.pdf/\\$file/BlackMTN_Derailment_report.pdf](http://www.transport.qld.gov.au/qt/LTASinfo.nsf/ReferenceLookup/BlackMTN_Derailment_report.pdf/$file/BlackMTN_Derailment_report.pdf)
- DeVaul, R.W., S. Dunn, 2001 “Real-Time Motion Classification for Wearable Computing Applications” December 7, 2001 (last accessed 3 March 2004)
<http://www.media.mit.edu/wearables/mithril/realtime.pdf>

- Donelson, J, III, R. L. Dicus, 2002, "Bearing defect detection using on-board accelerometer measurements", ASME/IEEE Joint Railroad Conference, 23-25 April 2002, pp.95-102
- ERRI C 209/RP 2, "Test and approval of railway vehicles from the points of view of dynamic behaviour, safety, track fatigue and ride quality – verification of the applicability of UIC Leaflet 518 Final Report, European Rail Research Institute, UTRECHT, July 1999
- ERRI, 1999, "Annual Report 1999", European Rail Research Institute, Utrecht, Netherlands, 1999
- Esveld, C., 1989, "Vehicle response analysis – a new and powerful tool for assessing track quality", De Rooi Publication, Rail Engineering International, vol 18, No 1, pp3-4, Chelmsford, UK.
- Esveld, C., 1990, "Vehicle reactions verses track geometry", *IEEE/ASME Joint Railroad Conference*, 1990, pp171-174
- Esveld, C., 1991, "Assessment of track quality vis vehicle reactions", *IHHA, Workshop on Maintenance of Way and Train Operation – Balancing the Conflicts*, pp. 185-190, Vancouver, Canada.
- Esveld, C., A.W.M. Kok, 1998, "Interaction Between Moving Vehicles and Railway Track at High Speed", *REI / Edition 1998, no. 3*
- Frohling, R.D., M. Tomas, W. Ebersohn, 1997. "Low frequency dynamic vehicle/track interaction: Instrumentation and measurement", *Proc. Sixth Int. Heavy Haul Conf.*, Cape Town, South Africa, pp. 462-474.
- Giancoli, D. C., 1988, *Physics for Scientists and Engineers with Modern Physics, 2nd Ed.*, Prentice-Hall International Editions. ISBN: 0 13 674052 9
- Gimenez, J.G., L.M. Martin, H. Sobejano, 1993, "Dynamic Vehicle Simulation. SDIVE Program", *Multibody Computer Codes in Vehicle System Dynamics*, (Supplement to V.S.D., Vol. 22)
- Goda, K., R. Goodall, 2003, "Fault-detection-and-isolation system for a railway vehicle bogie", 18th IAVSD Symposium, Japan, 2003
- Gorman, M., D. Roach, C. Cole, T. Mcleod, 2000, "The Development of a Train Dynamics Monitor", *CORE2000*, Adelaide.
- Guangxiong, Chen, Jin Xincan, 2001, "A Simulation Study on Influence of Periodic Irregularities on Derailment Safety of a Freight Car on Tangent Tracks", 7th *International Heavy Haul Conference*, 2001

- H.I. Andrews, 1986, *Railway Traction, The principles of Mechanical and Electrical Railway Traction, Studies in Mechanical Engineering Vol. 5*, Elsevier Science Publishers B.V., 1986
- Himelblau, H., A. G. Piersol, J. H. Wise, M. R. Grundvig, 1994, *Handbook for Dynamic Data Acquisition and Analysis*, IES-RP-DTE012.1, Design, Test and Evaluation Division Recommended Practice 012.1, IES/Institute of Environmental Sciences, Illinois, USA, 1994
- Irlam, M. J., 2004, "The Permanent Way, Construction and Maintenance of the Railroad", *Mike's Railway History, The way it was in 1935*, <http://mikes.railhistory.railfan.net/r081.html> (accessed 24-11-2004)
- Ishida, M., M. Uchida, S. Ono, 2001, "Prediction of the Growth of Track Irregularity using a Track Dynamic Model", *7th International Heavy Haul Conference*, 2001.
- Iwnicki, S., J. Stow, H.J.Parkinson, 1999, "Assessing railway vehicle derailment potential using neural networks", IMechE International Conference on Fault-Free Infrastructure, 1999, 147-155
- Kik, W., R. Menssen, D. Moelle, B. Bergander, Vincent, 2002, "Comparison of Results of Calculations and Measurements of DYASF-tests, a research project to investigate safety limits of Derailment at High Speeds", *Vehicle System Dynamics Supplement 37*, 2002, 543-553
- Kufver, B., 2000, *Optimisation of horizontal alignments for railways: Procedures involving evaluation of dynamic vehicle response*, Doctoral Thesis, Railway Technology, Department of Vehicle Engineering, Royal Institute of Technology, Stockholm, 2000
- Kuntzel, E., T. Q. Nguyen, 1997, "On Structure of Dyadic Symmetric Wavelets with Integer Coefficients", *1997 IEEE International Symposium on Circuits and Systems*, June 9-12, 1997, Hong Kong
- Li, D., T. Salahifar, J. Malone Jr., S. F. Kalay, 2001, "Development of Performance-based Track Geometry Inspection", *7th International Heavy Haul Conference*, 2001
- Markine, V.L., C. Esveld, 2000, "Determination of Train Speed Limits on Renewed Tracks using Tamping Machine and Numerical Optimisation", *Railway Engineering 2000*, 3rd Int.Conf. London, UK
- Mauer, L., 1995, "Determination of Track Irregularities and Stiffness Parameters with Inverse Transfer Functions of Track Recording Vehicles", *Vehicle System Dynamics Supplement 24*, 1995, 117-132

- McClanachan, Y. Handoko, M. Dhanasekar, D. Skerman, J. Davey, 2003, "Modelling Freight Wagon Dynamics", *18th IAVSD Symposium*, Japan, 2003
- Mertins, A., 1999, *Signal Analysis, Wavelets, Filter Banks, Time-Frequency Transforms and Applications*, John Wiley & Sons, ISBN: 0-470-84183-4
- Orange, N., Michell, M.(ed), 2004, "The "AK" Track Evaluation and Inspection Cars", *Newsletter No 6/2004*, Railway Technical Society of Australasia, SA Chapter, Adelaide, June 2004
- Parena, D., N. Kuka, W. Masmoudi, W. Kik, 1999, "Derailment Simulation, Parametric Study", *Vehicle Systems Supplement 33*, 1999, 155-167
- QR, 2003, Equipment Specification ES0186, *Rollingstock Data Requirements from Inertial Track Recording Systems*, Rollingstock Engineering Division Technical Services Group, Queensland Rail, QLD, 2003
- QR, 2004, Specification No. IS-OTI-531, *Specification for: Supply, delivery, installation, commissioning, acceptance testing and validation of a road/rail track geometry vehicle and an automated geometry measuring system*, Programmed Maintenance Services, Queensland Rail, QLD, 2004
- Rieckenberg, T., 2004, "Study of Undetected Derailments in Europe", *Track and Signal Magazine*, Vol.8, No.2, April-May-June 2004, 106-109
- Rogers, M. J. B., K Hrovat, K. McPherson, M.E. Moskowitz, T. Reckart, 1997, "Accelerometer Data Analysis and Presentation Techniques" <http://www.grc.nasa.gov/WWW/MMAP/PIMS/PDFs/ADAPT.pdf> (accessed 2 Nov 2004)
- Singh, S. P., F. D. Irani, S. K. Punwani, 1994, "Truck Suspension Specification for Automobile Transport", *Proceedings of the 1994 ASME/IEEE Joint Railroad Conference*, March 22-24, 1994, pp 133 – 139
- Smith, S. W., 1999, *A Scientists and Engineers Guide to Digital Signal Processing 2nd Edition*, California Technical Publishing, ISBN 0-9660176-6-8
- St.Clair, D. C., R. Reed, D. Mellor, R. M. Havira, B. Flachsbart, 2000, "Using Neural Networks to Automate the Detection of Rail Defects", *Automation, TONE: Volume 4: Miniture Robotics and Sensors for Nondestructive Testing and Evaluation*, American Society for Nondestructive Testing and Evaluation, 2000
- Stein, J. Y., 2000, *Digital Signal Processing a Computer Science Perspective*, John Wiley and Sons, Inc., ISBN 0-471-29546-9
- Strang, G., T. Nguyen, 1996, *Wavelets and Filter Banks*, Wellesley-Cambridge Press, ISBN: 0-9614088-7-1

- Suescun, A., L. M. Martin, J. G. Gimenez, J. Vinolas, 1995, "Use of Inverse Dynamics in the Development of Tilt Control Strategies for Rail Vehicles", *Proceedings of the 14th IAVSD Symposium, Arbor, Michigan, USA, August 21-25, 1995, Supplement to Vehicle System Dynamics*, Vol 25, pp 655-667
- Sun, Y.Q., 2002, *A wagon-track system dynamics model for the simulation of heavy haul railway transportation*, PhD Thesis, Centre for Railway Engineering, Central Queensland University
- Sun, Y.Q., M. Dhanasekar, 1999, "Analysis of rail track curved in plan", *Mechanics of Structures and Materials*, Bradford, ISBN 90 5809 107 4
- Sun, Y.Q., M. Dhanasekar, 2002, "Influence of the Railway Track Parameters to the Vertical and Lateral Impact", *CORE2002*, Wollongong
- Sun, Y.Q., M. Dhanasekar, B. Hagaman, 1999, "Analysis of Worn Rail Sections for Stress Concentration", *IHHA '99 STS – Conference*, Moscow, Russia, 239-243.
- Sun, Y.Q., M. Dhanasekar, D. Roach, 2002, "A 3D model for the lateral and vertical dynamics of wagon – track system." *Proc. Instn Mech. Engrs* Vol. 217 Part F, 31-45.
- Tew, G., K. Epp, M. Darby, R. Donnelly, G. Offereins, 2001, "The Role of Technology in the Operations of the BHP Iron Ore Railroad", *7th International Heavy Haul Conference*, 2001
- Vampire, Version 4.31 (Jan 2004) AEA Technology Rail, Derby, UK
www.aeat.co.uk
- Venkatachalam, V., L. Cazzanti, N. Dhillon, M. Wells, 2004 "Automatic Detection of Sound Recordings", *IEEE Signal Processing Magazine*, Vol. 21, No. 2, March 2004
- Wingren, J., 1997, *Track to carbody vibration transfer for a bogie rail vehicle*, Master of Science thesis, Railway Technology, Department of Vehicle Engineering, Royal Institute of Technology, Stockholm, Sweden.
- Xia, F., 2002, "Modelling of Wedge Dampers in the Presence of Two-Dimensional Dry Friction", *Vehicle System Dynamics Supplement 37*, 2002, 565-578
- Xia, F., H. True, 2003, "The Dynamics of The Three-piece-freight Truck", *18th IAVSD Symposium*, Japan, 2003

Xu, P., A. K. Chan, 2002, "Optimal Wavelet Sub-band Selection using Genetic Algorithm", *Geoscience and Remote Sensing Symposium, 2002. IGARSS '02. 2002 IEEE International*, Vol.3, 1441 – 1443

Appendix A Simulation Model Parameters

Table A-1 VAMPIRE™ Model Parameters for Simulations and Modal Analysis

BogSemiSpac	5.18	m	Bogie semi-spacing
WhlSemiSpac	0.838	m	Wheelset half axle spacing
YSemSpc	0.8	m	Primary suspension lateral semi-spacing
WheelRad	0.425	m	Wheel radius
SdbrsemSpac	0.616	m	Side support semi spacing
HalfCar	7.41	m	Half length of a car body
CoefWedge	0.3	Wedge	Wedge static friction coefficient
Stat	16	kN	Static load on wedge friction surface
Bodymass	66.1	Mg	Carbody mass (loaded)
	8.1	Mg	Carbody mass (unloaded)
Bodyroll	85.576	Mgm2	Carbody roll inertia (loaded)
	10.576	Mgm2	Carbody roll inertia (unloaded)
Bodypitch	647.182	Mgm2	Carbody pitch inertia (loaded)
	79.307	Mgm2	Carbody pitch inertia (unloaded)
Bodyyaw	652.982	Mgm2	Carbody yaw inertia (loaded)
	80.017	Mgm2	Carbody yaw inertia (unloaded)
Sidemass	0.447	Mg	Bogie side frame mass
Sideroll	0.101	Mgm2	Bogie side frame roll inertia
Sidepitch	0.1156	Mgm2	Bogie side frame pitch inertia
Sideyaw	0.1156	Mgm2	Bogie side frame yaw inertia
Bolstmass	0.465	Mg	Bogie bolster mass
Bolstroll	0.175	Mgm2	Bogie bolster roll inertia
Bolstpitch	0.115	Mgm2	Bogie bolster pitch inertia
Bolstyaw	0.176	Mgm2	Bogie bolster yaw inertia
Wheelsetmass	1.12	Mg	Wheelset mass
Wheelsetroll	0.4201	Mgm2	Wheelset roll and yaw inertia
Wheelsetpitch	0.1	Mgm2	Wheelset roll and yaw inertia
CoefAdapt	0.3	Friction	Friction coefficient of adapter
StatAdapt	84.388	kN	Static load on adapter
CentPlatePL	81.056	kN	Static pre-load on centre plate
PinSP	6.397	m	Coupler distance in x direction
CpHgt	0.785	m	Coupler distance in z-direction

Appendix B Matlab Code

B.1 EXAMPLE DATA ANALYSIS FORM – FBY 01-04 TO 06-08

This code requires MATLAB Signal Processing Toolbox™ and MATLAB Wavelet Toolbox™. The file handling code is specific to the file format and directory structure of the source files (not included). For clarity, the data path through the code is highlighted with **bold font**.

B.1.1 Code

```
function main()
% Author: Steven Bleakley

set(0, 'DefaultFigureVisible', 'off');

% clear all existing variables in memory

clear all

nfiles = 3 % number of data files to include in one figure

% file range
firstfile.path = 'T:\CQU\MEng\Data\2003 06 27 Field Data\03-27-6.001\'
firstfile.name = '03-27-6.004'
lastfile.path = 'T:\CQU\MEng\Data\2003 06 27 Field Data\03-27-6.006\'
lastfile.name = '03-27-6.008'

% initialise file counters
startfile = firstfile; % initialise
stopfile = firstfile;

% construct name for output file
filename = [firstfile.path((length(firstfile.path)-2):(length(firstfile.path)-1)),'-',
firstfile.name(10:11),'-', lastfile.path((length(lastfile.path)-
2):(length(lastfile.path)-1)),'-',lastfile.name(10:11)]

% loop through files reading nfiles of data into local variables and plotting the
% results to postscript pages
while
~isequal(fullfile(stopfile.path,stopfile.name),fullfile(lastfile.path,lastfile.name))

    [data,stopfile] = loaddata(startfile,nfiles,lastfile);

    FLBZ = (data(:,2)-2.5); % Front Left Body Z
    FLSZ = (-(data(:,3)-2.5)); % Front Left Sideframe Z
    RLBZ = (data(:,6)-2.5); % Rear Left Body Z
    RLSZ = (-(data(:,7)-2.5)); % Rear Left Sideframe Z
    RRBY = (data(:,10)-2.5); % Rear Right Body Y
    RRSZ = (-(data(:,11)-2.5)); % Rear Right Sideframe Z
    FRBZ = (data(:,14)-2.5); % Front Right Body Z
    FRSZ = (-(data(:,15)-2.5)); % Front Right Sideframe Z

    FLBY = (-(data(:,1)-2.5)); % Front Left Body Y
    FLSY = (-(data(:,4)-2.5)); % Front Left Sideframe Y
    RLBZ = (-(data(:,5)-2.5)); % Rear Left Body Z
    RLSY = (-(data(:,8)-2.5)); % Rear Left Sideframe Y
    RRBY = (-(data(:,9)-2.5)); % Rear Right Body Y
    RRSY = (data(:,12)-2.5); % Rear Right Sideframe Y
    FRBY = (-(data(:,13)-2.5)); % Front Right Body Y
    FRSY = (data(:,16)-2.5); % Front Right Sideframe Y

    % CONVERT BODY DATA INTO 5 DOF

    ROLL = (FRBZ - FLBZ); % Body Roll
```

```

    PITCH = (FRBZ - RRBZ);           % Body Pitch
    YAW   = (FLBY - RRBY);           % Body Yaw
    VERT  = (FLBZ + RRBZ)/2;         % Body Vertical
    LAT   = (RRBY + FLBY)/2;         % Body Lateral

% CONVERT DATA TO STANDARD LOCATIONS

FBZ      = (FLBZ + FRBZ)/2;         % Front Body Centre Vertical
FBY     = (FLBY + FRBY)/2;         % Front Body Centre Lateral
RBZ      = (RLBZ + RRBZ)/2;         % Rear Body Centre Vertical
RBY      = (RLBY + RRBY)/2;         % Rear Body Centre Lateral

FSY      = (FLSY + FRSY)/2;         % Front Bogie Centre Lateral
RSY      = (RLSY + RRSY)/2;         % Rear Bogie Centre Lateral

% create text for upper right hand corner of page
titletext = [...
    'Files: ',...
    startfile.path((length(startfile.path)-2):(length(startfile.path)-1)),'-
',startfile.name(10:11),...
    ' to ',...
    stopfile.path((length(stopfile.path)-2):(length(stopfile.path)-1)),'-
',stopfile.name(10:11),...
]

% create the data analysis page using the nominated data
createfigure(titletext, FBY);

% append the figure to the output file (postscript)
print(gcf, '-dpsc', '-append', filename);

% close the figure
close(gcf);
startfile = incfile(startfile);

end

%%% end of mainloop %%%

%%%%%%%%%%%%%%%%%%%%%%%%%%%%%%%%%%%%%%%%%%%%%%%%%%%%%%%%%%%%%%%%%%%%%%%%

function [data, stopfile] = loaddata(startfile,nfiles,lastfile)

% Load nfiles number of data files starting at startfiles
% Terminate if lastfile is found
% Return data in data and last-file-read in stopfile

d = zeros(1,16);
d(1,:) = [];
f = startfile;

for i = 1:nfiles
    f
    temp = DLMREAD(fullfile(f.path, f.name), '\t', 'E2..T15003');
    temp(5001,:) = [];           % extract GPS marks and delete line from data
    temp(10001,:) = [];
    d = [d; temp];              % append data
    if isequal(fullfile(f.path,f.name),fullfile(lastfile.path,lastfile.name))
        % terminate after last file read
        stopfile = f;
        break
    end
    if i ~= nfiles
        f = incfile(f);        % increment file
    end
end
stopfile = f;
data = d;

%%% end of function %%%

%%%%%%%%%%%%%%%%%%%%%%%%%%%%%%%%%%%%%%%%%%%%%%%%%%%%%%%%%%%%%%%%%%%%%%%%

function createfigure(figuretitle, DAT)

% Create the figure using the data in DAT
% place the text in figuretitle on the top right corner of the page

% create figure
figure1 = figure('PaperUnits', 'normalized',...
    'PaperType', 'A4',...
    'PaperOrientation', 'landscape',...
    'PaperPosition', [0.025 0.025 0.975 0.95]);

```

```

% place text in top right corner
set(gcf, 'DefaultAxesBox', 'on');
annotation1 = annotation(...
    figure1,'textbox',...
    'Position',[0.1 0.9702 0.85 0.02841],...
    'FontName','Arial',...
    'FontSize',12,...
    'LineStyle', 'none', ...
    'HorizontalAlignment', 'right', ...
    'FitHeightToText','off',...
    'String',figuretitle);

% scale signal from 0.1/g to 1/g
DAT = DAT*10;

% Filter and downsample signal
fp = 0.5; %Hz
fc = 10; %Hz
fs = 1000; %S/s
DAT = fftbpfilt(DAT,fp,fc,fs);
DAT = downsample(DAT,5);
fs = 200;

% create time vector
t = [1:length(DAT)]*1/fs;

% set up view window range
trange = [max(t)/6 5*max(t)/6];
nrange = trange*fs;

% Create plot1
% plot filtered signal
axes1 = axes('Position',[0.1 0.75 0.85 0.19],...
    'FontName','Arial',...
    'FontSize',12,...
    'XGrid','on',...
    'XMinorTick','on',...
    'YGrid','on',...
    'YTick',[-1:0.25:1],...
    'YTickLabel',{'','','-0.5','','0','','0.5','',''},...
    'XTickLabel',{''},...
    'Parent',figure1);
axis(axes1,[trange -1 1]); % |-[ - - - -]-|);
grid on
hold all
title('Front Body Lateral (0.5-10Hz filtered)');
ylabel('FBY(g)');
plot1 = plot(t,DAT,'Color','k','Parent',axes1);

% Create plot 2a
% Plot sliding RMS values
axes2 = axes('Position',[0.1 0.52 0.85 0.19],...
    'XAxisLocation','top',...
    'YAxisLocation','right',...
    'FontName','Arial',...
    'FontSize',12,...
    'XGrid','on',...
    'XMinorTick','on',...
    'YGrid','on',...
    'YTick',[0:0.05:0.25],...
    'YTickLabel',{'','','0.1','','0.2',''},...
    'XTickLabel',{''},...
    'XColor','m',...
    'YColor','m',...
    'Parent',figure1);
axis(axes2,[trange 0 0.25]);
grid on
hold all
xlabel('Pk-pk and RMS','Color','k');
ylabel('2sec RMS(g)','Color','m');
plot2 = plot(t, rms(DAT,256,1),'Color','m','Parent',axes2);

% Create plot 2b
% plot sliding Peak to Peak
axes2b = axes('Position',get(axes2,'Position'),...
    'Color','none',...
    'XColor','k',...

```

```

'YColor','k',...
'FontName','Arial',...
'FontSize',12,...
'XGrid','on',...
'XMinorTick','on',...
'YGrid','on',...
'YTick',[0:0.3:1.5],...
'YTickLabel',{' ',' ','0.6',' ','1.2',' '},...
'XTickLabel',{' ',' ',' ',' ',' '},...
'Parent',figure1);
axis(axes2b,[trange 0 1.5]);
grid on
hold all
ylabel('1sec PK-PK(g)','Color','k');
plot2b = plot(t, pk2pk(DAT,200,1),'Color','k','Parent',axes2b);

% Create plot 3
% Plot wavelet coefficients

axes3 = axes('Position',[0.1 0.29 0.85 0.19],...
'FontName','Arial',...
'FontSize',12,...
'Parent', figure1,...
'Layer', 'top',...
'XLim', nrange,...
'YLim', [1 6]);
hold all

%   haar   freq
%   scale  (Hz)
%=====
%   16     12.4514
%   32     6.2257
%   64     3.1128
%   128    1.5564
%   256    0.7782
%   512    0.3891

scales = [16 32 64 128 256 512];
C = cwt(DAT,scales,'haar','absq1b');
axis ij
set(axes3,'YTickLabel',{'12.5','6.2','3.1','1.6','0.8','0.4'},'XTickLabel',{' '});
ylabel('freq(Hz)');
xlabel(' ');
title('Haar wavelet for scales: 16 32 64 128 256 512')
map = ones(240,3) - gray;
colormap(map);

% Create plot 4
% Plot Spectrogram

axes4 = axes('Position',[0.1 0.06 0.85 0.19],...
'FontName','Arial',...
'FontSize',12,...
'XGrid','on',...
'XMinorTick','on',...
'YGrid','on',...
'YMinorTick','on',...
'Box', 'on',...
'Layer', 'top',...
'Parent',figure1);
grid on
hold all
ylabel('f(Hz)');

NFFT = 256;
[A,F,T] = specgram(DAT,NFFT,fs,NFFT,192);
T(1:3) = [];
plot4 = imagesc(T,F,A);
axis(axes4,[trange 0 11]);
axis xy
ylabel('freq(Hz)');
title('256pt FFT, 64pt shift, Hanning window');
xlabel('time(sec)');

%%% end of function %%%

%%%%%%%%%%%%%%%%%%%%%%%%%%%%%%%%%%%%%%%%%%%%%%%%%%%%%%%%%%%%%%%%%%%%%%%%

function sigout = fftbpfilt(sigin,fp,fc,fs)

```

```

% FFT band pass filter
% lower cut-off = fp
% upper cut-off = fc
% sampling rate = fs

sx = fft(signin);
len = length(sx);
sx((len*fc/fs):(len*(1-fc/fs)))=0;
sx(1:fix(len*fp/fs))=0;
sx(fix(len*(1-fp/fs)):len)=0;
sigout = real(ifft(sx));

%%% end of function %%%

%%%%%%%%%%%%%%%%%%%%%%%%%%%%%%%%%%%%%%%%%%%%%%%%%%%%%%%%%%%%%%%%%%%%%%%%

function sigout = rms(signin,window,step)

% Calculate the RMS value of SIGIN
% over WINDOW points
% sliding in steps of STEP points

MS = zeros(1,length(signin));
for i = 1+window/2:step:(length(signin)-window/2)
    MS(i) = sum(signin((i-window/2):(i+window/2)).^2)/window;
end
sigout = sqrt(MS);

%%% end of function %%%

%%%%%%%%%%%%%%%%%%%%%%%%%%%%%%%%%%%%%%%%%%%%%%%%%%%%%%%%%%%%%%%%%%%%%%%%

function sigout = pk2pk(signin,window,step)

% WINDOW in points
% STEP in points

PK2PK = zeros(1,length(signin));
for i = 1+window/2:step:(length(signin)-window/2)
    PK2PK(i) = max(signin((i-window/2):(i+window/2))) - min(signin((i-
window/2):(i+window/2)));
end
sigout = PK2PK;

%%% end of function %%%

%%%%%%%%%%%%%%%%%%%%%%%%%%%%%%%%%%%%%%%%%%%%%%%%%%%%%%%%%%%%%%%%%%%%%%%%

function newfile = incfile(oldfile)

% Increment the file name by 1
% When filenumber reaches 99, clear to 00 and increment the directory by 1

filepath = oldfile.path;
filename = oldfile.name;
filenum = str2double(filename((length(filename)-4):length(filename))); % get file
number
filenum = filenum + 0.001; % inc file number
if filenum > 6.099
    filenum = 6.0;
    filepath = incpath(filepath);
end
filenumstr = num2str(filenum,'%5.3f') ;
filename((length(filename)-4):length(filename))= filenumstr;
% Check that new file exists
if ~isequal(exist(fullfile(filepath,filename)), 2)
    error('File not found.')
end
newfile.name = filename;
newfile.path = filepath;

%%% end of function %%%

%%%%%%%%%%%%%%%%%%%%%%%%%%%%%%%%%%%%%%%%%%%%%%%%%%%%%%%%%%%%%%%%%%%%%%%%

function newpath = incpath(oldpath)

% NEWPATH = INCPATH(OLDPATH)
% eg '03-27-6.002/' -> '03-27-6.003/'

path = oldpath;
pathnum = str2double(path((length(path)-5):(length(path)-1))); % get path number
pathnum = pathnum + 0.001; % inc path number
pathnumstr = num2str(pathnum,'%5.3f'); % field = 5, precision = 3

```

```

path((length(path)-5):(length(path)-1)) = pathnumstr;
newpath = path;

%%% end of function %%%

%%%%%%%%%%%%%%%%%%%%%%%%%%%%%%%%%%%%%%%%%%%%%%%%%%%%%%%%%%%%%%%%%%%%%%%%

function newpath = decpath(oldpath)

% NEWPATH = INCPATH(OLDPATH)
% eg '03-27-6.002/' -> '03-27-6.001/'

path = oldpath;
pathnum = str2double(path((length(path)-5):(length(path)-1))); % get path number
pathnum = pathnum - 0.001; % inc path number
pathnumstr = num2str(pathnum,'%5.3f'); % field = 5, precision = 3
path((length(path)-5):(length(path)-1)) = pathnumstr;
newpath = path;

%%% end of function %%%

%%% end of code %%%

```

B.1.2 Sample Data Plot

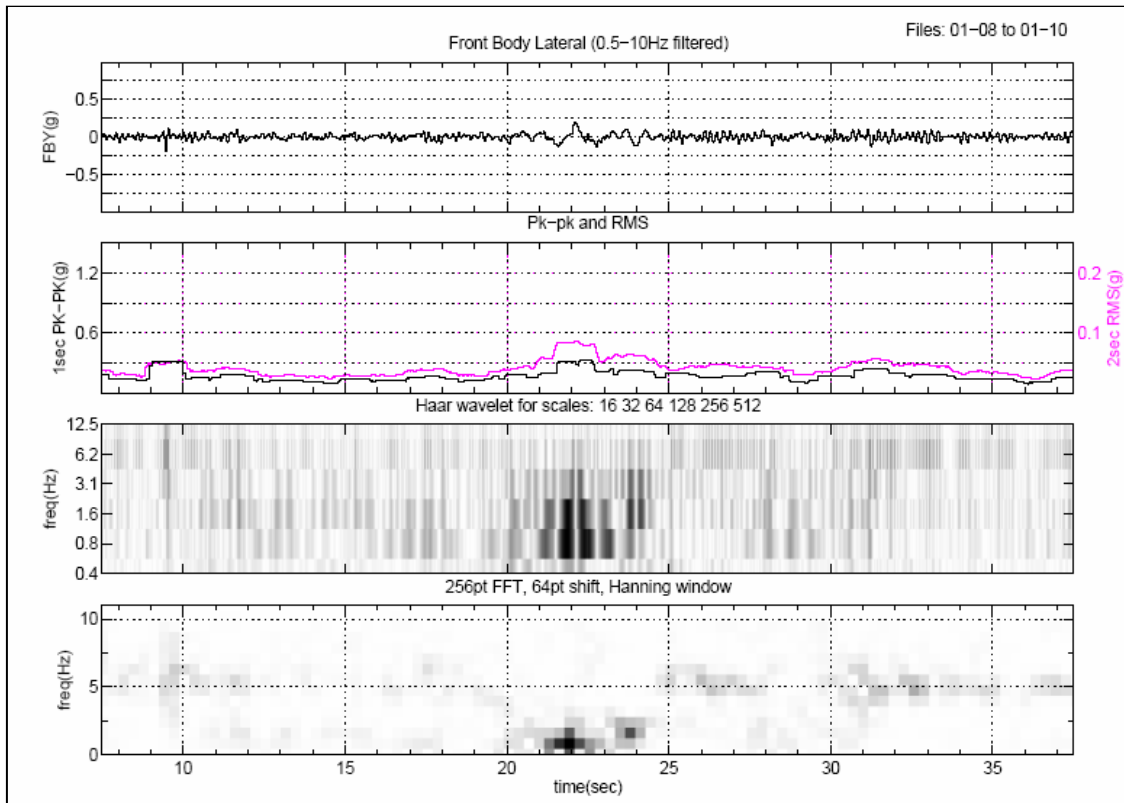


Figure B-1 Example Data Analysis Page (CD01:\FBY 01-04 to 06-08.pdf, page 5)

Appendix C Known Issue Health Card Algorithm

An issue with the algorithm implemented on the prototype Health Card for the initial test was identified during subsequent offline time-frequency analysis of field data. The algorithm applied a 256pt FFT with 128pt shift and a Hanning window. In Figure C-2, spectrograms (1), and (3) have the same configuration. As Figure C-1 illustrates, a transient signal moving from one time location to another aligns differently with the local FFT windows. If the transient aligns with the centre of the window, all of its spectral content will appear in the FFT of the signal multiplied by that window. Alternately, if the transient signal lies at the boundary between two windows, the spectral content is shared between the two.

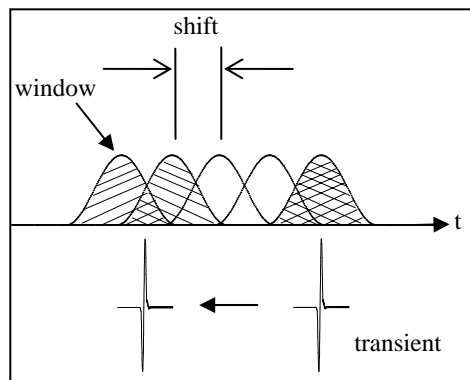


Figure C-1 Windowing and Shift

Figure C-2 demonstrates the effect. The local spectrum of the transient signal in (1) at 24sec is shared over two windows. When the signal is shifted to 8sec in (3), the frequency information is contained within a single window.

More consistent results were achieved by increasing the overlap of the windows. Spectrograms (2) and (4) were calculated with 200pt overlap (i.e. 56pt shift). There is negligible difference between the spectra of the time shifted transient.

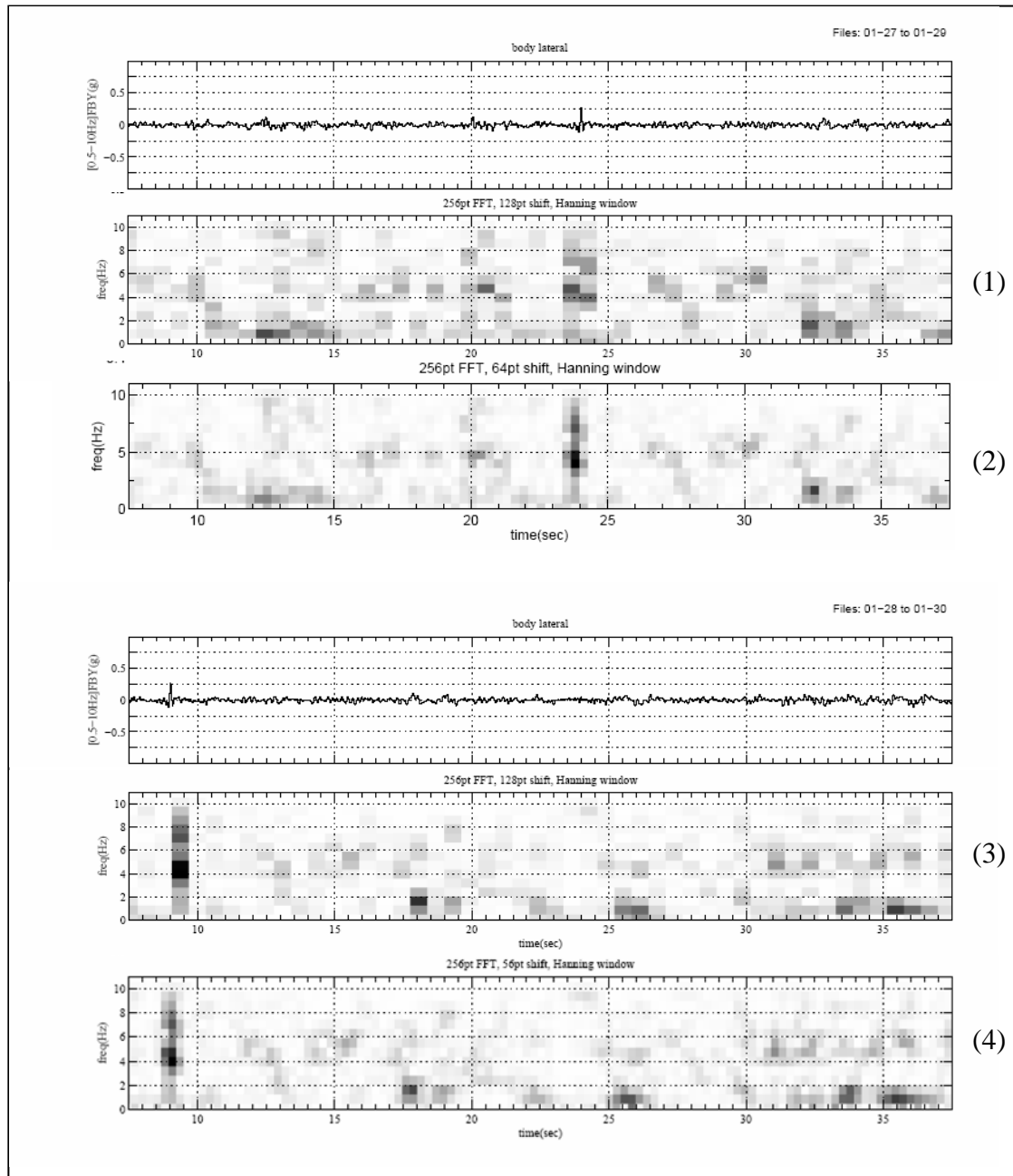


Figure C-2 Comparison of Adequate and Inadequate FFT Overlap

Reducing the shift requires the FFT to be calculated more often, which would cause additional load on the processing resources. For Health Card, the trade-off between time shift invariance and processing load can be managed as the code is optimised. For the offline analysis, a 64pt shift was used. This could be implemented on Health Card using blocks of 64pts instead of 128.